FARADAY ROTATION OF ELECTROMAGNETIC WAVES IN WAVEGUIDES CONTAINING GASEOUS DISCHARGE PLASMAS WITH APPLIED LONGITUDINAL MAGNETIC FIELDS

BY

JAMES EDGAR ETTER

B.S., University of Illinois, 1946
M.S., University of Illinois, 1948

THESIS

SUBMITTED IN PARTIAL FULFILLMENT OF THE REQUIREMENTS
FOR THE DEGREE OF DOCTOR OF PHILOSOPHY IN ELECTRICAL ENGINEERING
IN THE GRADUATE COLLEGE OF THE
UNIVERSITY OF ILLINOIS, 1951

URBANA, ILLINOIS

UNIVERSITY OF ILLINOIS

THE GRADUATE COLLEGE

July 7, 1954

I HEREBY RECOMMEND THAT THE THESIS PREPARED UNDER MY SUPERVISION BY JAMES E. ETTER

ENTITLED FARADAY ROTATION OF ELECTROMAGNETIC WAVES IN WAVE-GUIDES CONTAINING GASEOUS DISCHARGE PLASMAS WITH APPLIED LONGITUDINAL MAGNETIC FIELDS

BE ACCEPTED IN PARTIAL FULFILLMENT OF THE REQUIREMENTS FOR THE DEGREE OF DOCTOR OF PHILOSOPHY IN ELECTRICAL ENGINEERING

L Goldstein
In Charge of Thesis

Eb Jordan
Head of Department

Recommendation concurred in†

C E Shroder
H. Day
Henry Van Foerster
P W Kelchum

Committee on Final Examination†

† Required for doctor's degree but not for master's

5M 4-54—54947

TABLE OF CONTENTS

ACKNOWLEDGMENT

The author wishes to express his appreciation for the guidance and encouragement given him during the period of his research by his advisor, Professor L. A Goldstein, Director of Gaseous Electronics Research at the University of Illinois, Urbana, Illinois.

He is also indebted to the members of the Electron Tube Research Group for their suggestions and criticisms. In particular, the author wishes to thank Professor M. Gilden and Mr. A. Dougal who contributed many hours in the design of the equipment and the recording of data.

The author gratefully acknowledges the support of the Air Force Cambridge Research Center under whose contract AF 19 (604)-524 the research was accomplished.

James E. Etter

July 7, 1954
Urbana, Illinois

SECTION I

INTRODUCTION

A. Subject

Faraday in 1845 used a beam of plane polarized visible light as a probe to investigate the properties of matter under the influence of magnetic fields. He found that the plane of polarization of the light wave traversing transparent media, which were immersed in longitudinal magnetic fields, had been rotated a certain angle. This angle was found to be proportional to the length of medium traversed, and to the intensity of the magnetic field. Faraday also observed that if the light was reflected after one transit through the medium the angle of rotation was doubled. This is the non-reciprocity inherent to this effect.

These experiments led Faraday to believe that this phenomenon was general in that it was not restricted to magnetic materials. He further hoped experiments of this kind would lead to the distinction between the magnetic properties of matter, namely para- and diamagnetism. This, however, was not realized since all para-and diamagnetic materials investigated by him and others with the aid of light rotated the plane of polarization in the same direction. For the dielectrics and range of magnetic fields investigated by Faraday and others at frequencies in the visible light spectrum, the magnitude Θ of the rotation is expressed by

$$\Theta = V B_o L \quad .$$

L is the length of medium traversed, B_o is the static magnetic field, and V is a factor called the Verdet constant which depends

upon the particular material considered.

A satisfactory explanation of this Faraday effect was not reached until years after its discovery. It has been interpreted in terms of the Fresnel decomposition of a linearly polarized light wave into two oppositely rotating circularly polarized waves, each of half amplitude of the original wave. These oppositely rotating circularly polarized waves propagate in the magnetized medium with different velocities. After traversing the medium these two components combine again into a linear wave, provided their amplitudes are equal, but rotated with respect to the original polarization in the sense of the direction of rotation of the faster component. If N_+ is the index of refraction of the wave rotating to the right for an observer looking at the source, and N_- is that for the oppositely rotating wave, the rotation θ in radians is expressed as

$$\theta = (N_- - N_+) \frac{\omega}{2c} L \quad .$$

ω is the angular frequency of the light wave, c is the velocity of light in free space, and L is the length of the medium traversed. The difference, $N_- - N_+$, between the indices of refraction is deduced from consideration of the Zeeman effect. For frequencies in the range of visible light ($\omega \sim 10^{15}$) and magnetic fields of a few thousand gauss, the corresponding Faraday rotation per unit length of medium is quite small. As an example, using glass as the dielectric material, the rotation due to a magnetic field of one thousand gauss is about 30 minutes of arc per centimeter length traversed. At microwave frequencies, however, the

Faraday rotation may be made much larger.

Two media, recently investigated, which produce large Faraday rotations for microwave frequencies are the ferromagnetic dielectrics (ferrites) and the electron gases of gaseous discharge plasmas. Both media become anisotropic in the presence of a dc magnetic field, but a different property is concerned in each case. In the presence of an rf electric field, the motion of the free electrons of the plasma about the applied magnetic field leads to a tensor of dielectric constant. In the magnetized ferrite, an rf magnetic field causes precession of the magnetization about the applied field, and a tensor of magnetic susceptibility arises. Such media wherein the rf propagation is altered by a dc magnetic field are designated as gyromagnetic.

The propagation of electromagnetic waves in magnetized ferrites has been treated extensively, both experimentally and theoretically, and this work is reported in current publications. No detailed account of the Faraday rotation of guided waves propagated through an electron gas medium is as yet published.

The subject of this thesis is an experimental investigation of the Faraday rotation of guided electromagnetic waves using the electron gases of gaseous discharge plasmas as the gyromagnetic material. In addition, associated phenomena such as resonances and polarization changes are considered.

B. Historical Summary

1. Experimental

The propagation of guided electromagnetic waves through electron gases in magnetic fields was first observed by Goldstein, Lampert, and Heney[4],[5] in 1951.

Goldstein, Lampert, and Heney reported both Faraday rotation and polarization transformation in circular wave guides and resonance phenomena in guides of rectangular cross section, where polarization changes cannot occur. The procedure used to obtain Faraday rotation in the circular guide was essentially as follows: A linearly polarized TE_{11} wave was launched in waveguide of circular cross-section. The waveguide contained a discharge tube filling the cross-section of the guide for a distance of five inches, and a magnetic field was applied to the discharge along the guide axis by locating this section in the core of a solenoid. Polarizations of the waves on either side of the discharge were measured by probing the radial electric field at the guide periphery. The radial probes were inserted in short sections of the guide which could be mechanically rotated about the axis of the guide. Measurements were made on a 10 μ sec duration rf pulse propagated through the electron gas of a pulsed gaseous discharge plasma at various times in the discharge decay after removal of the discharge excitation pulse of 5 μ sec duration. Propagation at frequencies between 4600 and 5500 megacycles was studied for magnetic fields up to about 3500 gauss maximum value.

By these experiments, Goldstein and his group established

1. Very large angles of rotation, of the order of 90 degrees or more per air guide wavelength of electron gas.

2. Resonance behaviour of the rotation in the region where

the electron cyclotron frequency is near the rf signal frequency.

3. Departure from linear polarization in the resonance region, and nearly pure circular polarization at resonance, and

4. Demonstration of the non-reciprocity by an analogue of the crossed Nicol prisms experiment with circularly polarized waves.

These results were interpreted in terms of the decomposition of the linear TE_{11} wave into components of opposite circular polarization of differing propagation constants within the anisotropic electron gas, much the same as the Fresnel decomposition of linear polarized light is used to explain the Faraday rotation for frequencies in the visible spectrum.

The work of Goldstein and his associates constitutes the extent of published experimental results of study of guided waves in an anisotropic electron gas medium.

2. Theoretical

The relation, $\vec{D} = \|\epsilon_e\| \cdot \vec{E}$, which gives the rf electric displacement $\vec{D}$ in terms of the electric field $\vec{E}$ within an electron gas in a uniform dc magnetic field is obtained from solutions to the equation of motion of the electrons. Representative derivations have been given by Lorentz,[8] Booker,[1] Turner,[18] and others. In the particular case where the magnetic field is uniform and in the z direction, the dielectric tensor $\|\epsilon_e\|$ is of the form

$$\|\epsilon_e\| = \begin{Vmatrix} \epsilon & -i\eta & 0 \\ i\eta & \epsilon & 0 \\ 0 & 0 & \epsilon_z \end{Vmatrix}$$

where $i = \sqrt{-1}$. The axis along the applied magnetic field, here the z-axis, is referred to as the gyroaxis. The dependence of the tensor elements upon the magnetic field and the discharge parameters are given in Section II. It is noted here that for the electron gas of a discharge plasma ϵ, η, and ϵ_z are in most cases nearly real quantities, and independent of the coordinates.

Theoretical treatments of guided wave propagation along the gyroaxis of gyromagnetic electron gas media having the above dielectric tensor form have been given by Suhl and Walker,[16],[17] Gamo,[2] and Van Trier.[19] In all cases, the medium was assumed lossless in order to accomplish the analyses. This is a reasonable

assumption for most cases of propagation in a gyromagnetic electron gas of a plasma, since at microwave frequencies little loss occurs except in the vicinity of resonances.

For waveguides of circular cross-section filled with a uniform gyromagnetic electron gas, Suhl and Walker[16] were the first to give the characteristic equation which relates the propagation constants of the various modes of propagation to the frequency of the electromagnetic wave. They found the two lowest modes to be neither transverse electric or transverse magnetic, but that they reduce to oppositely rotating circularly polarized TE_{11} waves as the magnetic field is removed. These two modes, called TE_{11}- limit, are those of importance to Faraday rotation. A Verdet constant which relates the rotation to small applied magnetic fields was given. In a subsequent paper[17] Suhl and Walker present an extended analysis for the case of ferrites, and indicate the procedure for an electron gas. Approximate expressions for the propagation constants are given for limiting values (very small and very large) of the applied magnetic field.

The characteristic equation and some other expressions discussed by Suhl and Walker have also been given by Gamo. Van Trier has presented a portion of their results in a more general form, and has considered special cases of other than circular cross-section waveguides.

C. Procedure

The investigations were begun with an experimental set-up similar to that used by Goldstein et al, and by preliminary experiments the qualitative aspects of the Faraday rotation phenomenon were measured. These results were used as a guide in the making of modifications necessary to obtain quantitative data.

The problems associated with the experiments could be divided into two categories: First, those concerning the production and description of discharge plasmas within the cylindrical waveguide, and second, the measurement of rf propagation through the plasmas in dc magnetic fields.

The discharge plasmas were obtained by using a pulsed discharge technique which provided plasmas of practical dimensions and uniformity within the waveguide. The parameters of the plasmas were then determined from measurements of their effective dielectric constant by microwave transmission measurements.[3],[10]

Usual waveguide techniques were used in the propagation studies. The main features of this equipment were:

1. A phase bridge, which enabled the velocity of propagation within the plasma to be measured,

2. A wave analyzer, which provided a much more sensitive measurement of wave polarization than radial probes, and

3. A launching scheme which could excite any polarization of a TE_{11} wave in circular waveguide.

Theoretical values of the propagation constants of the modes of propagation in the gas filled waveguide were obtained by evaluating the analysis of Suhl and Walker for a limited range of plasma

parameters. For completeness, their derivation of the equations which describe propagation in the plasma filled waveguide have been included as Appendix A.

D. Summary of Results

The results of the investigation confirmed the previous observations of Goldstein, Lampert, and Heney concerning the propagation of linear TE_{11} waves in circular cross-section waveguide. By observing the propagation of individual oppositely circularly polarized waves, the validity of interpreting the Faraday effect of linear waves in terms of circularly polarized components was demonstrated.

It was found that the propagation of the circularly polarized waves was described by the detailed theory of Suhl and Walker. Good quantitative agreement was obtained for discharge plasmas which conformed closest to the assumptions of the analysis, and in general for all plasmas, qualitative agreement was found. At low magnetic fields, the rotation of the plane of polarization of the linear wave was measured to be directly proportional to the applied magnetic field intensity. The constant of proportionality relating the rotation and magnetic field intensity agreed closely to the theoretical value of the appropriate Verdet constant.

From the results of the investigation, two applications of Faraday phenomena in gaseous discharge plasmas are evident. First, the effect may be used in the study of the decay of discharge plasmas in magnetic fields. The rotation of the plane of polarization is readily measured, and can be related to the electron density of the plasma. Secondly, the properties of the anisotropic plasma can be utilized in microwave engineering devices for microwave propagation control. The non-reciprocity is important in this respect, and can be used in one-way transmission

applications analogous to the ferrite gyrator.[6] Attenuators, phase shift devices, etc., are also possible uses.

SECTION II

PROPAGATION IN AN UNBOUNDED PLASMA

The simple magneto-ionic theory of propagation[1],[7],[15] describes the Faraday effect of plane waves in unbounded electron gases with superimposed static magnetic fields. This theory cannot be applied rigorously to guided wave Faraday rotation because effects due to the conducting walls of the waveguide cannot be neglected. However, a consideration of the phenomena in the infinite medium does show qualitatively the influence of the plasma parameters upon the propagation of electromagnetic waves and the Faraday effect, and these results aid in the interpretation of the guided wave case.

A. The Gaseous Discharge Plasma as a Medium for Wave Propagation

A comprehensive description of that portion of a discharge called the plasma is found in "The Plasma State of Gases" by Rompe and Steenbeck.[13] To simplify the mathematical description here the plasma is defined simply as that region of a discharge having relatively high and equal concentrations of positive and negative charged particles. It is assumed that no net space charge and no static electric fields exist in the plasma.

If the discharges are further limited to those gases which do not form negative ions, the negatively charged particles of the plasma are frec electrons, and the positive particles are much heavier positive ions. For such discharges it has been demonstrated that the properties of the plasma due to the presence of high frequency electromagnetic fields depend for the most part on the free electron gas.[13]

The electron gas is described, for the purposes of electromagnetic wave propagation, by the following two parameters:

1) N, the electron density, given as the number of electrons per unit volume, and

2) ν , the average number of collisions per second of an electron with the gas atoms.

Under the above assumptions, the motion of the electrons in the presence of an electric field varying in time as exp $i\omega t$ and a static uniform magnetic field H_0 leads to an effective dielectric constant, $\| \epsilon_e \|$, of tensor form. If orthogonal cyclindrical coordinates u, v, z are chosen, so that H_0 lies along z, $\| \epsilon_e \|$ is written as

$$\left\| \epsilon_e \right\| = \begin{Vmatrix} \epsilon & -i\eta & 0 \\ i\eta & \epsilon & 0 \\ 0 & 0 & \epsilon_z \end{Vmatrix} .$$

The tensor elements are:

$$\epsilon = \epsilon_0 \left[1 + \frac{q^2(1-ib)}{\sigma^2 - (1-ib)^2} \right] ,$$

$$\eta = \epsilon_0 \left[\frac{\sigma q^2}{\sigma^2 - (1-ib)^2} \right] ,$$

and $$\epsilon_z = \epsilon_0 \left[1 - \frac{q^2}{1-ib} \right] .$$

In the above $q = \frac{\omega_p}{\omega}$, $\sigma = \frac{\omega_H}{\omega}$, and $b = \frac{\nu}{\omega}$. ω_p is the angular plasma frequency, and is related to the electron density N by $\omega_p = \left(\frac{Ne^2}{\epsilon_0 m}\right)^{1/2}$, and ω_H is given by $\omega_H = \frac{e\mu_0 H_0}{m} = \frac{eB_0}{m}$.

Also

e = electron charge,

m = electron mass,

ϵ_0 = permittivity of free space,

and μ_0 = permeability of free space.

The variation of ϵ and η with σ is shown in Figs. 1 and 2 for the case b = 0. The other element, ϵ_z, is not a function of the applied magnetic field.

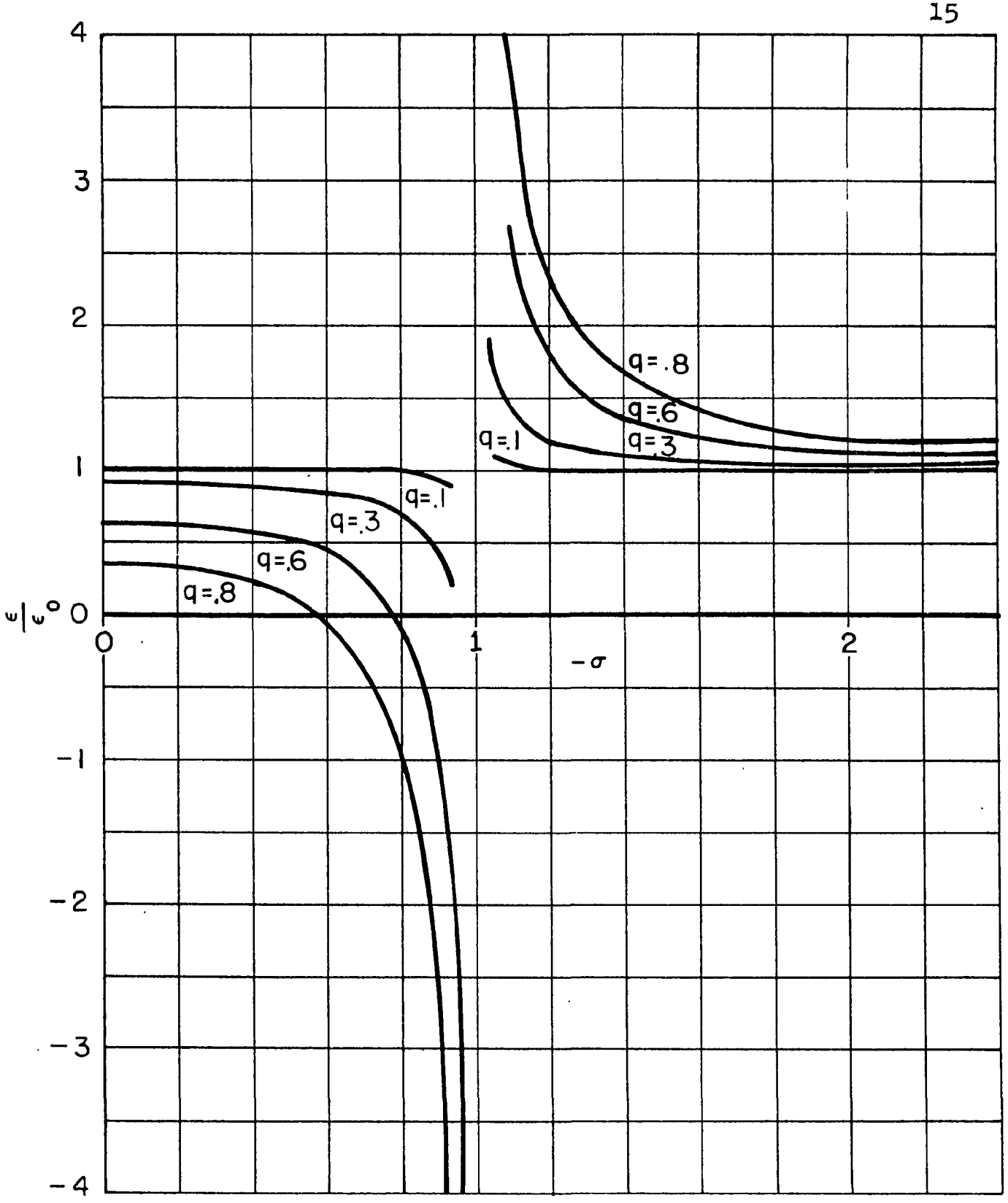

Figure 1. Variation of ϵ with the Magnetic Field Parameter σ.

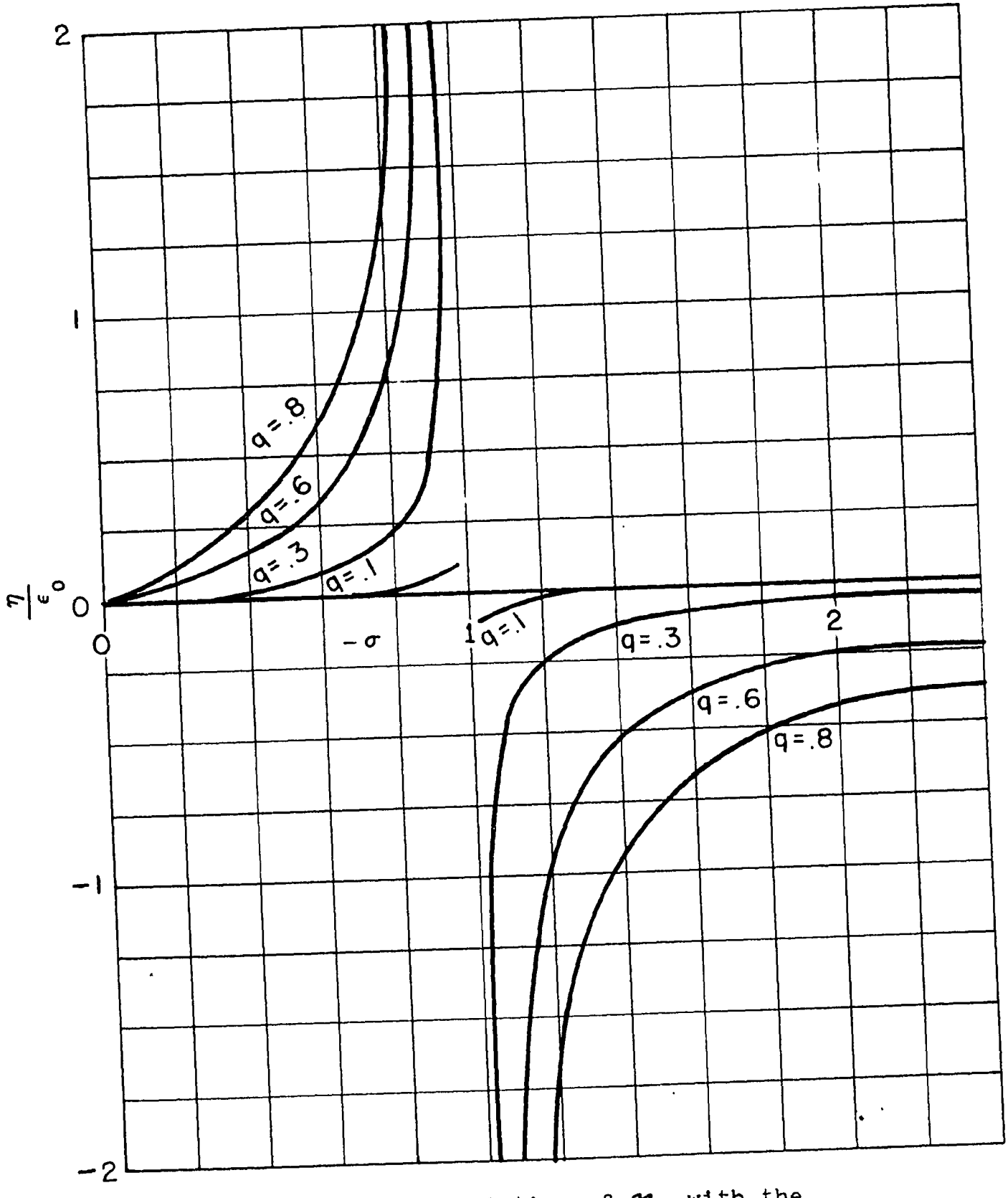

Figure 2. Variation of η with the Magnetic Field Parameter σ.

B. Propagation of Uniform Plane Waves in the Unbounded Medium

Electromagnetic waves in the anisotropic electron gas medium satisfy Maxwell's equations

$$\nabla \times \vec{E} = -\dot{\vec{B}} \qquad \text{and} \qquad \nabla \times \vec{H} = \dot{\vec{D}}$$

where $\vec{B} = \mu_0 \vec{H}$ and $\vec{D} = \|\epsilon_e\| \cdot \vec{E}$. Assuming uniform plane wave solutions which vary as $\exp i\omega t - \gamma z$ where $i = \sqrt{-1}$, these relations reduce to

$$(\omega^2 \mu \epsilon + \gamma^2) E_x - i\omega^2 \mu \eta E_y = 0 \tag{2.1}$$

and

$$i\omega^2 \mu \eta E_x + (\omega^2 \mu \epsilon + \gamma^2) E_y = 0 . \tag{2.2}$$

$\gamma = \alpha + i\beta$ where α and β are respectively attenuation and phase constants Solving 2.1 and 2.2 for the propagation constants of uniform waves results in

$$\gamma_{+,-}^2 = -\omega^2 \mu_0 (\epsilon \pm \eta) , \tag{2.3}$$

a familiar result[15] of magneto-ionic propagation theory.

The wave with propagation constant γ_+ will be called the plus wave and that with γ_- the minus wave

Substitution of γ_+ and γ_- into equation (2.1) shows that the electric field components E_x and E_y of the two waves satisfy

$$\left(\frac{E_x}{E_y} \right)_{+,-} = \mp i . \tag{2.4}$$

Fom this relationship the plus and minus waves are seen to be oppositely rotating circularly polarized waves. By a circularly polarized wave is meant one whose electric field pattern in any

plane perpendicular to the direction of propagation rotates about the axis of propagation. In this particular case, since the waves are uniform, the transverse electric fields also are everywhere circularly polarized.

Neglecting the terms in $\|\epsilon_e\|$ arising from electron collisions, the phase velocities of the plus and minus waves propagating in a lossless anisotropic electron gas are

$$v_+ = c\left[\frac{1}{1-\frac{q^2}{1-\sigma}}\right]^{1/2}, \tag{2.5}$$

and

$$v_- = c\left[\frac{1}{1-\frac{q^2}{1+\sigma}}\right]^{1/2} \tag{2.6}$$

where c is the velocity of light in vacuum.

The phase velocities, plotted as the square of the ratio of phase velocity to velocity of light, are shown in Fig. 3 as a function of σ. Curves for several values of the parameter q are given. The velocity of propagation of plus waves, as can be seen, is little changed by variation of the magnetic field. Their relative phase velocity is always greater than unity starting at $\frac{v_+}{c} = (1-q^2)^{-1/2}$ for $-\sigma = 0$ and decreasing asymptotically toward unity as $-\sigma$ becomes very large. This behaviour is understood by noting that the natural cyclotron motion of electrons is opposite to the electric field rotation and that increasing the static magnetic field reduces electron displacement. By increasing the electron density at a given magnetic field the phase velocity is increased.

In contrast, Fig. 3 shows the phase velocity of a minus wave to always increase with increasing magnetic field. Starting at $-\sigma = 0$, where the phase velocity is the same as that of the plus

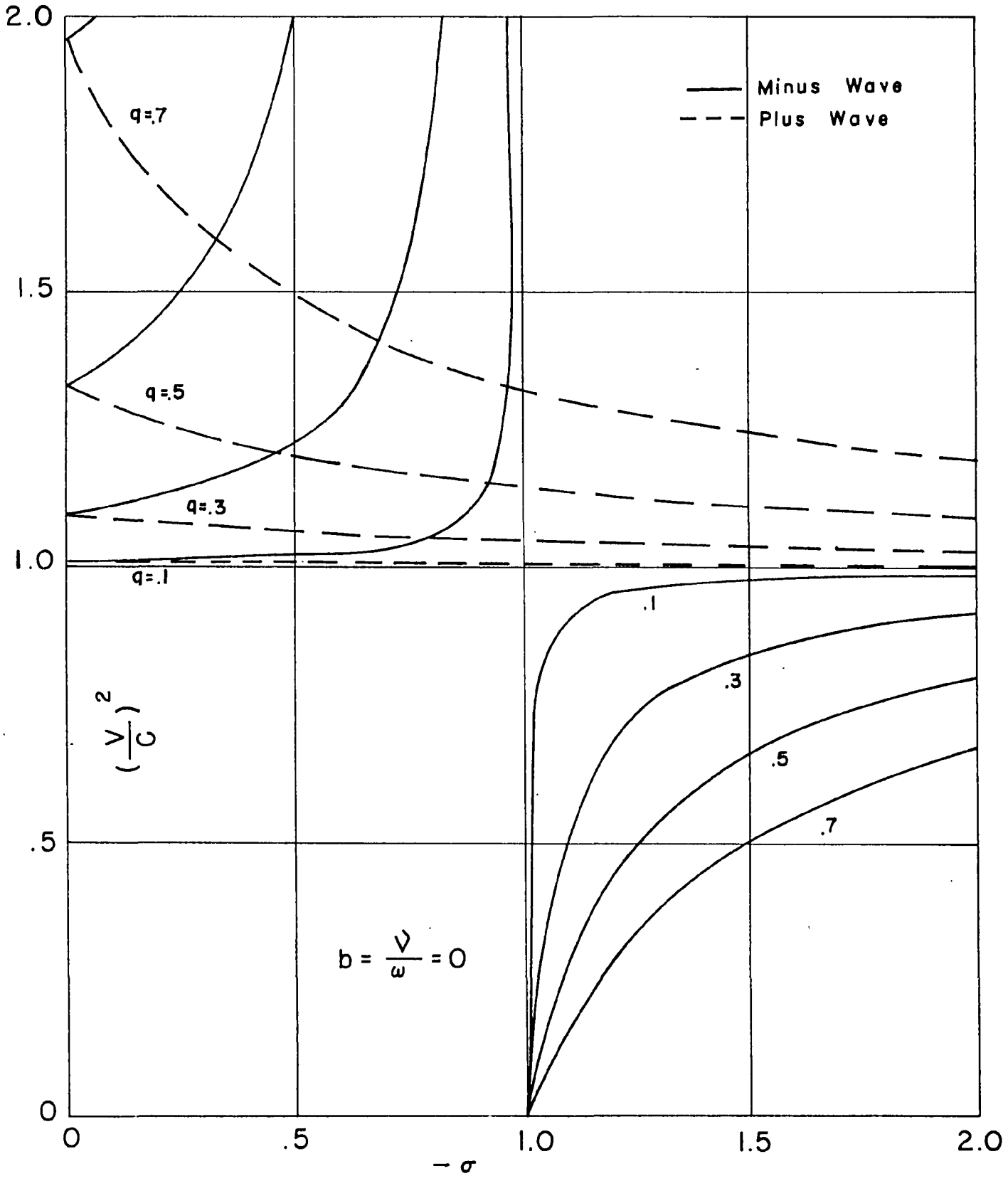

Figure 3. Phase Velocities of Uniform Waves in an Unbounded Electron Gas Neglecting Electron-Atom Collisions.

wave the phase velocity increases without limit until the wave cuts off at $-\sigma = 1 - q^2$. The minus wave reappears with zero phase velocity just as $-\sigma$ exceeds unity. For larger magnetic fields the phase velocity increases, approaching that of propagation in free space as $-\sigma$ becomes very large. As for the plus wave, increasing the electron density for fixed magnetic field increases the phase velocity.

The large variations of $\frac{v_-}{c}$ at values of $-\sigma$ near unity are due to "gyro-resonance" of the electrons. The natural cyclotron motion of the electrons is in the same sense as the minus wave electric field rotation.

When electron collisions are considered, the phase velocity and the attenuation of the minus wave vary with magnetic field as shown in Fig. 4a. $\left(\frac{v_-}{c}\right)^2$ is plotted as a function of magnetic field for several values of b the ratio of collision frequency to angular signal frequency. From Fig. 4a it is seen that an increase of the collision frequency results in a decrease of the variation of phase velocity with magnetic field. The minus wave loses its cutoff and continues to propagate throughout the region of gyroresonance. Passing through the gyroresonance the phase velocity decreases with applied magnetic field. As in the lossless case, the phase velocity always increases with magnetic field for values of magnetic field away from the resonance.

Propagation at magnetic fields near those required for gyroresonance is accompanied by increased attenuation of the minus wave This is shown in Fig. 4b. The maximum value of absorption which occurs at resonance decreases with increasing collision

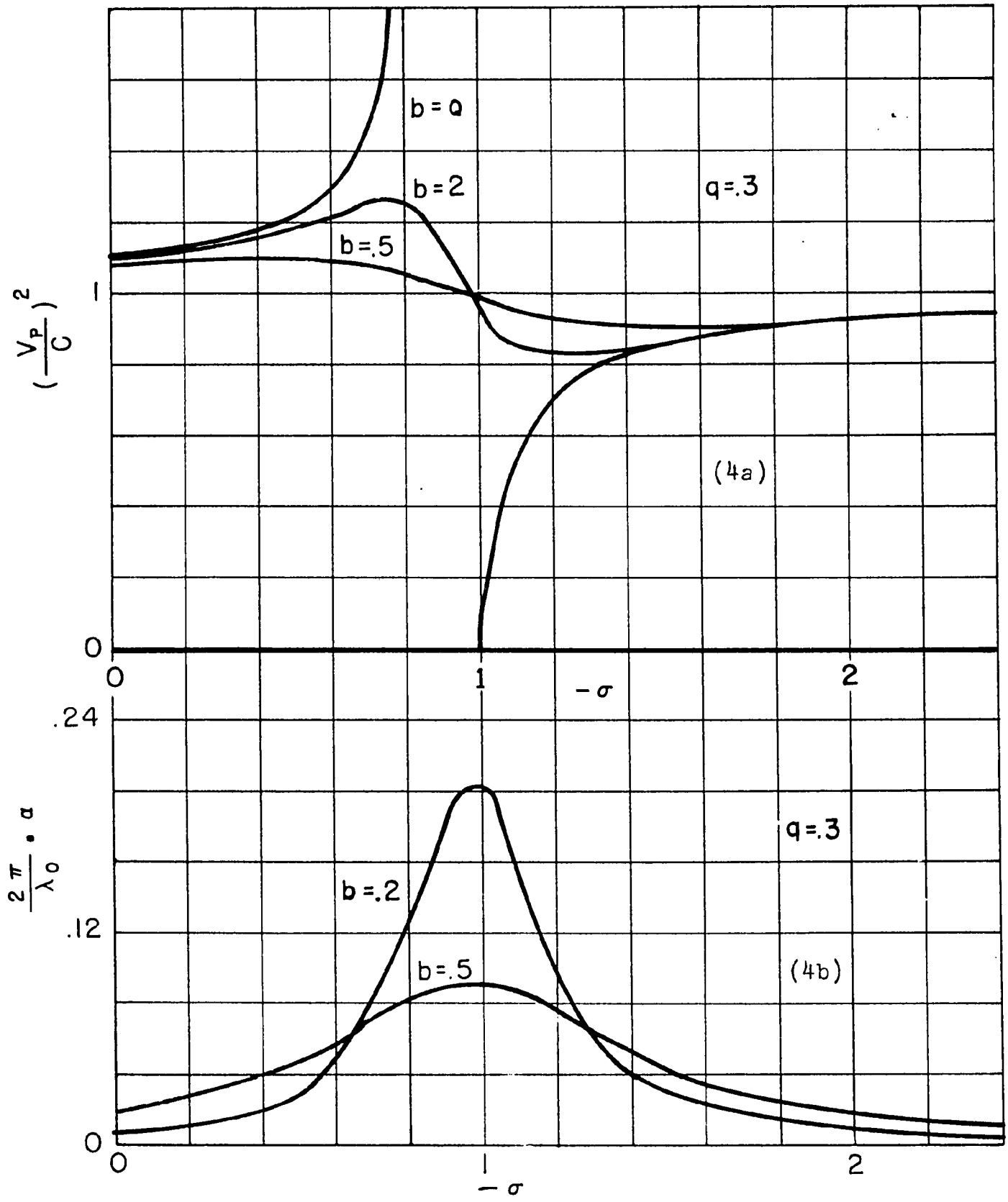

Figure 4. Propagation of the Minus Wave in an Unbounded Electron Gas Considering Electron-Atom Collisions.

frequency.

The inclusion of losses does not significantly alter the variation of phase velocity of the plus wave with magnetic field.

Up to now, the discussion of the propagation of the plus and minus waves has assumed the direction of positive magnetic field to be the same as the direction of wave propagation. Reversing the magnetic field interchanges the propagation constants of the two waves. This is seen from the expression $\gamma^2_{+,-} = -\omega^2 \mu_0 (\epsilon \pm \eta)$ by noting that ϵ and η are respectively even and odd functions of the applied magnetic field.

C. The Faraday Rotation of Linear Waves in the Unbounded Medium

A uniform linear wave within the gyromagnetic electron gas medium can be expressed as the sum of plus and minus waves propagating along the same axis.

As has been mentioned, the plus and minus waves have uniform electric fields entirely transverse to the direction of propagation along the static magnetic field. Because of this uniformity, the behaviour of the waves can be expressed in terms of the electric field at any point in the transverse plane. For the purposes of this discussion. cylindrical coordinates r, φ, z oriented with respect to the rectangular system x, y, z as shown in Fig. 5 will be employed.

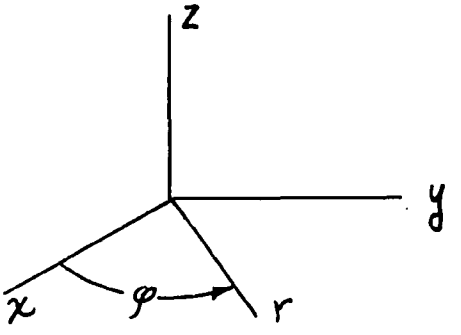

Figure 5. The Coordinate Systems

The fields of the two waves have x and y components

$$(E_x)_{+,-} = \frac{E_{+,-}}{2} e^{i\omega t - \gamma_{+,-} z} \quad \text{and} \quad (E_y)_{+,-} = i \frac{E_{+,-}}{2} e^{i\omega t - \gamma_{+,-} z} \qquad (2.7)$$

assuming propagation in the positive z direction.

If. at z = 0, plus and minus waves of equal amplitudes $E_{+,-} = E_0$ are excited, the resultant total electric field components are by superposition

$$E_x = \frac{E_0}{2} e^{i\omega t}\left(e^{-\gamma_+ z} + e^{-\gamma_- z}\right) \quad \text{and} \quad E_y = i\frac{E_0}{2} e^{i\omega t}\left(e^{-\gamma_+ z} - e^{-\gamma_- z}\right). \tag{2.8}$$

If both circularly polarized components propagate without attenuation. the resultant field is from equation 2.8,

$$E_x = \frac{E_0}{2} e^{i\omega t}\left(e^{-i\beta_+ z} + e^{-i\beta_- z}\right) \quad \text{and} \quad E_y = \frac{iE_0}{2} e^{i\omega t}\left(e^{-i\beta_+ z} - e^{-i\beta_- z}\right)$$

so that by division,

$$\frac{E_y}{E_x} = \tan\left(\frac{\beta_+ - \beta_-}{2}\right) z \quad . \tag{2.9}$$

Equation 2 9 shows that the resultant of the circularly polarized modes is a linear wave, with the plane of polarization $\varphi = 0$ at $z = 0$. The plane of polarization rotates $\frac{\beta_+ - \beta_-}{2}$ radians with unit length in the positive z direction. The sense of the rotation is the same as that of the circularly polarized component with greater phase velocity.

For the lossless medium, the angle of rotation, θ, of the plane of polarization is

$$\theta = \frac{\beta_+ - \beta_-}{2} L = \frac{\omega L}{2c}\left[\left(1 - \frac{q^2}{1-\sigma}\right)^{1/2} - \left(1 - \frac{q^2}{1+\sigma}\right)^{1/2}\right]. \tag{2.10}$$

L is the length of the anisotropic medium.

For q and σ small equation 2.10 is given approximately by

$$\theta \cong -\frac{\omega L}{2c}\sigma q^2 = V_e B_0 L \tag{2.11}$$

where V_e is a Verdet constant for the electron gas. In terms of the electron gas density N

$$\gamma_e = \frac{|e^3|\,N}{2m^2\omega^2}\sqrt{\frac{\mu_0}{\epsilon_0}} \qquad (2.12)$$

If after traversing a unit length of the medium in the positive z direction the linear wave is reflected the plane of polarization of the reflected wave does not return to $\varphi = 0$ at $z = 0$. The anisotropic electron gas is not a reciprocal medium for transmission of uniform linear waves.

Upon reflection the plus and minus wave components of the reflected linear wave are propagating opposite to the direction of positive applied magnetic field. As shown previously, the phase constants of the two waves are interchanged by the apparent magnetic field reversal so that the plane of polarization of the reflected wave is rotated through an additional $\frac{\beta_+ - \beta_-}{2} L$ radians at $z = 0$. The relative angle between the planes of polarization of the incident and reflected linear waves at $z = 0$, is $(\beta_+ - \beta_-)L$ radians or twice the rotation caused by one traversal. Successive traversals and reflections further multiply the amount of rotation.

When plus and minus waves of equal amplitude and phase are excited in the lossy anisotropic medium the resultant wave is linearly polarized only at the point of excitation ($z = 0$). The unequal attenuation of the circular components causes an increasing departure from linearity with propagation of the wave. The field at any point can be expressed as the superposition of a linear and a circular wave. Assuming the minus wave to be attenuated more than the plus wave, equation (2.8) gives

$$E_x = E_o\, e^{-\alpha_- z} \cos \frac{\beta_- - \beta_+}{2} z \quad \cos\left(\omega t - \frac{\beta_- - \beta_+}{2} z\right)$$

$$+ \frac{E_o}{2}\left(e^{-\alpha_+ z} - e^{-\alpha_- z}\right) \cos\left(\omega t - \beta_+ z\right) \qquad (2.13)$$

and

$$E_y = -E_o\, e^{-\alpha_- z} \sin \frac{\beta_- - \beta_+}{2} z \quad \cos\left(\omega t - \frac{\beta_- - \beta_+}{2} z\right)$$

$$- \frac{E_o}{2}\left(e^{-\alpha_+ z} - e^{-\alpha_- z}\right) \sin\left(\omega t - \beta_+ z\right) \quad . \qquad (2.14)$$

The first members on the right half portions of 2.17 and 2.18 yield a linear wave with plane of polarization at $\varphi = \frac{\beta_+ - \beta_-}{2} z$. The second half represents a plus wave.

Equations 2.13 and 2.14 are parametric equations of an ellipse, and the field represented by the pair is said to be elliptically polarized. The major axis of the ellipse occurs at $\varphi = \frac{\beta_+ - \beta_-}{2} z$ and is the plane of polarization of the elliptic wave.

The ratio of the major to the minor axis of the polarization ellipse is called the axial ratio. In terms of the attenuation constants the axial ratio expressed in db is

$$\text{Axial ratio db} = 20 \log_{10} \frac{e^{-\alpha_- z} + e^{-\alpha_+ z}}{e^{-\alpha_- z} - e^{-\alpha_+ z}} \quad .$$

For a linear wave the axial ratio is infinite. A circularly polarized wave in comparison has zero db axial ratio. Frequently the terms axial ratio and ellipticity are used interchangeably.

SECTION III

PROPAGATION IN CIRCULAR WAVEGUIDE

In circular waveguide filled with a homogeneous anisotropic electron gas the characteristic equation yielding the phase constants of the modes of propagation has been given by Suhl and Walker.[16] The two lowest modes are oppositely rotating circularly polarized waves and are neither purely transverse electric or transverse magnetic types. They do reduce to the corresponding TE_{11} circularly polarized modes as the static magnetic field is removed from the gas, and are therefore called TE_{11}-limit waves.

Faraday rotations of linear TE_{11} waves coupled through a length of anisotropic electron gas are related to the phase velocities of the TE_{11}- limit waves propagating within the electron gas.

A. The Field Quantities

In a circular wave guide of radius r_0 and filled with a lossless anisotropic dielectric with dielectric tensor

$$\|\epsilon_e\| = \begin{Vmatrix} \epsilon & -i\eta & 0 \\ i\eta & \epsilon & 0 \\ 0 & 0 & \epsilon_z \end{Vmatrix},$$

the expressions for the field quantities, following Suhl and Walker, are

$$\mathcal{E}_z = \left[\frac{J_m(\chi_1 r)}{J_m(\chi_1 r_0)} - \frac{J_m(\chi_2 r)}{J_m(\chi_2 r_0)} \right] \ell^{im\varphi} , \tag{3.1}$$

$$\mathcal{E}_r = -\frac{i}{\beta'} \left[\frac{1}{r} \frac{J_m(\chi_1 r)}{J_m(\chi_1 r_0)} \frac{1}{\chi_1^2} \left\{ (1-\chi_1^2) F_m(\chi_1 r) + m h_1 \right\} \right. \tag{3.2}$$

$$\left. - \frac{1}{r} \frac{J_m(\chi_2 r)}{J_m(\chi_2 r_0)} \frac{1}{\chi_2^2} \left\{ (1-\chi_2^2) F_m(\chi_2 r) + m h_2 \right\} \right] \ell^{im\varphi} ,$$

$$\mathcal{E}_\varphi = \frac{1}{\beta'} \left[\frac{1}{r} \frac{J_m(\chi_1 r)}{J_m(\chi_1 r_0)} \frac{1}{\chi_1^2} \left\{ h_1 F_m(\chi_1 r) + m(1-\chi_1^2) \right\} \right.$$

$$\left. - \frac{1}{r} \frac{J_m(\chi_2 r)}{J_m(\chi_2 r_0)} \frac{1}{\chi_2^2} \left\{ h_2 F_m(\chi_2 r) + m(1-\chi_2^2) \right\} \right] \ell^{im\varphi} , \tag{3.3}$$

$$\mathcal{H}_z = i\beta' \left[\frac{1}{h_1} \frac{J_m(\chi_1 r)}{J_m(\chi_1 r_0)} - \frac{1}{h_2} \frac{J_m(\chi_2 r)}{J_m(\chi_2 r_0)} \right] e^{im\varphi} , \tag{3.4}$$

$$\mathcal{H}_r = - \left[\frac{1}{r} \frac{J_m(\chi_1 r)}{J_m(\chi_1 r_0)} \frac{1}{\chi_1^2} \left\{ h_1 F_m(\chi_1 r) + m \right\} \right.$$

$$\left. - \frac{1}{r} \frac{J_m(\chi_2 r)}{J_m(\chi_2 r_0)} \frac{1}{\chi_2^2} \left\{ h_2 F_m(\chi_2 r) + m \right\} \right] e^{im\varphi} , \tag{3.5}$$

and $$\mathcal{H}_\varphi = -i \left[\frac{1}{r} \frac{J_m(\chi_1 r)}{J_m(\chi_1 r_0)} \frac{1}{\chi_1^2} \left\{ F_m(\chi_1 r) + m h_1 \right\} \right.$$

$$\left. - \frac{1}{r} \frac{J_m(\chi_2 r)}{J_m(\chi_2 r_0)} \frac{1}{\chi_2^2} \left\{ F_m(\chi_2 r) + m h_2 \right\} \right] e^{im\varphi} . \tag{3.6}$$

In the above expressions $F_m(u) = u J_m'(u) / J_m(u)$ where $J_n(u)$ is a Bessel function of the first kind, order n. $J_n'(u)$ denotes the derivative of $J_n(u)$ with respect to the argument u.

χ_1, χ_2, h_1, and h_2 are parameters which are to be evaluated, and n may take any integral value, positive or negative. The details of the derivation of the field expressions are given in Appendix A.

In the above equations all lengths are measured in units of $1/\beta_z$, where $\beta_z = \omega (\mu_0 \epsilon_0)^{1/2} (1 - q^2)^{1/2}$. The quantity $\mathcal{H}$ is related to the magnetic field intensity H by $\mathcal{H} = (\mu_0/\epsilon_z)^{1/2} H$ and β' is related to β, the phase constant by $\beta' = \beta/\beta_z$.

In the new system, script letters $\mathcal{E}$ and $\mathcal{H}$ are used to denote field quantities, and r, φ, z are distances along the usual cylindrical coordinates r, φ, z measured in the new unit of length. The derivations are made in this system and can be

written in conventional units from the given relations.

For an electron gas with a tensor of dielectric constant having elements as given on page 14 the relations between h_1, h_2 χ_1, χ_2, and β', expressed in terms of σ and q, are from Appendix A:

$$h_1 + h_2 - \sigma h_1 h_2 = \frac{\sigma}{1-q^2} \quad , \tag{3.7}$$

$$\frac{1-\sigma h_1}{1-h_1^2}\left[h_1 F_m\left(\sqrt{\frac{1-h_1^2}{1-\sigma h_1}}\, r_0\right) + m\right] = \frac{1-\sigma h_2}{1-h_2^2}\left[h_2 F_m\left(\sqrt{\frac{1-h_2^2}{1-\sigma h_2}}\, r_0\right) + m\right] \quad , \tag{3.8}$$

$$\chi_{1,2}^2 = \frac{1-h_{1,2}^2}{1-\sigma h_{1,2}} \quad , \tag{3.9}$$

and

$$(\beta')^2 = -h_1 h_2 \quad . \tag{3.10}$$

B Modes of Propagation in the Isotropic Plasma-Filled Waveguide

At $\sigma = 0$, the effective dielectric constant ϵ_e of a uniform lossless electron gas is scalar and has the value $\epsilon_e = \epsilon_o (1 - q^2)$. The possible modes of propagation are thus the usual TE and TM modes in cylindrical wave guide of radius r_o and a dielectric medium of $\epsilon_e = \epsilon_o (1 - q^2)$. At $\sigma = 0$, the phase constants β_o' of the propagating modes will be evaluated for $r_o = 2.055$ and $q = 0.3$.

Setting $\sigma = 0$ in equations 3.7 and 3.8 results in

$h_1 + h_2 = 0$ and (3.11)

$$F_n \left[(1 - h_{1,2}^2)^{\frac{1}{2}} \times 2.055 \right] = 0. \quad (3.12)$$

n will be restricted to values plus and minus unity.

To represent a propagating mode, $(\beta')^2$ must be a positive quantity. From equation 3.10 it is seen that h_1 and h_2 are therefore of opposite sign. h_1 will be chosen to be the positive member of the pair.

The values of h satisfying 3.12 are determined from the roots of $F_n(u)=0$. From usual identities[9] it can be shown that $F_{+1}(u)=F_{-1}(u)$, so that the roots are the same for n= +1 or n= -1. Zeros of $F_{+1}(u)$ occur for $u^2 > 0$, and are the zeros, u_{1m} of $J_1'(u)$. Hence

$$2.055 (1 - h_{1,2}^2) = u_{1m} \text{ where } u_{1m} = 1.841, 5.33, 8.54 \ldots \quad (3.13)$$

Of the roots u_{1m}, only $u_{11}=1.841$ satisfies the conditions that $h_1 > 0$ and $u^2 > 0$. Equation 3.13 then simplifies to $2.055(1-h_1^2)^{\frac{1}{2}} = 1.841$, from which $h_1 = -h_2 = .445$ and $\beta_o' = .445$. These are solutions for both values of n.

Inserting these values of h_1 and h_2 into the field expressions, equations 3.1 through 3.6 results in the solution for propagating modes in the isotropic ($\sigma = 0$) electron gas:

$$E_z = 0,$$

$$E_r = -\frac{n\beta_z}{r k_c^2}\left(\frac{\mu_o}{\epsilon_z}\right)^{1/2} J_n(k_c r)\; e^{i(\omega t - \beta_o z + n\varphi)},$$

$$E_\varphi = -\frac{i\beta_z}{k_c}\left(\frac{\mu_o}{\epsilon_z}\right)^{1/2} J_n'(k_c r)\; e^{i(\omega t - \beta_o z + n\varphi)},$$

$$H_z = J_n(k_c r)\; e^{i(\omega t - \beta_o z + n\varphi)}, \qquad (3.14)$$

$$H_r = -\left(\frac{\epsilon_z}{\mu_o}\right)^{1/2}\frac{\beta_o}{\beta_z} E_z,$$

$$\text{and } H_\varphi = \left(\frac{\epsilon_z}{\mu_o}\right)^{1/2}\frac{\beta_o}{\beta_z} E_r,$$

where $n = \pm 1$ and $k_c^2 = \beta_o^2 - \beta_z^2$.

Equations 3.14 are the field equations of oppositely rotating circularly polarized TE_{11} waves with phase constant $\beta = \beta_o$.[11]

C. Modes of Propagation in the Anisotropic Plasma-Filled Waveguide

1. The Approximate Solution for Small Magnetic Fields

For a small anisotropy, that is σ only slightly different than zero, an expression for the phase constants of the modes can be obtained.

The function $F_{\pm 1}(u)$ satisfies the differential equation[17]

$$u \frac{d F(u)}{du} + \left[F(u)\right]^2 + u^2 - 1 = 0 \qquad (3.15)$$

so that at $\sigma = 0$, when it has been shown $u=u_{11}$ and hence $F_{\pm}(u_{11})= 0$, equation 3.15 reduces to

$$\frac{d F_{\pm 1}(u)}{du} = \frac{1-u_{11}^2}{u_{11}} \qquad (3.16)$$

Approximating $F_{\pm 1}(u)$ by the first term of the Taylor series expansion about $u=u_{11}$ by means of eq. 3.17 results in

$$F_{\pm 1}(u_{11}+\Delta u) = \frac{1-u_{11}^2}{u_{11}} \Delta u + \ldots . \qquad (3.17)$$

at $\sigma = 0$, the solutions to 3.7 and 3.8 will be denoted by $h_1=h_0$, $h_2= -h_0$, and $\beta_0'=h_0$. For a slight change in σ the solution may be written as $h_1=h_0 + \zeta$, $h_2= -h_0 + \xi$ and $(\beta')^2 \cong (\beta_0')^2 - \beta_0'(\xi - \zeta)$ where ξ and ζ are small quantities.

Substituting these values of h_1 and h_2 into $u = \sqrt{\frac{1-h^2}{1-\sigma h}}\, h_0$, the incremental changes $\Delta u = u - u_{11}$, are found to be, for $h=h_1$,

$$(\Delta u)_{h=h_1} = u_{11}\left(\frac{\sigma h_0}{2} - \frac{\zeta h_0}{1-h_0^2}\right) ,$$

and for $h = h_2$,

$$(\Delta u)_{h=h_2} = u_{11}\left(-\frac{\sigma h_0}{2} + \frac{\xi h_0}{1-h_0^2}\right) \quad .$$

Using the expansion given by equation 3.16, the $F_n(u)$ for h_1 and h_2 become

$$F(u_{11}+\Delta u_{h_1}) \cong (1-u_{11}^2)\left[\frac{\sigma h_0}{2} - \frac{\xi h_0}{1-h_0^2}\right]$$

and $$F(u_{11}+\Delta u_{h_2}) \cong (1-u_{11}^2)\left[\frac{-\sigma h_0}{2} + \frac{\xi h_0}{1-h_0^2}\right] \quad .$$

Substituting the approximate expressions for $F_n(h)$, $h_1 = h_0 + \xi$, and $h_2 = -h_0 + \xi$ into equation (3.8) then gives

$$(u_{11}^2-1)\left[(\beta')^2-(\beta_0')^2\right](1+\sigma\beta_0') + 2m\sigma\left[\frac{q^2}{1-q^2} - (\beta')^2 + (\beta_0')^2\right] = 0. \quad (3.18)$$

Differentiating 3.18 with respect to σ and evaluating the differential at $\sigma = 0$,

$$\left.\frac{d\beta'}{d\sigma}\right|_{\sigma=0} = \frac{-mq^2}{\beta_0'(u_{11}^2-1)(1-q^2)} \quad . \quad (3.19)$$

The phase constants of the two waves ($n = \pm 1$) are thus for small σ given by

$$\beta'_{+,-} = \beta_0' + \sigma\frac{d\beta'}{d\sigma} = \beta_0' + \frac{\mp\sigma q^2}{\beta_0'(u_{11}^2-1)(1-q^2)} \quad . \quad (3.20)$$

Equation 3.20 shows the addition of the magnetic field causes a splitting in the propagation constants of the two waves. The initial changes in the phase constants are directly proportional to the applied magnetic field B_0 and of opposite sign for the two waves.

2. The Solution for other than Small Magnetic Fields

For values of σ not in the neighborhood of zero, the phase constants cannot be approximated as in the preceding paragraphs and full solutions to equations 3.7 and 3.8 are required.

Because of the form of equation 3.8, h_1 and h_2 cannot be expressed explicitly in terms of σ, q, n, and λ_0. By assigning numerical values to these quantities, h_1 and h_2 can be evaluated by a graphical procedure.

The graphical analysis was completed for the following set of conditions:

1. Electron density of 3.1×10^{10} electrons per cm^3. ($\frac{\omega_p}{\omega} = .3$ for $\omega = \pi \times 10^{10}$).
2. Waveguide inner diameter 1.62 inches.
3. Signal frequency of 5×10^9 cps., and
4. Applied magnetic field intensities between zero and those required for twice gyro resonance at the given signal frequency ($0 \leq |\sigma| \leq 2$).

For the above values, β_z and λ_0 are

$$\beta_z = \omega (\mu_0 \epsilon_0)^{1/2} (1 - q^2)^{1/2} = .9985$$

and $$\lambda_0 = r_0 \beta_z = 2.055.$$

In the graphical analysis, the phase constants of the two modes of propagation found by the approximate solution for σ only slightly different than zero were extended to larger values of magnetic field. The mode obtained for n equal plus or minus one will be referred to as the plus or minus TE_{11}- limit wave.

To illustrate the method of graphical analysis, the field expressions of the plus wave for $\sigma = .2$ will be obtained.

For $\sigma = .2$ and $n = +1$, equations 3.7 and 3.8 are

$$h_1 + h_2 - .2\, h_1\, h_2 = .2/.91. \tag{3.21}$$

and

$$\frac{1-.2\,h_1}{1-h_1^2}\left[h_1 F_1\left(\sqrt{\frac{1-h_1^2}{1-.2\,h_1}}\, 2.055\right) + 1\right] = \frac{1-.2\,h_2}{1-h_2^2}\left[h_2 F_1\left(\sqrt{\frac{1-h_2^2}{1-.2\,h_2}}\, 2.055\right) + 1\right] . \tag{3.22}$$

$F_{+1}(u)$ is shown in Fig. 6 as a function of u^2.

Denoting the expression on either side of equation 3.22 by $G_n(h)$ equation 3.22 may be written simply as $G_{+1}(h_1)=G_{+1}(h_2)$, which is to be evaluated for $\sigma = .2$ and $\lambda_o = 2.055$.

Figure 7 shows $G_{+1}(h)$ evaluated as a function of h for these values of σ and λ_o .

As shown in the $G_{+1}(h)$ plot, horizontal lines of $G_{+1}(h)$= constant are constructed and intersect the curve at equal values of $G_{+1}(h)$. Each pair of h determined from the intersections is a solution to $G_{+1}(h_1)=G_{+1}(h_2)$.

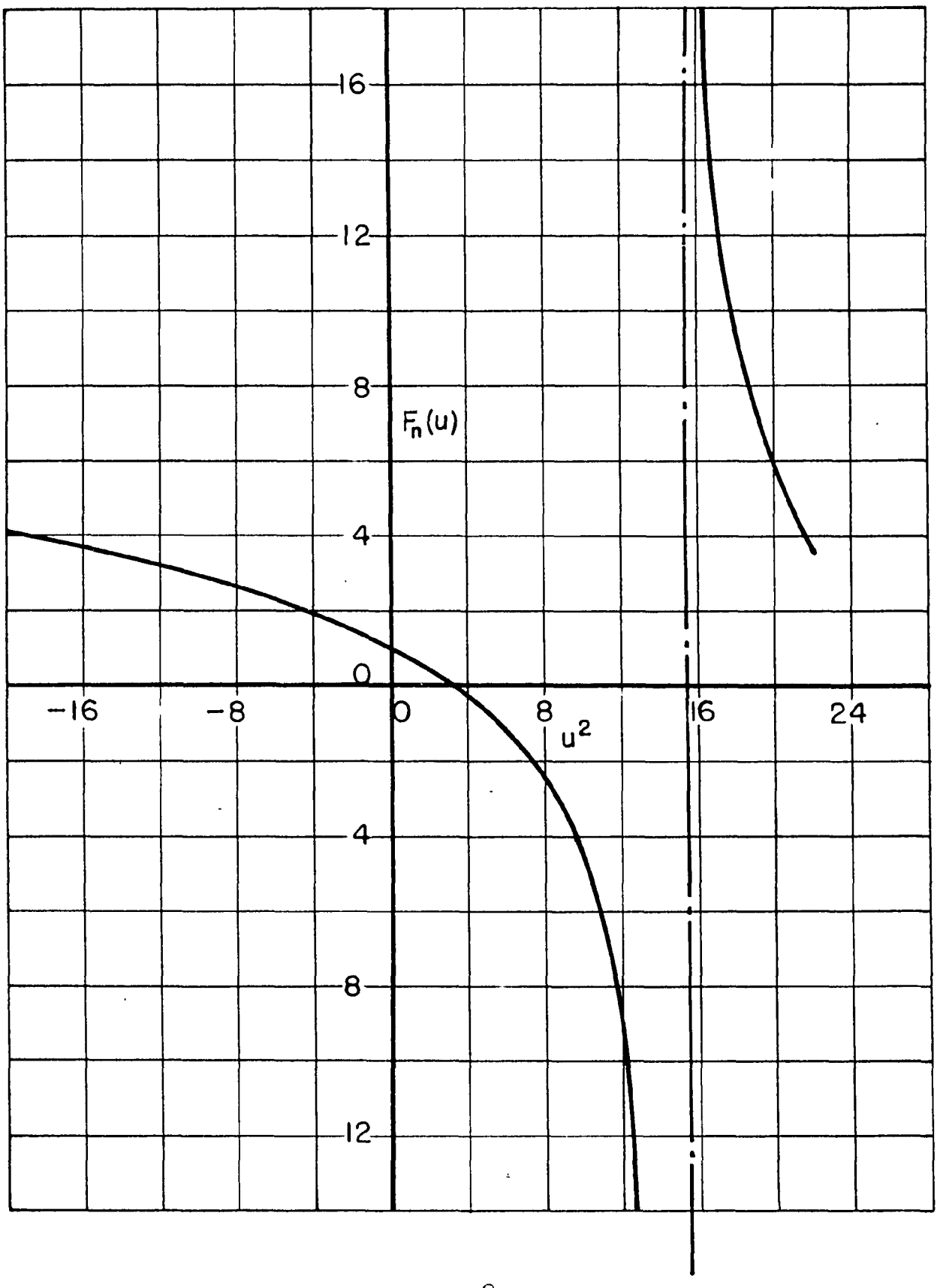

Figure 6. $F_n(u)$ versus u^2 for $n = \pm 1$

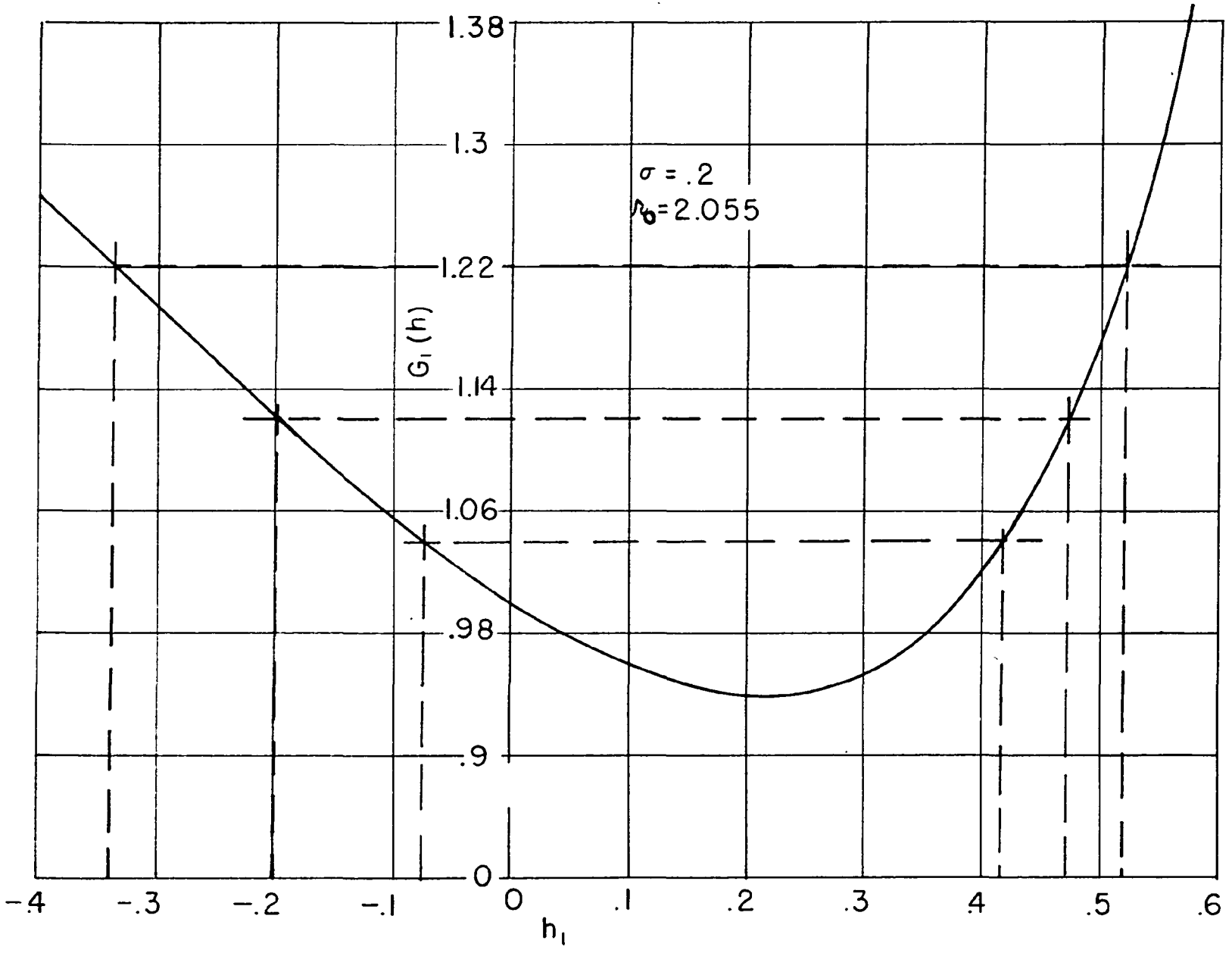

Figure 7. Graphical Solution of $G_1(h_1) = G_1(h_2)$

After obtaining many pairs of h_1, h_2 from the $G_{+1}(h)$ plot, values of $(\beta')^2 = -h_1 h_2$ computed from each pair are plotted as a function of h_1. The curve obtained from these values is shown in Fig. 8. On the same coordinates $(\beta')^2$ vs h_1 is also presented, as obtained from equation (3.21).

The intersection of the two curves of Fig. 8 occurs for $(\beta')^2$ and h_1 which satisfy simultaneously equations 3.21 and 3.22. For this particular case h_1 and $(\beta')^2$ were found to have the values $h_1 = .5208$ and $(\beta')^2 = .1750$. The remaining quantities necessary to completely evaluate the field expressions are obtained from equations 3.9 and 3.10 and are $h_2 = -0.3359$, $\chi_1 = .902$, and $\chi_2 = .912$.

In similar manner, solutions were obtained for sufficient number of values of σ to construct curves of β_- and β_+ for constant q and Λ_0.

The magnetic field in the preceding example was assumed to be applied in the negative z direction. To obtain solutions for $n = \pm 1$ for magnetic fields in the positive z direction, it is not necessary to repeat the graphical analysis. Solutions for negative magnetic fields can be related directly to those for positive fields by considering equations 3.7 and 3.8.

If $h_1 = a$, $h_2 = -b$ are the solutions of 3.11 and 3.12 obtained graphically for $\sigma = \sigma_0$ and $n = \pm 1$, direct substitution of $h_1 = b$, $h_2 = -a$ into equations 3.7 and 3.8 shows that these values are solutions for $\sigma = -\sigma_0$ and $n = \mp 1$. Therefore, reversal of the magnetic field interchanges the phase constants and field expressions of the plus and minus waves.

Fig. 9 shows curves of β_- and β_+ versus σ for static

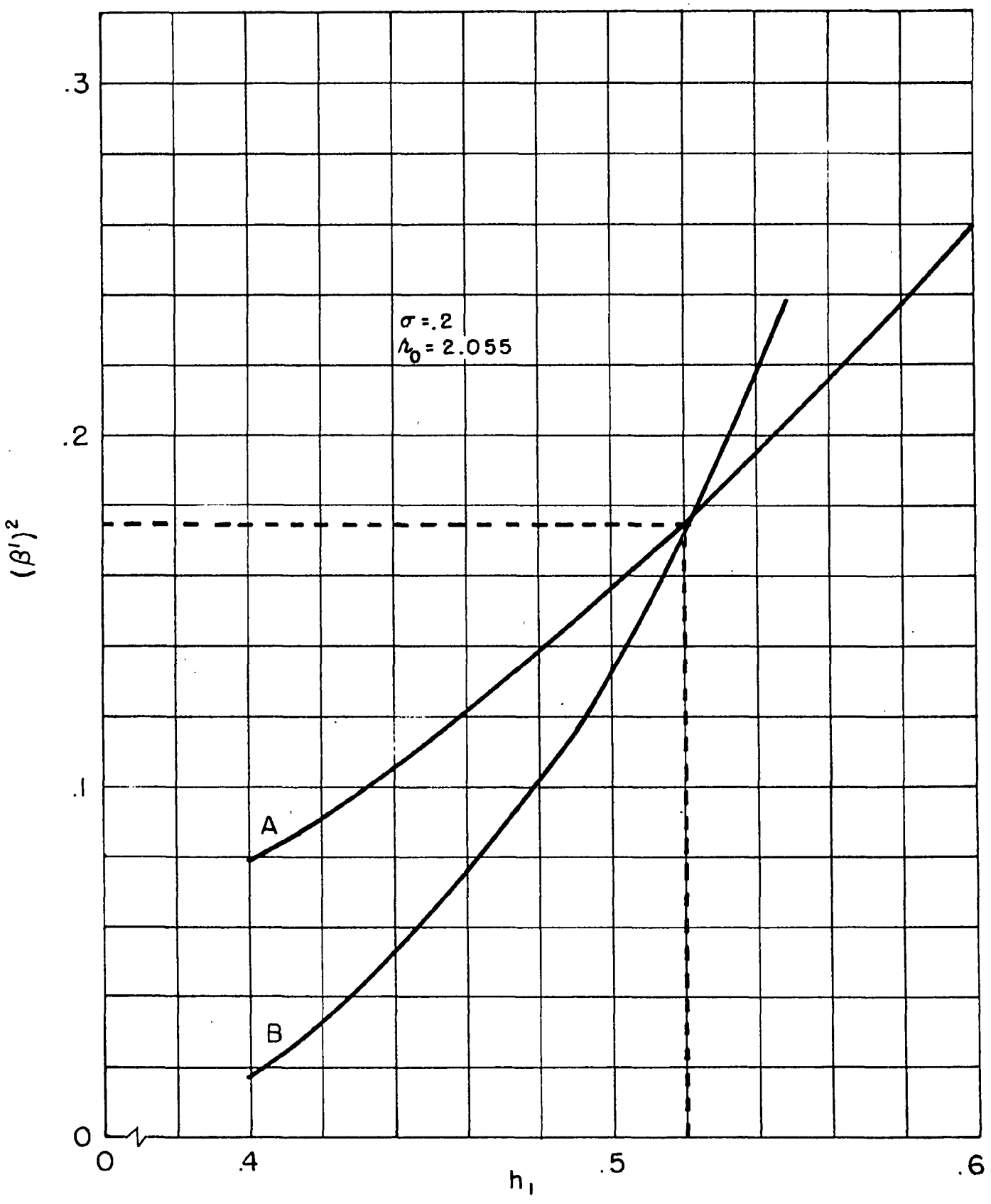

Figure 8. $(\beta')^2$ versus h_1

A. Equation 3.21
B. Solution of Equation 3.22

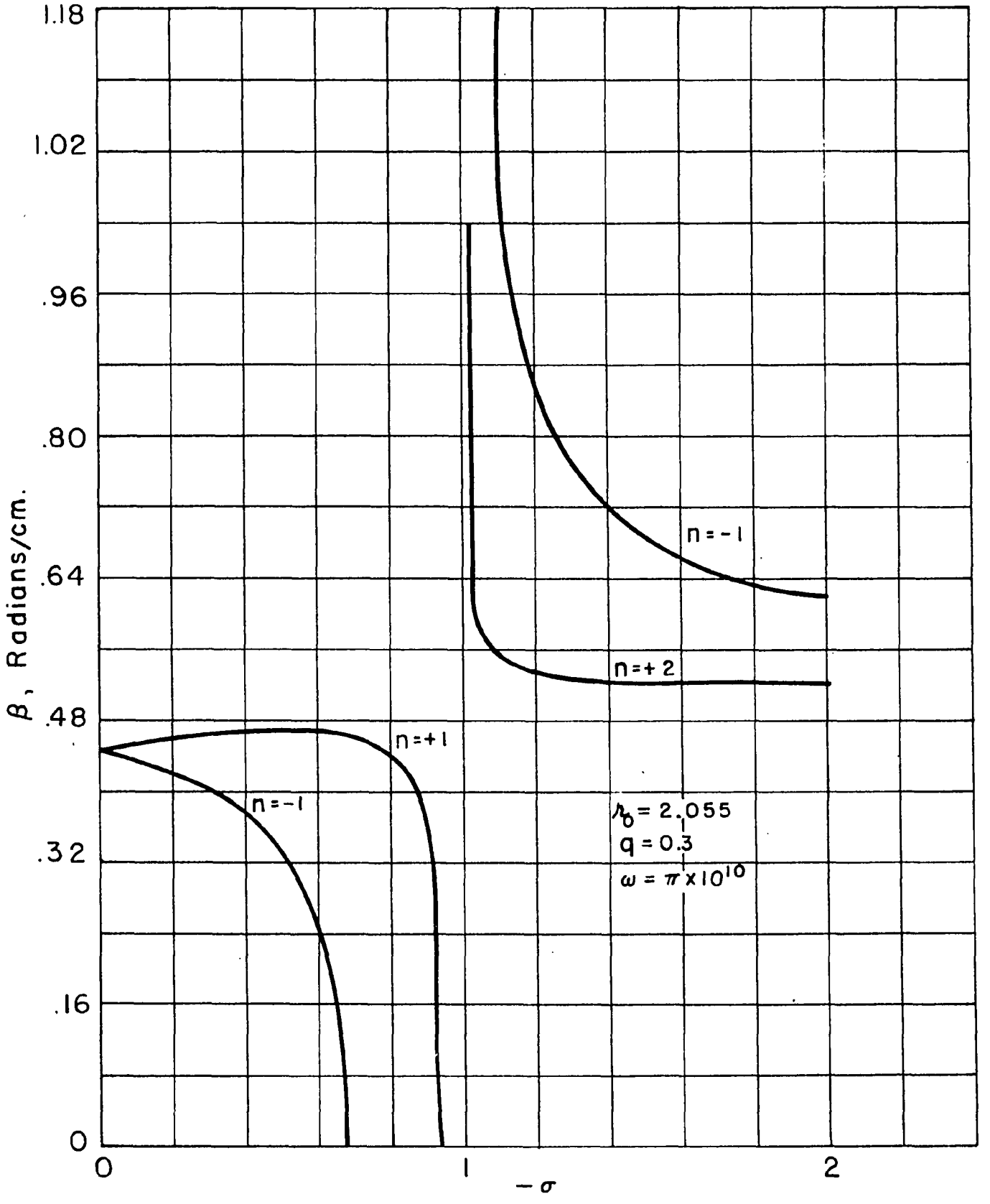

Figure 9. Phase Constants of the TE_{11} Limit Waves.

applied magnetic fields directed in the positive Z sense. Values of q and λ_0 are $q = 0.3$ and $\lambda_0 = 2.055$. Except for the region in the neighborhood of $-\sigma = 1$, the phase constants of the wave guide modes behave very much like those of plus and minus uniform waves in the unbounded medium. The major difference is the resonant dispersion of the guided plus wave.

Both the $n = -1$ and $n = +1$ waves exhibit cut-off at magnetic fields less than required for gyroresonance ($-\sigma = +1$). The values of $-\sigma$ at cut-off of the TE_{11}- limit waves are determined from equations 3.7 and 3.8 by setting $(\beta')^2 = h_1 h_2 = 0$. Since one of the h must also become zero at cutoff, the other satisfies

$$h = \frac{\sigma}{1 - q^2} \tag{3.23}$$

and

$$G_m(h) = m \quad . \tag{3.24}$$

Solving 3.23 and 3.24 for a magnetic field in the positive direction. the cutoffs were found to occur at $-\sigma = .665$ for the minus wave and $-\sigma = .93$ for the plus wave.

3. The Electric Field Components

Although the electric field components of the TE_{11}- limit waves change with the value of the applied static magnetic field, they remain similar to those of the "isotropic" ($\sigma \approx 0$) TE_{11} waves. The greatest deviation is to be expected to occur for magnetic fields in the region of electron gyroresonance.

Fig. 10 shows the magnitude of the electric field components of the minus TE_{11} limit wave at $-\sigma = .5$ and $-\sigma = 1.2$. The distribution of the isotropic field quantities are included for comparison. Values of $\mathcal{E}_r$ and $\mathcal{E}_\varphi$ for $-\sigma < .5$ and $-\sigma > 1.2$ lie between. In general as $-\sigma$ approaches unity from larger values, the field becomes more uniform within the guide cross-section. The differences between the TE_{11}- limit wave and the isotropic TE wave transverse electric fields are not great for magnetic fields below resonance.

The relative magnitude of $\mathcal{E}_z$, a component which does not exist for the TE_{11} wave, is given in Fig. 11. For $-\sigma < 1$, the maximum intensity of $\mathcal{E}_z$ is less than one percent of that of the other electric field components. Above $-\sigma = 1$, its magnitude is somewhat greater. From equation 3.1 it is seen that $\mathcal{E}_z$ is zero at the center of the guide ($r = 0$) and at the guide wall ($r = r_a$). The maximum value, for the cases computed, occurs for a distance from the guide center just greater than half the radius.

The polarization of the transverse electric field within the waveguide is established from equations 3.2 and 3.3. At $r = 0$, division of 3.2 and 3.3 results in

$$\left(\frac{\mathcal{E}_r}{\mathcal{E}_\varphi}\right)_{+,-} = \mp i \quad .$$

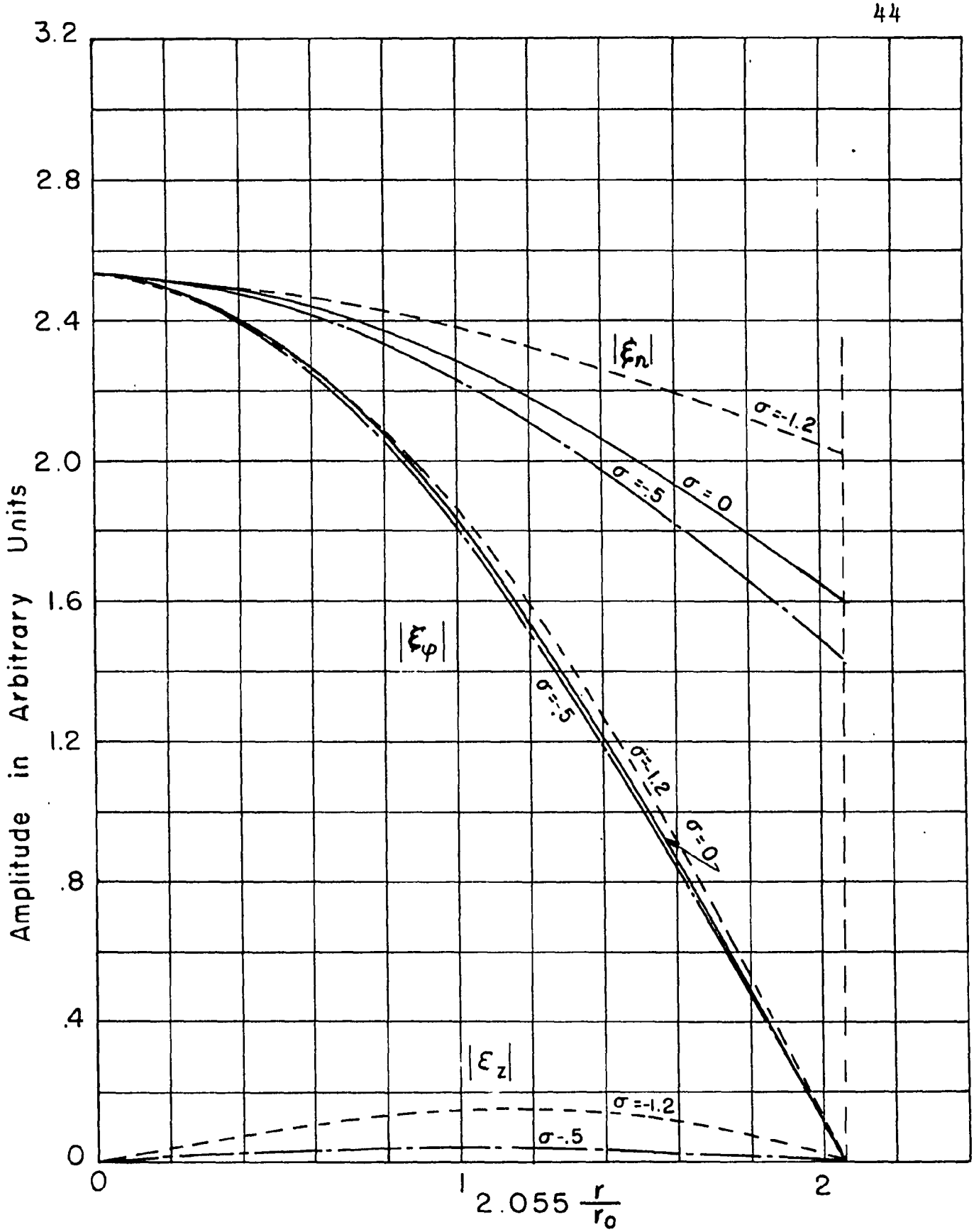

Figure 10. Radial Distribution of the Electric Field Components of the Minus TE_{11} Limit Wave
r_o= waveguide radius

Therefore the transverse electric fields of the plus and minus limit waves are oppositely circularly polarized at the center of the guide. The polarization of the transverse field at other values of r is obtained from $\mathcal{E}_r$ and $\mathcal{E}_\varphi$ evaluated for specific values of q, σ, and r_0.

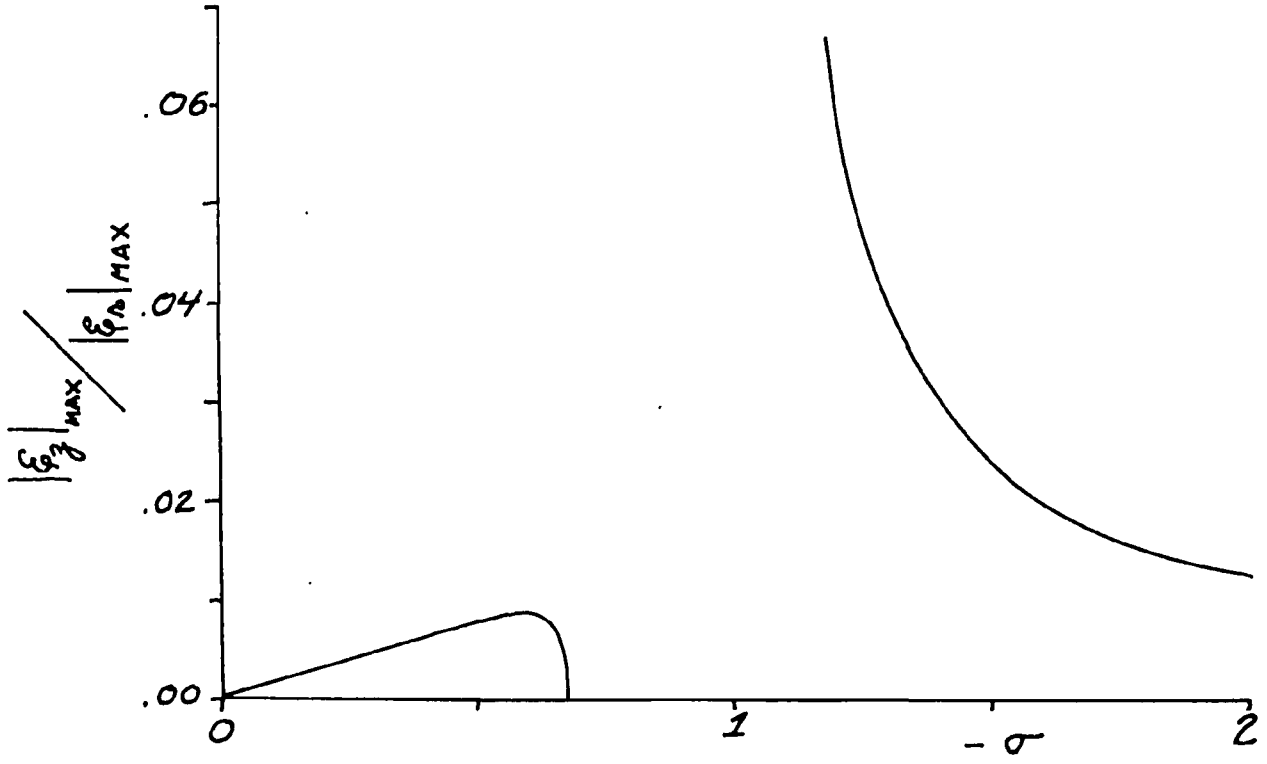

Figure 11. Relative Magnitude of the Maximum Value of $\mathcal{E}_\varphi$ of the Minus Wave $q = 0.3$, $\omega = \pi \times 10^{10}$, $r_0 = 2.055$

D. Faraday Rotation of TE_{11} Waves

To relate the Faraday rotation of linear TE_{11} waves in cylindrical guide to the plus and minus waves described in the preceding sections a short description of the TE_{11} waves and the method of obtaining the rotation is necessary.

The linearly polarized TE_{11} mode, which is the lowest mode of propagation in cylindrical guide, has a transverse electric field pattern as shown in Fig. 12.

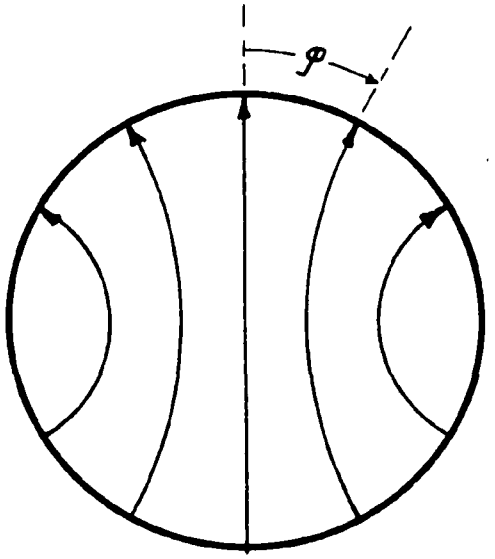

Figure 12. Transverse Electric Field Pattern of the Linear TE_{11} Wave in Cylindrical Waveguide

The radial electric field at the periphery of the guide wall is sufficient to identify TE_{11} waves, and for the linear wave has the form $E_r = A \cos\varphi \exp i(\omega t - \beta z)$. The position of maximum radial field is taken as the plane of polarization. For instance the wave as sketched in Fig. 12 has radial electric field variation $E_r = A \cos\varphi$, so that the plane of polarization is given by $\varphi = 0$.

The linear TE_{11} wave may be expressed as the sum of two equal amplitude circularly polarized TE_{11} waves of opposite senses of rotation. The circularly polarized TE_{11} waves have transverse electric field patterns identical to the linearly polarized wave, but the patterns as a whole rotate about the axis of the waveguide in either sense. The peripheral field of the linear wave in terms of the circular waves is given by

$$E_r = A \cos\varphi \; e^{i\omega t} = \frac{A}{2} e^{i(\omega t - \beta z + \varphi)} + \frac{A}{2} e^{i(\omega t - \beta z - \varphi)} . \qquad (3.25)$$

A TE_{11} wave with variation $\exp i(\omega t - \beta z + \varphi)$ is called a plus TE_{11} wave; that with variation as $\exp i(\omega t - \beta z - \varphi)$, a minus TE_{11} wave.

The sense of rotation of the plus and minus TE_{11} waves is the same as the plus and minus uniform waves in the unbounded medium described in Section II.

The polarization of the electric fields are not the same, however. While for the infinite medium, the plus and minus waves have plus and minus circular polarization of the electric field at every point, the plus and minus TE_{11} and TE_{11}- limit waves have plus and minus circular polarization of the electric field only at the center of the waveguide. The db axial ratio of the electric field polarization across the wave guide radius is shown in Fig. 13. The polarization at the waveguide wall is linear since boundary conditions require $E_\varphi = 0$ for $r = r_o$.

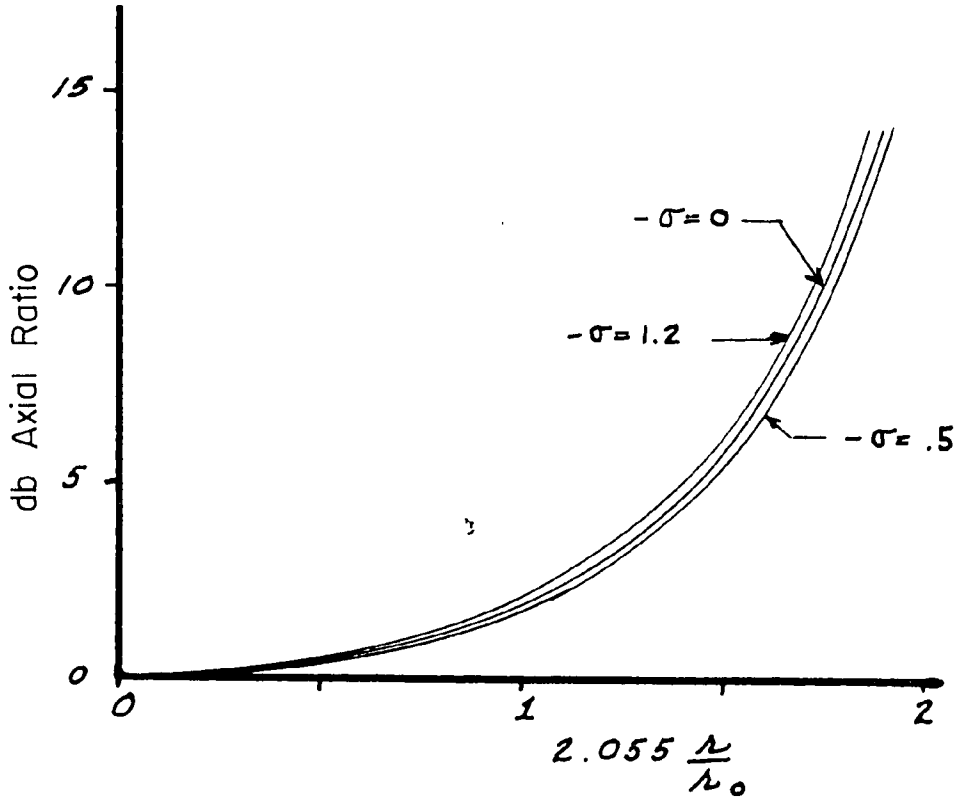

Figure 13. Polarization of the transverse electric field of the minus TE_{11} - limit wave as a function of r, the distance from the waveguide axis. (r_0 is the waveguide radius).

In waveguide filled with isotropic dielectric, the TE_{11} circularly polarized waves propagate with identical attenuation and phase constants. If however, differing phase shifts and attenuation are introduced in the propagation, the result is no longer the initially linearly polarized TE_{11} wave. The linear wave of equation 3.25, after relative phase shifts and attenuations of the circular components, would have radial field of the form

$$E_r = A\, e^{i(\omega t - \beta z - \Phi_+ + \varphi)} + B\, e^{i(\omega t - \beta z - \Phi_- - \varphi)} \quad . \quad (3.26)$$

If unequal attenuation of the two components occurs, the radial field is no longer zero for any value of φ, but does have maximum and minimum values, which are 90 degrees apart. The ratio of the larger to the smaller radial field is called the axial ratio of the elliptic TE_{11} wave. In terms of the amplitudes A and B of the circular components,

$$\text{db axial ratio} = 20 \log \frac{A + B}{A - B} ,$$

where $A > B$.

The plane of maximum radial electric field defines the plane of polarization of the elliptic wave, and for the wave described by equation 3.23 is given by

$$\theta = \frac{\Phi_+ - \Phi_-}{2}$$

To produce Faraday rotation of guided TE_{11} linear waves, unequal phase shifts of the two components of opposite circular polarization are introduced in propagation through a portion of the waveguide filled with the anisotropic electron gas medium (region b, Fig. 14).

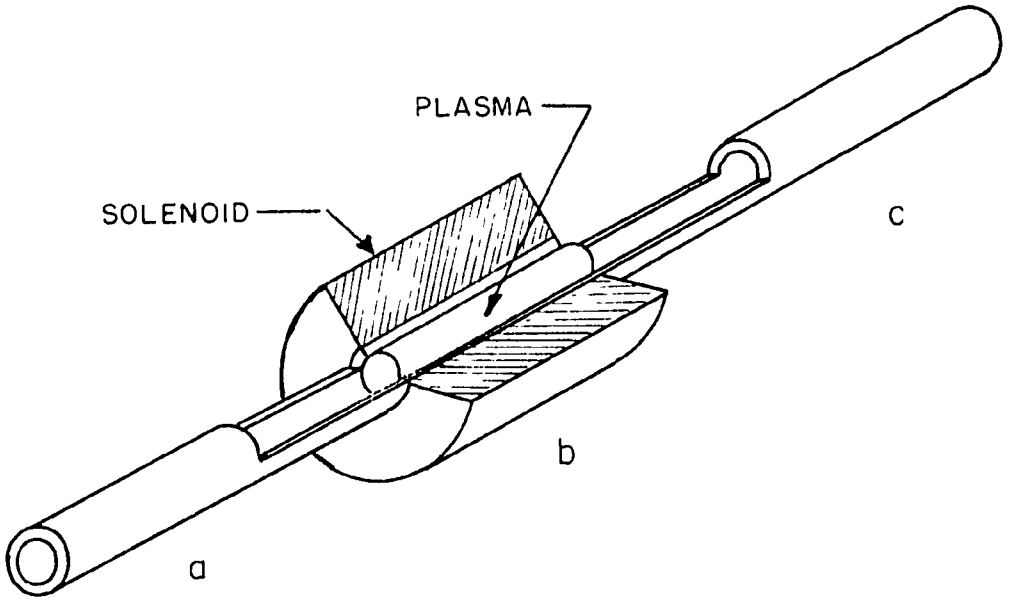

Figure 14. Cutaway View of the Circular Waveguide Containing a Discharge Plasma

An incident linear wave propagates in arm "a" with unchanged polarization. At the interface between a and b, the incident linear wave excites waves within the anisotropic electron gas filled section. These waves in turn excite, at the interface between b and c, TE_{11} waves which form the transmitted wave.

As long as the discontinuity between interfaces is small, which will be the case for small anisotropies and small electron densities, each circularly polarized component of the incident TE_{11} wave will couple only to its corresponding TE_{11}- limit wave within the anisotropic region and, after propagation through the electron gas the limit waves excite only the corresponding circularly polarized TE_{11} waves. A phase shift between the components of the transmitted wave has thus been introduced, and is directly obtained from the difference in phase of these TE_{11} limit

waves.

This phase difference is given by $(\beta_+ - \beta_-)$ L, where L is the length of region b, and the plane of polarization of the resultant transmitted wave has been rotated by an angle $\theta = \frac{\beta_+ - \beta_-}{2}$ L radians. From equation 3.20, we obtain

$$\frac{\beta_+' - \beta_-'}{2} = \frac{-\sigma q^2}{\beta_0' (u_{11}^2 - 1)(1 - q^2)} \quad , \qquad (3.27)$$

which is the expression for angle of rotation per unit length of the plasma filled guide, for σ and q small. Writing 3.27 in terms of a Verdet constant V, where θ = VBL results in

$$V = \sqrt{\frac{\mu_0}{\epsilon_0}} \frac{|e^3| N}{f^2 m^2} \frac{\lambda q_0}{\lambda_a 4\pi^2 (u_{11}^2 - 1)} \quad . \qquad (3.28)$$

For larger magnetic fields, the transverse field patterns of TE_{11} and TE_{11}- limit waves become increasingly different. In addition, the TE_{11}- limit waves acquire a longitudinal component of electric field. Under these conditions, a circular TE_{11} wave can no longer be assumed as exciting only its corresponding TE_{11}- limit wave at the air anisotropic dielectric interface, since the presence of other modes is required to match the fields at the boundary. This presents a very formidable analytical problem, particularly when two such interfaces must be considered. The description of the fields at the interface may be of general interest, but in view of the correlation of experimental results with calculations which neglect the discontinuities at the interfaces, this was not attempted.

The quantity $\frac{\beta_+ - \beta_-}{2}$, which is proportional to the angle of rotation of the transmitted TE_{11} wave (neglecting interface effects) is shown in Fig. 15.

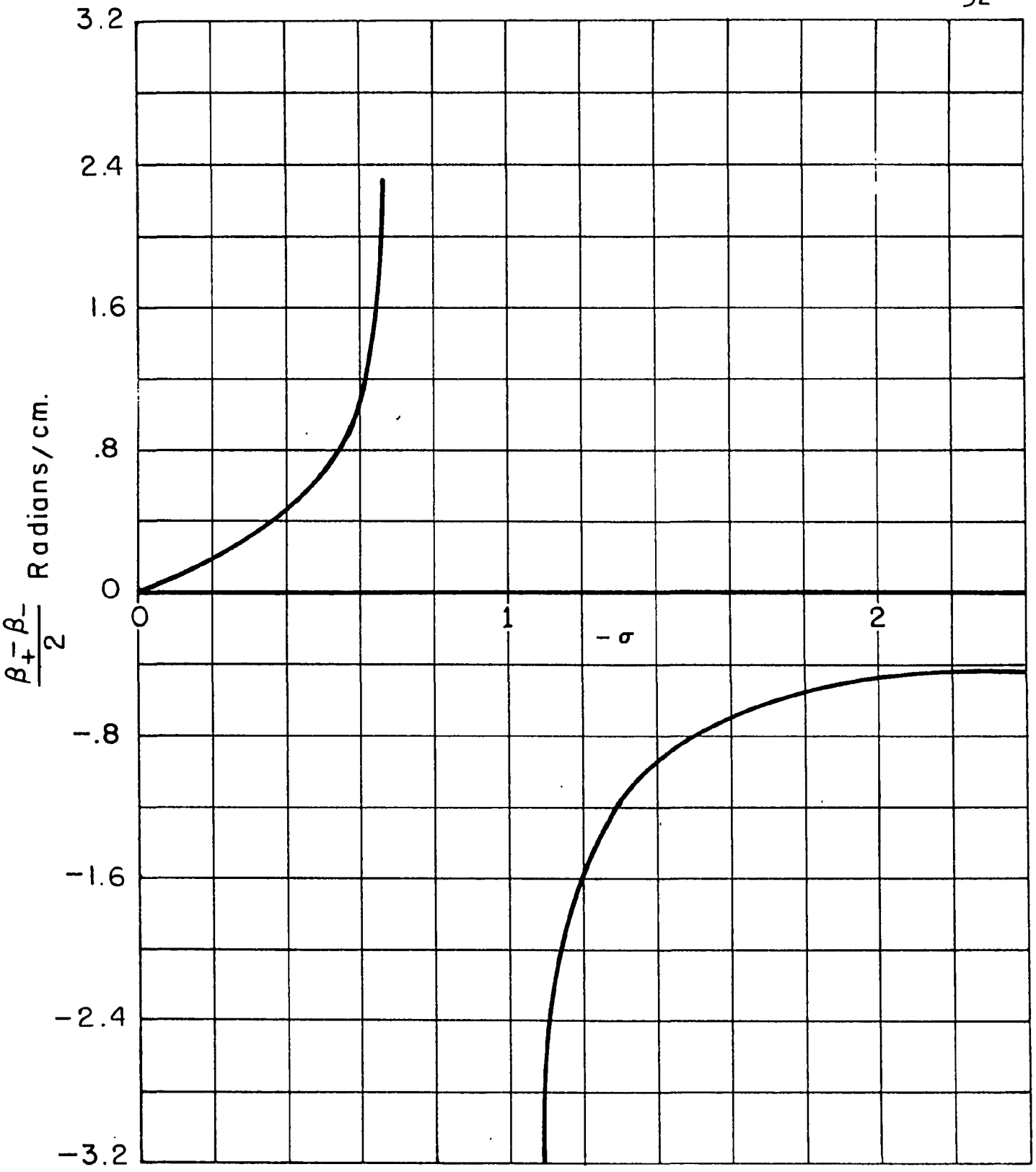

Figure 15. Difference in Phase Constants of the TE_{11} Limit Waves

SECTION IV

THE APPARATUS AND DISCHARGE OPERATION

A. Description of the Apparatus

The apparatus which was used to measure the Faraday rotation and the phase and insertion loss of waves propagated through the anisotropic gaseous discharge plasmas is shown in Fig. 16. The photograph shows the waveguide circuits the solenoid which provided the magnetic field, and a portion of the vacuum system. The discharge tube located in the waveguide section within the solenoid core is not visible.

1. The Waveguide Circuit

The waveguide circuit served the purposes of launching known polarizations of the TE_{11} wave in the cylindrical waveguide containing the electron gas, and determining the relative amplitude, phase, and polarization of the TE_{11} wave coupled through the elec tron gas. A schematic diagram is given in Fig. 17.

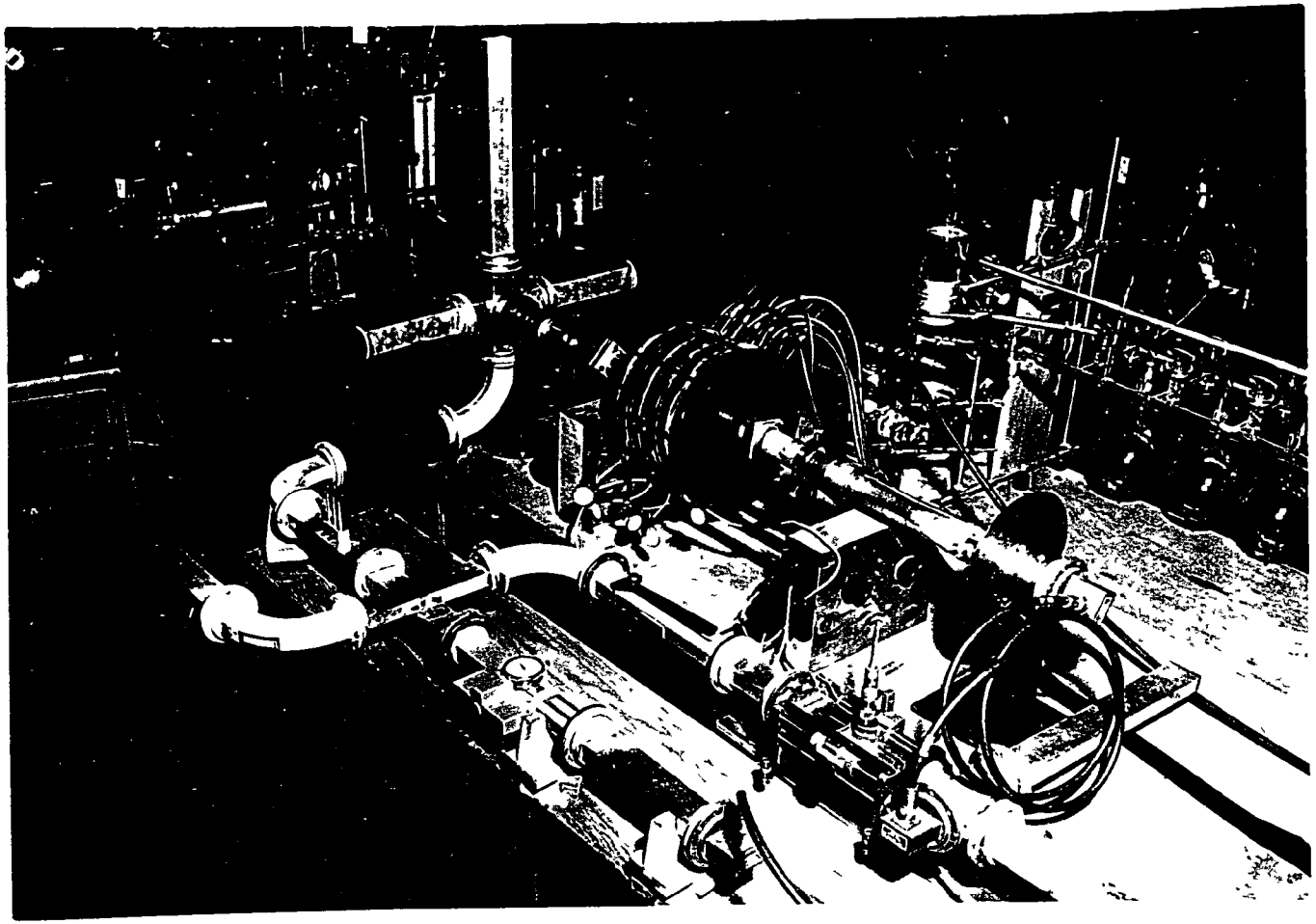

Figure 16. Photograph of Apparatus

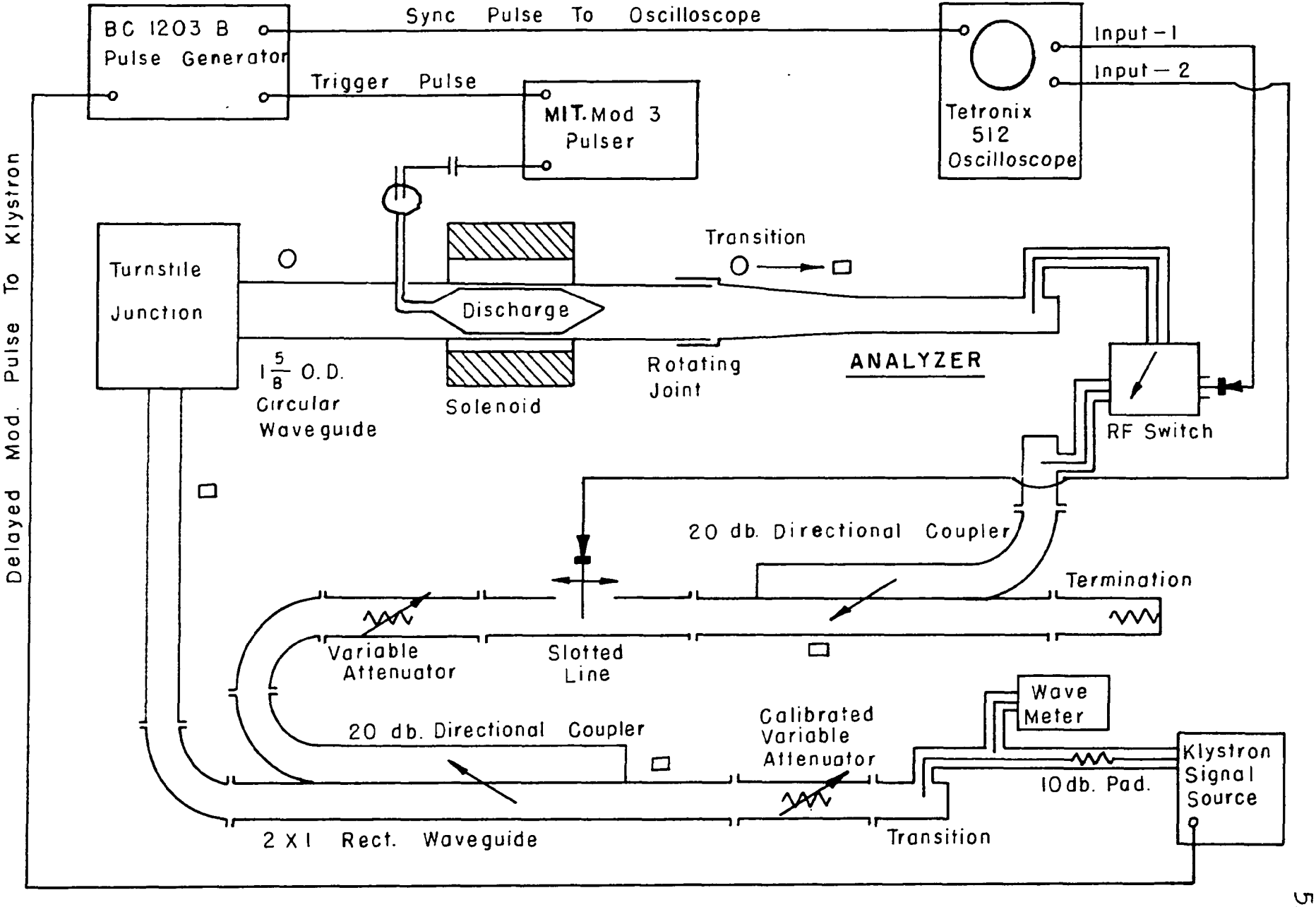

Figure 17. Schematic Diagram of the Apparatus

The microwave signal source, a Sperry type 2k43 reflex klystron, was capable of delivering approximately 250 milliwatts in the frequency range between 4200 and 5700 mc. The signal from the klystron was fed by coaxial cable to the rectangular waveguide input, shown in the lower center of the photograph, Fig. 16. A wavemeter and a 10 db fixed attenuator pad inserted in the coaxial feed are not visible. Following the waveguide input was a calibrated attenuator with dial indicator, and a directional coupler, which delivered a reference signal to the left arm of the phase bridge. The phase bridge circuit is identified in the photograph as that rectangular waveguide section containing the traveling probe.

Beyond the coupler, a 90 degree curve and a twist section joined the waveguide to the bottom arm of a turnstile junction, which was connected to the cylindrical waveguide passing through the solenoid. As shown on the left side of the photograph of Fig. 16, a turnstile is essentially a symmetrical junction of one cylindrical and four rectangular waveguides. A complete description of turnstile properties is given by Montgomery, Dieke, and Purcell.[11]

The rectangular arms of the junction were operated in the TE_{10} mode. By feeding the bottom arm and adjusting the positions of shorts in the two side arms, any configuration of TE_{11} waves could be excited in the cylindrical waveguide. The TE_{11} wave launched by the turnstile will be referred to as the "incident" TE_{11} wave.

The discharge tube was located in the cylindrical waveguide in the core of the solenoid. To the right of the solenoid, the cylindrical guide joined to the "wave analyzer".

The wave analyzer decomposed the wave coupled through the discharge (designated the "transmitted" wave) into linear TE_{11} waves of orthogonal planes of polarization. This was accomplished by a cylindrical to rectangular waveguide transition. Only the linearly polarized component of the transmitted wave with plane of polarization identical to that of the rectangular guide was transformed into the rectangular waveguide TE_{10} mode. The other linear TE_{11} component at orthogonal polarization was attenuated to a negligible amplitude by a resistance pad within the analyzer.

Rotating the analyzer to positions of polarization coinciding with the major or the minor axis of the transmitted wave resulted in a maximum or a minimum of signal amplitude transformed to the rectangular waveguide. The signal amplitudes were determined from the response of a crystal detector. The plane of polarization of the analyzer in these positions was read from an angularly calibrated disc scale, the back of which is visible in the photograph. The smallest subdivision of the scale corresponded to one half degree of rotation.

In addition to the crystal detector, the wave coupled to the analyzer could also be referred to the phase bridge by coaxial cable and a directional coupler. This is shown in the lower right of Fig. 16.

The phase bridge was used to determine changes in phase between the reference signal from the turnstile feed arm and the signal delivered to the analyzer. The operation of waveguide

phase bridges has been described by Samuel and Crandell.[14] The oppositely propagating signals formed a standing wave in the rectangular waveguide. The position of the minimum of the standwave pattern as determined from the traveling probe amplitude response indicated phase balance of the bridge. A shift of phase of $\Delta\Theta$ degrees of the analyzer signal from an initial balance phase caused the position of the standing wave minimum to shift a distance Δs given by

$$\Delta S = \frac{\Delta\Theta}{720}\ \lambda_g \qquad (4.1)$$

where λ_g is the wavelength in the bridge waveguide. A delay or advance in the phase of the analyzer signal shifted the balance position toward or away from the reference signal input. The position of the bridge probe was measurable within .1 mm.

2. The Solenoid

It was decided to investigate propagation through the electron gas for applied magnetic field strengths up to twice that required for electron gyroresonance at a frequency of 5×10^9 cps. This required a maximum field strength of about 3500 Oersteds throughout the volume of the discharge.

The solenoid used in the experiments can be seen in the center of Fig. 16. The solenoid consisted of five component coils separated by jackets for water cooling. Water cooling was necessary to prevent overheating when operating at maximum current. Approximately five kilowatts was dissipated in the coils at the maximum coil current of 25 amperes.

Soft iron flanges were provided on each end of the solenoid to help provide a uniform magnetic field intensity over greater axial lengths than would a simple solenoid. The distribution of the axial field intensity, and the position of the discharge tube within the field are shown in Fig. 18. The effective cylindrical portion of the discharge tube was situated in that region of the solenoid core measured as having a field uniform within 2 percent. The maximum axial magnetic field intensity H_{max} in oersteds was related to the solenoid current I in amperes by $H_{max} = 150\ I$. This calibration was accurate to within 2%.

The direct current supply was a motor-generator set, whose output voltage was adjusted by variation of the generator field excitation.

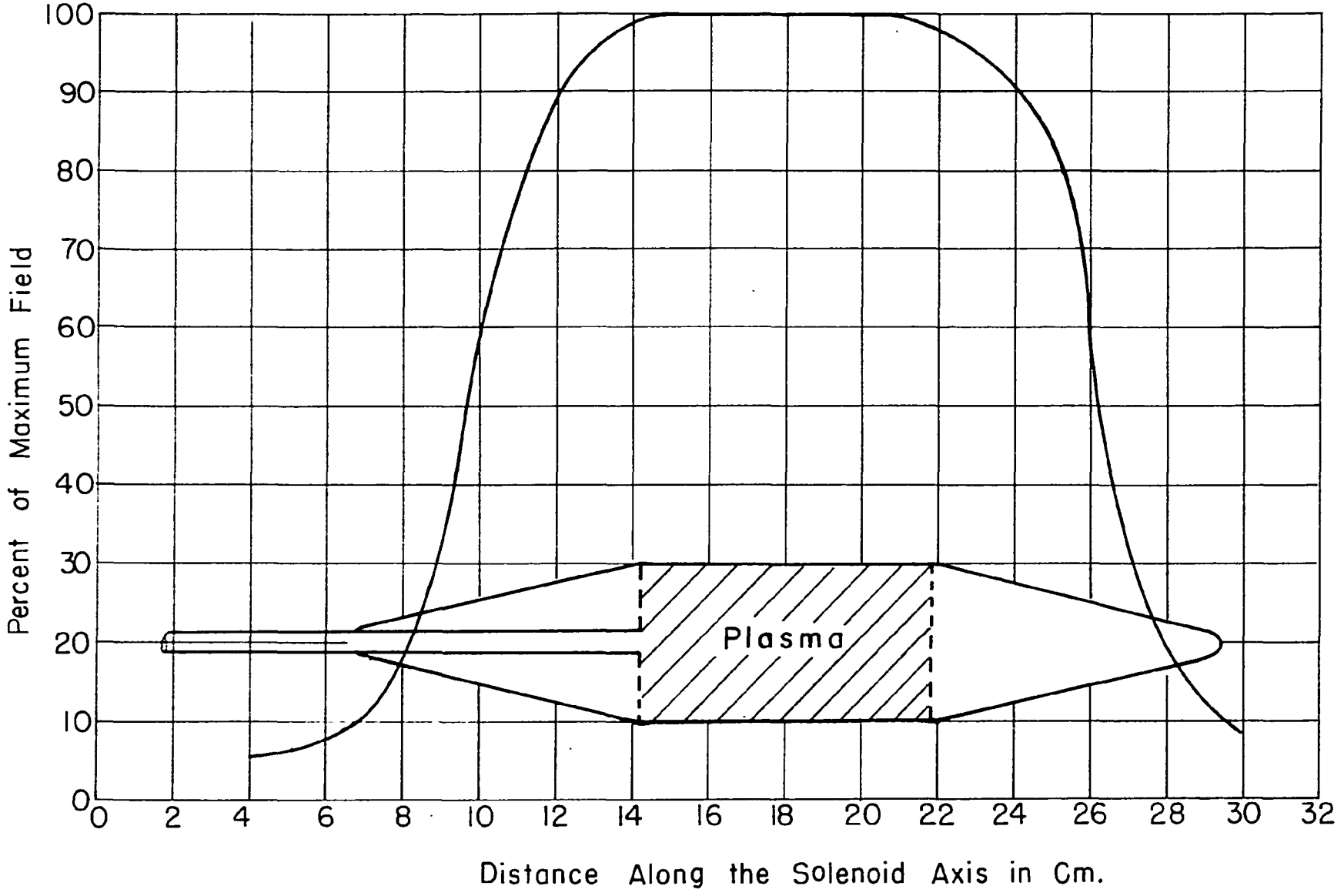

Figure 18. Position of the Discharge Plasma with Respect to the Axial Magnetic Field Intensity.

3. The Discharge Tube and Vacuum System

There were two important factors to be considered in the design of the discharge tube. First, the tube when inserted in the waveguide should introduce little or no discontinuity to wave propagation. If small reflections do occur, they should be independent of the polarization of the propagating waves. In other words, the discontinuity should not cause the excitation of a propagating mode of differing polarization. The second factor to be considered was the geometry of the region in which the discharge is created. The electron density in this region should be nearly uniform throughout a volume with well defined length in order to attempt correlation between the experimental results and those calculated.

The discharge tube shown in Fig. 19 was designed with these factors in mind and was used in the final experiments. The details of the construction and the position of the tube in the waveguide are given in Fig. 20. The cross-section of the central portion of the tube nearly filled the cross-section of the waveguide, and the ends were tapered to reduce reflection of microwaves from the glass. Mica inserts were located at the beginning of the tapers to prevent diffusion of the electron gas into the tapered end sections. The cylinder formed by the glass wall and the mica inserts thus provides a constant volume of the discharge.

The anode, in the form of a circular platinum wire ring of largest possible diameter inside the discharge tube, was electrically grounded to the waveguide by a fine wire connection brought through the glass wall of the tube and through a small

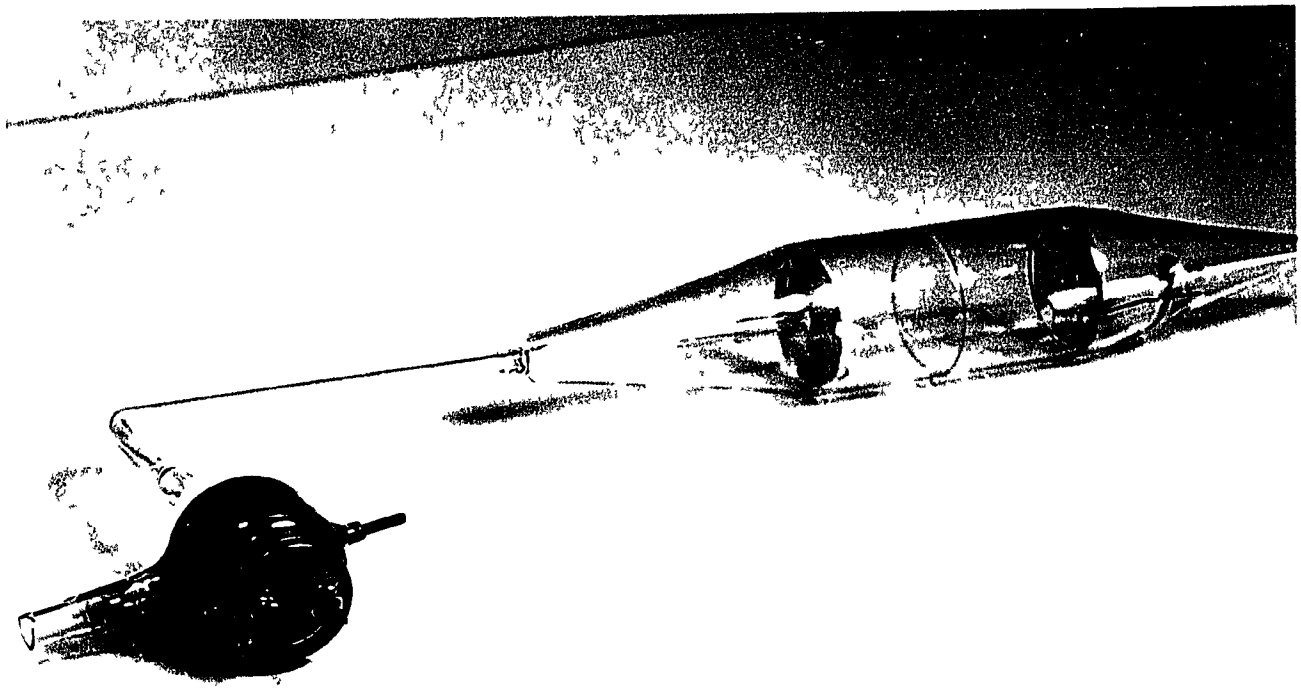

Figure 19. Photograph of
Discharge Tube.

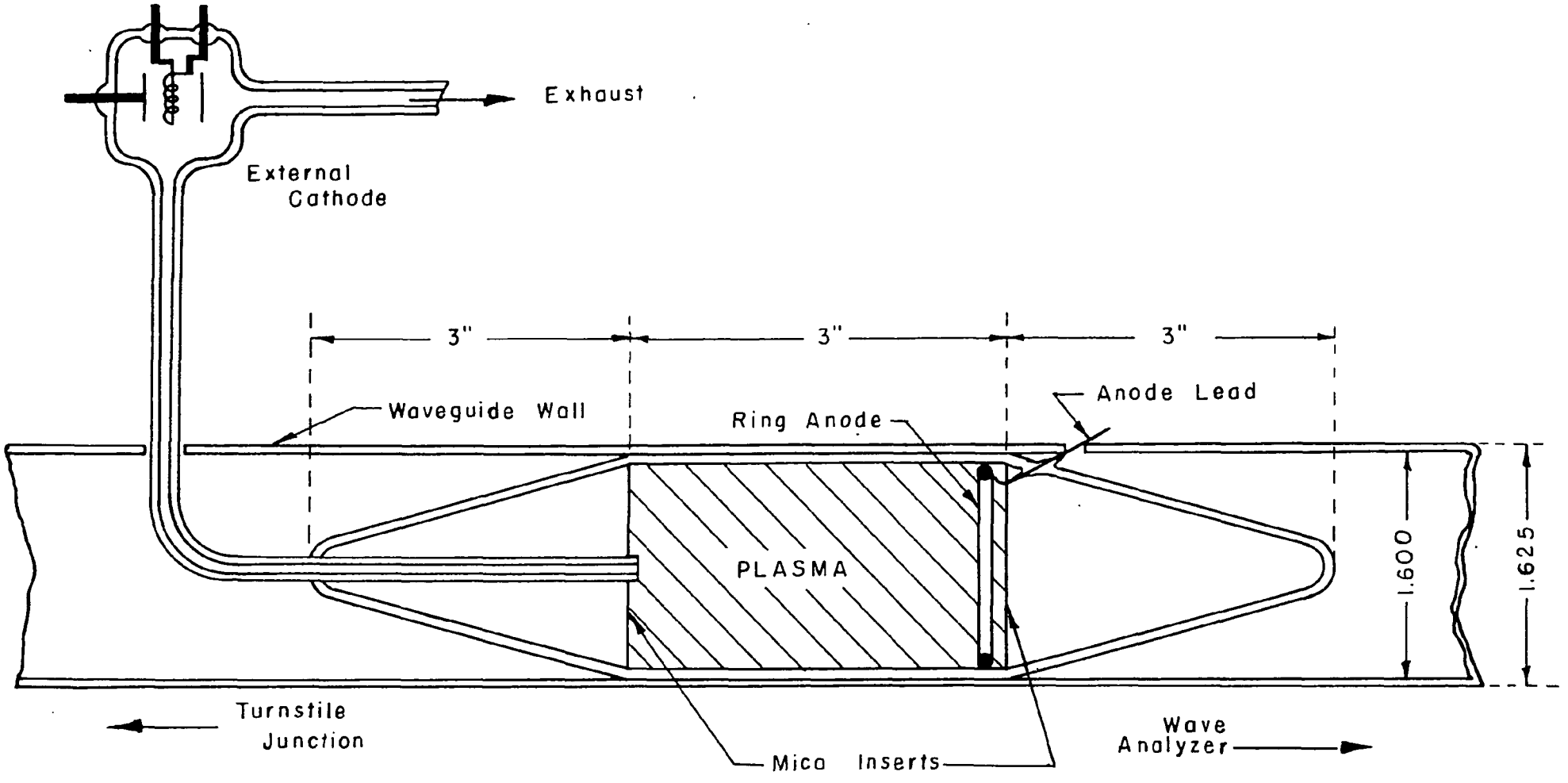

Figure 20. Sketch of the Discharge Tube

hole in the waveguide wall. The overall VSWR caused by the tube structure was measured to be 1.5 or less between 4850 and 5050 mc.

The tube was evacuated through an exhaust tubulation, which entered the waveguide through a small circular opening, passed through the center of the tube taper, extending just through a hole in the mica insert. On the exhaust tubulation, outside the waveguide, was located the cathode of the discharge tube as shown in Figs. 19 and 20.

After evacuation and degassing, the tube was filled with gas at the desired pressure. Neon, helium, and argon supplied in one liter pyrex bulbs from Linde Air Products were connected to the vacuum manifold by a stopcock system. Pressures below 20 mm of Hg were measured by a butyl pthalate manometer, and a Wallace-Tiernan type FA 160051 absolute pressure indicator was used for pressures between 20 and 200 mm of Hg. To remove condensable impurities a liquid nitrogen cooled charcoal trap was attached to the system. The estimate of the amount of non-condensable impurities in the commercial rare gases is one part in 10^6.

B. Operation of the Pulsed Discharge

The discharge in the tube was created by pulsing the external cathode to a large negative potential of 2 microseconds duration at a repetition rate of 250 pulses per second. The time for decay between excitations was thus four milliseconds.

The negative voltage pulse applied to the cathode was obtained from a MIT Mod 3 hard tube pulser, triggered by a free-running BC-1203 B pulse generator. The sweep of a Tetronix model 512 oscilloscope was also initiated simultaneous to the breakdown pulse. In addition, a second pulse from the BC-1203-B generator, which could be delayed continuously from 10 to 3500 microseconds with respect to the breakdown pulse, was used to pulse modulate the klystron oscillator output.

Because of the variable delay, the time of propagation of the rf signal pulse to be studied could be positioned at any desired time during the plasma decay. The envelope of the rf signal as detected by a crystal rectifier located either at the bridge probe or the analyzer output was amplified and presented visually on the oscilloscope trace triggered by the discharge breakdown pulse. The delay between the breakdown and the rf signal transmission was measured from the calibrated sweep speed of the oscilloscope.

During each breakdown pulse, an electron gas of high density and high thermal energy was formed within the tube. This initial density was estimated to be much greater than 10^{11} electrons per cm^3, which is the value calculated to completely reflect an incident 5000 mc rf signal.

In the time interval after a breakdown pulse, the values of electron density and temperature decrease due to electron loss processes and collisions with gas atoms. The approximate variation of electron density and temperature in the decay is represented in Fig. 21. The reproduceability of the breakdown and the decay was good, as evidenced by the absence of jitter between successive signals presented on the oscilloscope.

Under most discharge conditions used in these experiments, the electron temperature was reduced by collisions to the temperature of the neutral gas atoms (assumed to be room temperature) within a few tens of microseconds after the breakdown pulse. In contrast, the decay of the electron density was much slower; in these experiments this occured with a time constant of about one millisecond.

This difference in the electron temperature and density decay was utilized by delaying the rf propagation to such time for which the electron temperature was known, so that the electron collision frequency could be estimated from the relation

$$\nu_c = \bar{v}\, p_o P_m \qquad (12)$$

where

$\bar{v}$ = average electron velocity at room temperature,

p_o = gas pressure corrected to zero degrees centigrade.

and P_m = probability of collision for momentum transfer.

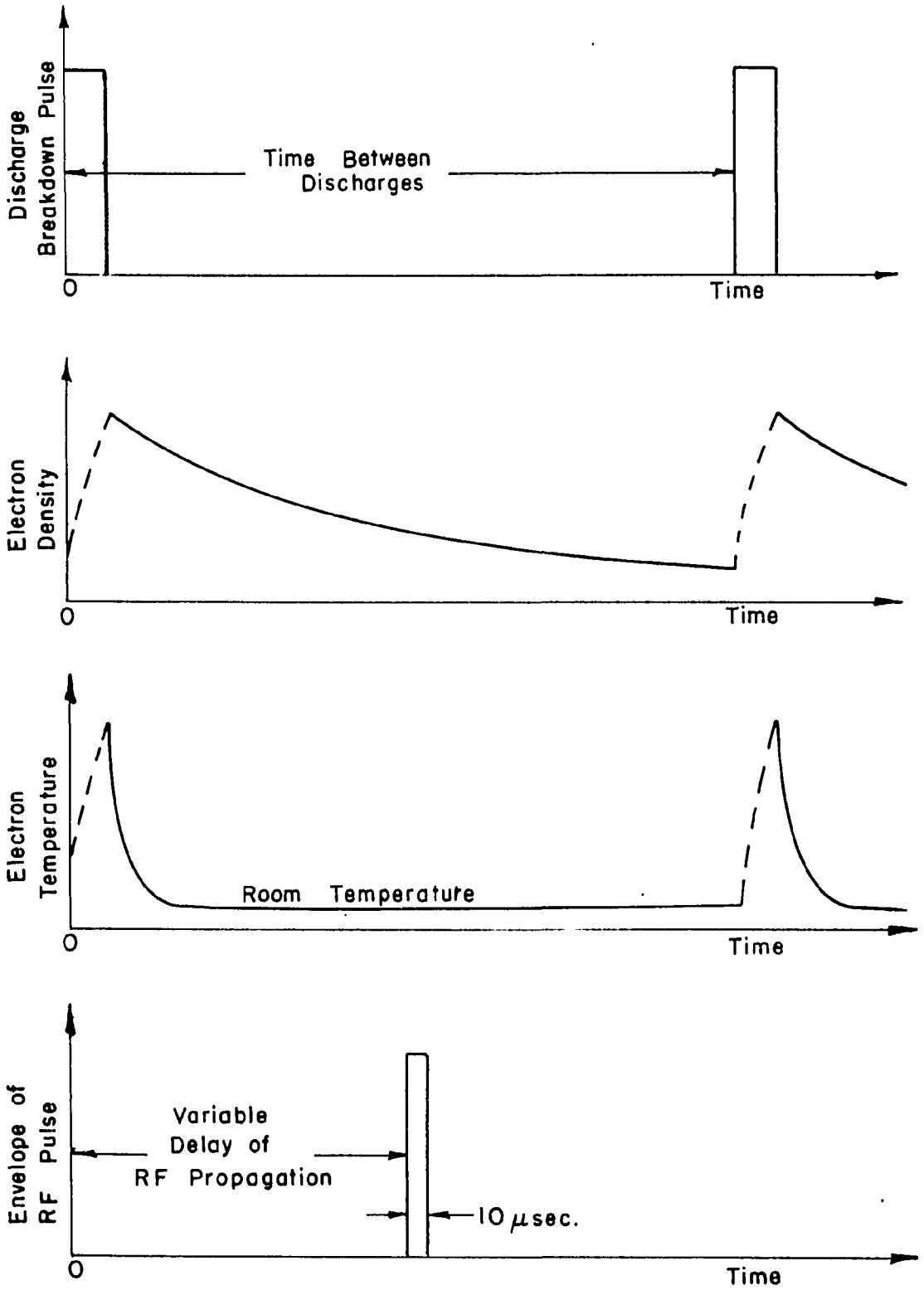

Figure 21. The Plasma Decay and the Time Sequence of Pulsed Operation.

Because of the slower electron density decay, a sufficient electron density (10^9 to 10^{10} per cm^3) to have measurable effects upon the transmission of the rf signal existed after thermal equilibrium had been reached.

Delaying the transmission of the rf pulse also allowed large spatial variations of electron density created during the breakdown to be smoothed by diffusion and recombination.

The cylindrical shape of the discharge within the waveguide lended itself directly to the transmission method of low-loss dielectric constant measurements.[3][10] For low loss electron gases, the wavelength in the gas is a function of the electron density alone, and $\frac{\omega_p}{\omega}$ is calculable from the measured values of the phase constant.

In the absence of a static magnetic field, the effective complex dielectric constant of an electron gas in a plasma is given by $\epsilon_e = \epsilon_0\left(1 - \frac{q^2}{1 - ib}\right)$ if uniform electron density is assumed. The exact relations between $\frac{\omega_p}{\omega}$, $\frac{\nu}{\omega}$, and the attenuation and phase constant of TE_{11} waves propagating in a cylindrical waveguide filled with the electron gas are then[3]

$$\left(\frac{\omega_p}{\omega}\right)^2 = \left(\frac{\lambda}{\lambda_g}\right)^2\left[1 + \left(\frac{m}{54.6}\right)^2 - \left(1 - \frac{\delta}{360}\right)^2\right]\left[1 - \left(\frac{\nu}{\omega}\right)^2\right] \qquad (5.1)$$

and

$$\frac{\nu}{\omega} = \frac{2m}{54.6}\left(1 - \frac{\delta}{360}\right)\left[1 + \left(\frac{m}{54.6}\right)^2 - \left(1 - \frac{\delta}{360}\right)^2\right]^{-1} . \qquad (5.2)$$

m and s are respectively the db change of attenuation and degrees

change of phase shift from empty guide propagation due to one air filled guide wavelength λ_g of electron gas. λ is the wavelength of propagation in free space.

If in expression 5.1, $(m/54.6)^2$ is negligible when compared to $\delta/180$, and $\frac{\nu}{\omega} << 1$, the relation for $\frac{\omega_p}{\omega}$ becomes

$$\frac{\omega_p}{\omega} \cong \frac{\lambda}{\lambda_g}\left(\frac{\delta}{180}\right)^{1/2} \quad . \tag{5.3}$$

In most of our experiments, the terms involving m and ν/ω were negligible, and the approximate relation, eq. 5.3, could be used.

In the measurements δ was obtained from the measurement of the total phase shift, Δ, introduced in the transmitted wave by the presence of the electron gas within the discharge tube. A 10 μsec duration, 5000 Mc freq. rf pulse was propagated through the tube in the absence of the pulsed discharge, and zero phase balance of the phase bridge determined. With the discharge operating in the absence of the magnetic field, phase balance was again obtained at the desired delay of the rf pulse with respect to the discharge pulse. The shift in bridge balance then gave the total phase shift introduced in the transmitted wave.

The measured total shift Δ, is exactly related to δ only for the conditions that the length of the discharge is an integral number of half wavelengths in the medium, otherwise the reflections at the air-electron gas interfaces must be considered.

The reflection coefficient, Γ_i, for the interface was calculated to be .09 or less for $\frac{\omega_p}{\omega} \leq 0.3$, $\nu/\omega = 0$ so that the theoretical deviation of Δ due to the interfaces, which is of the order of Γ_i^2 (11), was negligible. Under these conditions

δ was given directly by $\delta = \frac{\lambda_g}{L} \Delta$ where L is the length of the discharge. At 000 mc, the ratio λ_g/L was 1.5.

From the values of $\frac{\omega_p}{\omega}$ calculated from measured phase shifts the density of the electron gas at the time of transmission was obtained. It must be noted, however, that a value of $\frac{\omega_p}{\omega}$ determined in this manner is an effective value in that it gives the electron density parameter of an assumed gas of uniform density which would produce the observed change in phase shift.

SECTION V

EXPERIMENTAL PROCEDURE AND RESULTS

Measurements of the propagation of a microwave klystron pulse through gaseous discharge plasmas were made for each of the opposite circular polarizations of the incident TE_{11} wave. The Faraday effect was measured directly by using the linear polarization of the incident wave. Insofar as was possible, an attempt was made to investigate separately the effects of the average electron density and collision frequency. Fairly complete data was taken for an initial average electron density such that $q = 0.3$, the condition for which the phase constants of the TE_{11}- limit waves had been evaluated and a comparison to these calculated values could be made.

A. Propagation of Circularly Polarized Waves

To obtain circular polarization of the incident TE_{11} wave, the shorts in the turnstile side arms were adjusted to give minimum variation of the magnitude of the analyzer detector response as the analyzer was rotated about its axis. These adjustments were made with no discharge present. A variation of less than .2 db could be obtained, so that the power excited in other than the desired circular polarization was down approximately 40 db. The sense of the rotation of the circularly polarized wave was determined by feeding the analyzer signal to the phase bridge

and measuring the change in phase as the analyzer was rotated. From the variation, exp $i(\omega t \pm \varphi)$ of a plus or minus wave field, a rotation in the plus sense of the analyzer caused the phase of the analyzer output to decrease (increase) if a plus (minus) wave was incident to the analyzer.

Having established the mode of propagation in the empty circular guide, zero phase balance of the analyzer signal was obtained with the analyzer position fixed, and with no discharge present. The discharge was then initiated and the time of transmission of the rf pulse through the decay of the electron gas was adjusted to such time when the electron density, as measured by the phase shift method, gave a desired $\frac{\omega_p}{\omega}$ ratio.

Keeping the discharge excitation, time of rf transmission, and the analyzer position unchanged, the magnetic field was then applied to the discharge. Measurements of the changes of phase and magnitude of the analyzer signal were made for increasing values of magnetic field intensity. Since the phase shift and insertion loss measurements required switching the analyzer signal from the phase bridge to the crystal detector, separate runs of magnetic field variation were made to obtain each type of data.

All the initial conditions (electron density, zero phase balances, and incident wave polarization) were rechecked at the end of each run. In addition, the polarization of the transmitted wave was observed over the entire range of magnetic field. It was found that as the insertion loss became greater than 20 db, the transmitted wave began to depart from nearly circular polarization in a somewhat erratic manner. There are many possible causes of the apparent loss of circular polarization. These

may include discharge inhomogeneity, rf reflections at the tube interfaces, the slightly imperfect circular polarization of the incident wave, and the imperfection of the wave analyzer. At insertion losses greater than 20 db, there was insufficient signal at the analyzer to make phase measurements, and, as a result, the transmitted wave could not completely be described. Since the polarization of the transmitted wave could not be determined at these low signal amplitudes, insertion losses of greater than 20 db measured with fixed analyzer position cannot be interpreted as strictly the result of circular wave propagation in the electron gas.

1. Propagation of the Minus Wave

With minus circular polarization of the incident wave, the transmitted wave was found to be of similar polarization over appreciable ranges of discharge pressure and applied magnetic field. Where nearly circular polarizations (axial ratio of the order of 1 db or less) of the incident and transmitted wave were retained with variation of the magnetic field, the change in phase between the reference arm signal and that from the analyzer in a fixed position was directly interpreted as the change in phase of a mode of minus circular polarization propagating through the discharge. Phase shift data for discharges in helium and neon at pressures of 5, 10, and 20 mm. are shown in Figs. 22 and 23. The corresponding insertion loss curves are given in Figs. 24 and 25.

For each pressure and gas the time of propagation of the rf pulse was adjusted so that with no applied magnetic field, an increase in phase of 43° was introduced by the discharge. This phase increase corresponded to an average phase constant $\beta_o' = .445$ in the electron gas medium, and to $q = 0.3$ for $\nu/\omega \leq 1/10$.

Comparison of the data shows the measured phase shift and insertion loss agree qualitatively with those of uniform minus wave propagation through a medium of constant electron density described in Section II.

The solid curves in Figs. 22 and 23 are the computed values of the phase of the analyzer signal assuming minus TE_{11}- limit propagation through the plasma. A constant value of electron density corresponding to $q = 0.3$ was used in the computations, and the length of the anisotropic medium was taken as the distance between the mica inserts of the discharge tube.

The computed values of phase shift assume ν to be zero which is not the case for an electron gas in a plasma. For these experiments, ν, the electron collision frequency, can be estimated as $\nu = 3.3 \times 10^{7}\ p_o$ in neon and $\nu = 1.8 \times 10^{8}\ p_o$ in helium. p_o is the gas pressure corrected to mm of Hg at zero degrees centigrade. These values of ν were calculated from $\nu = \bar{v} P_m p_o$ where $\bar{v}$ is the average velocity of electrons at room temperature. The values of P_m used were 3.3 for neon and 18 for helium as given by Phelps, Fundingsland, and Brown.[12] Thus at room temperature, and equal pressures, the electron collision frequency is about six times as great in helium than in neon.

Some idea of the effect of a finite but small value of ν/ω

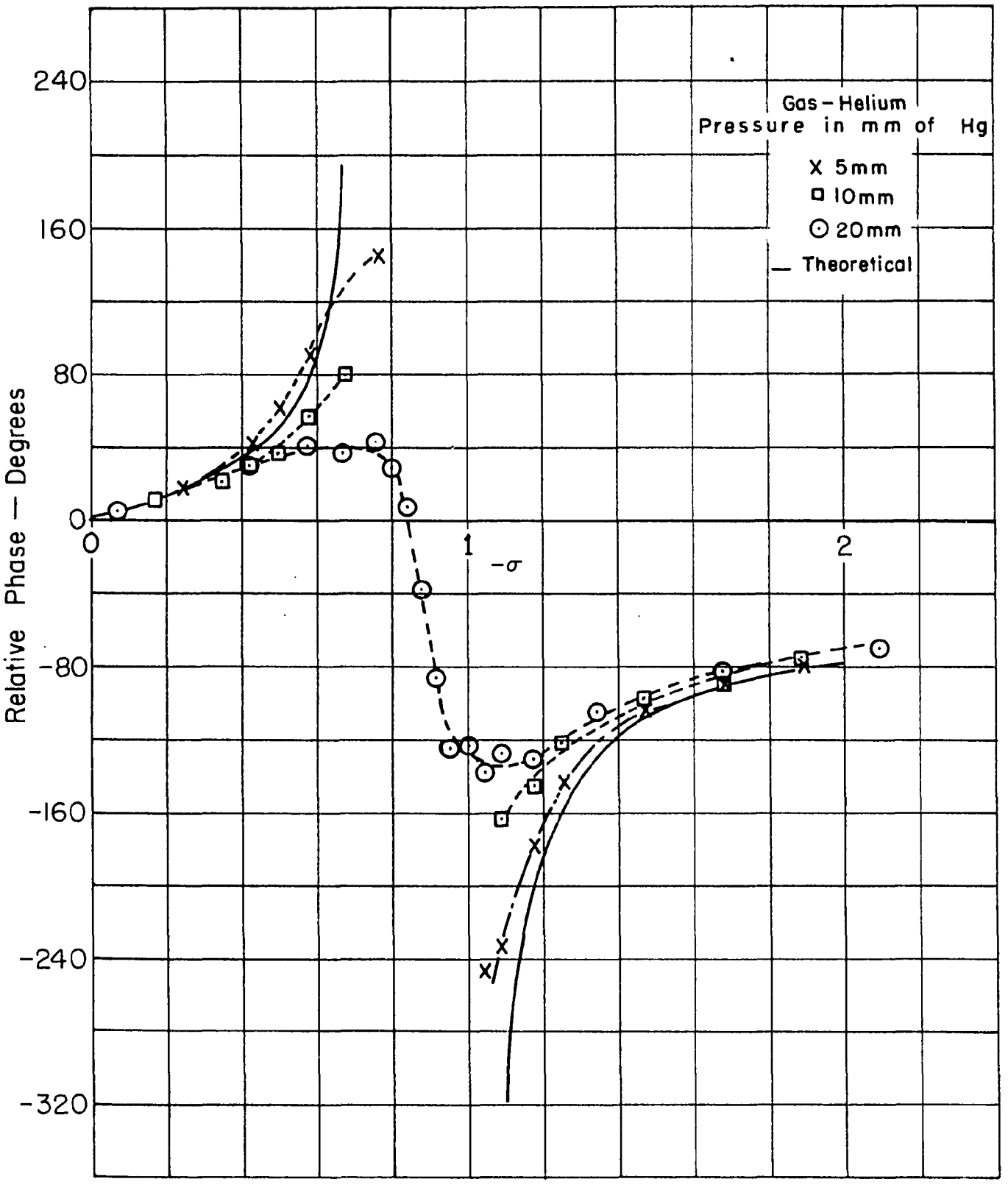

Figure 22. Phase of the Analyzer Signal - Incident Minus Wave and Helium Discharge

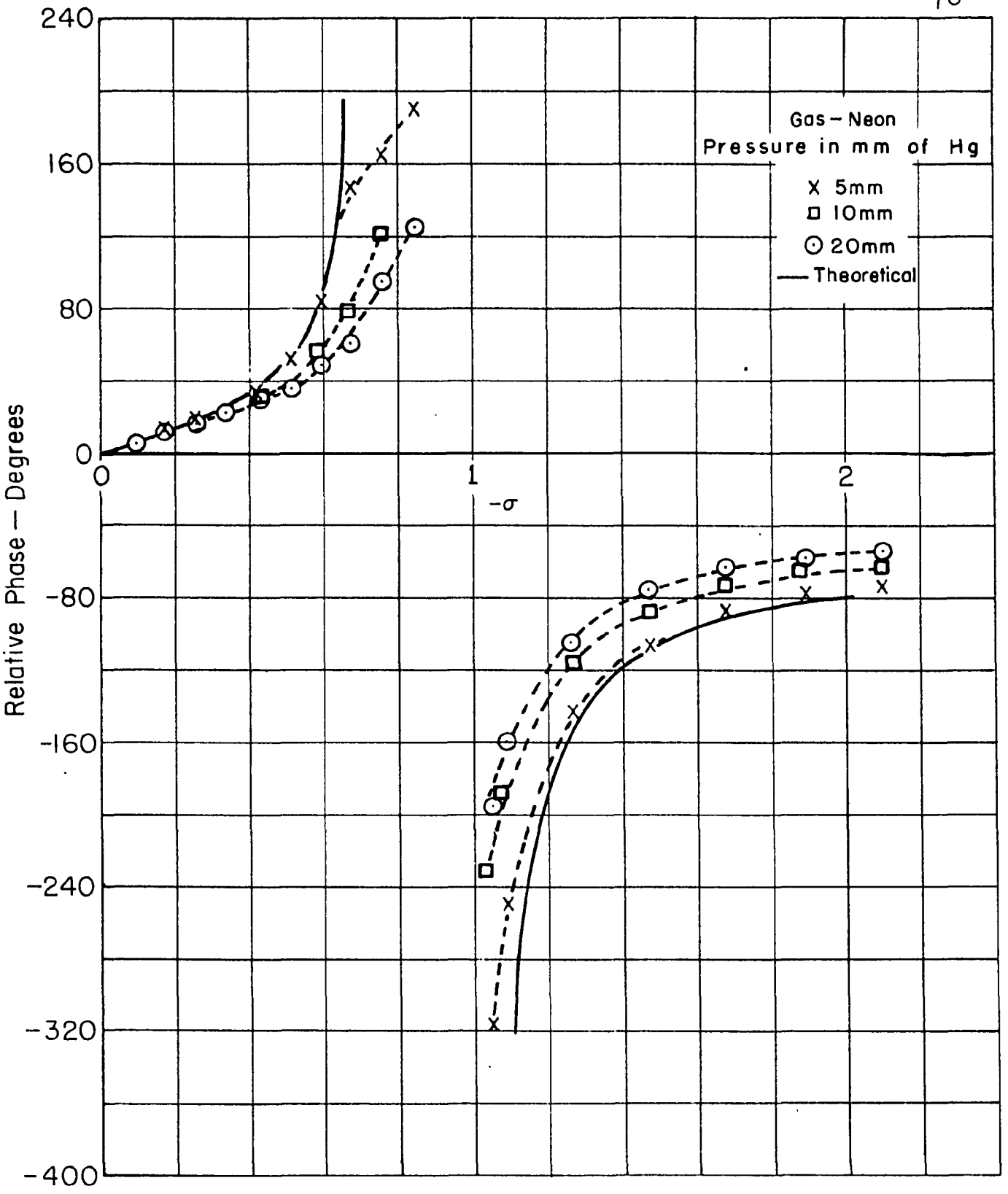

Figure 23. Phase of the Analyzer Signal - Incident Minus Wave and Neon Discharge

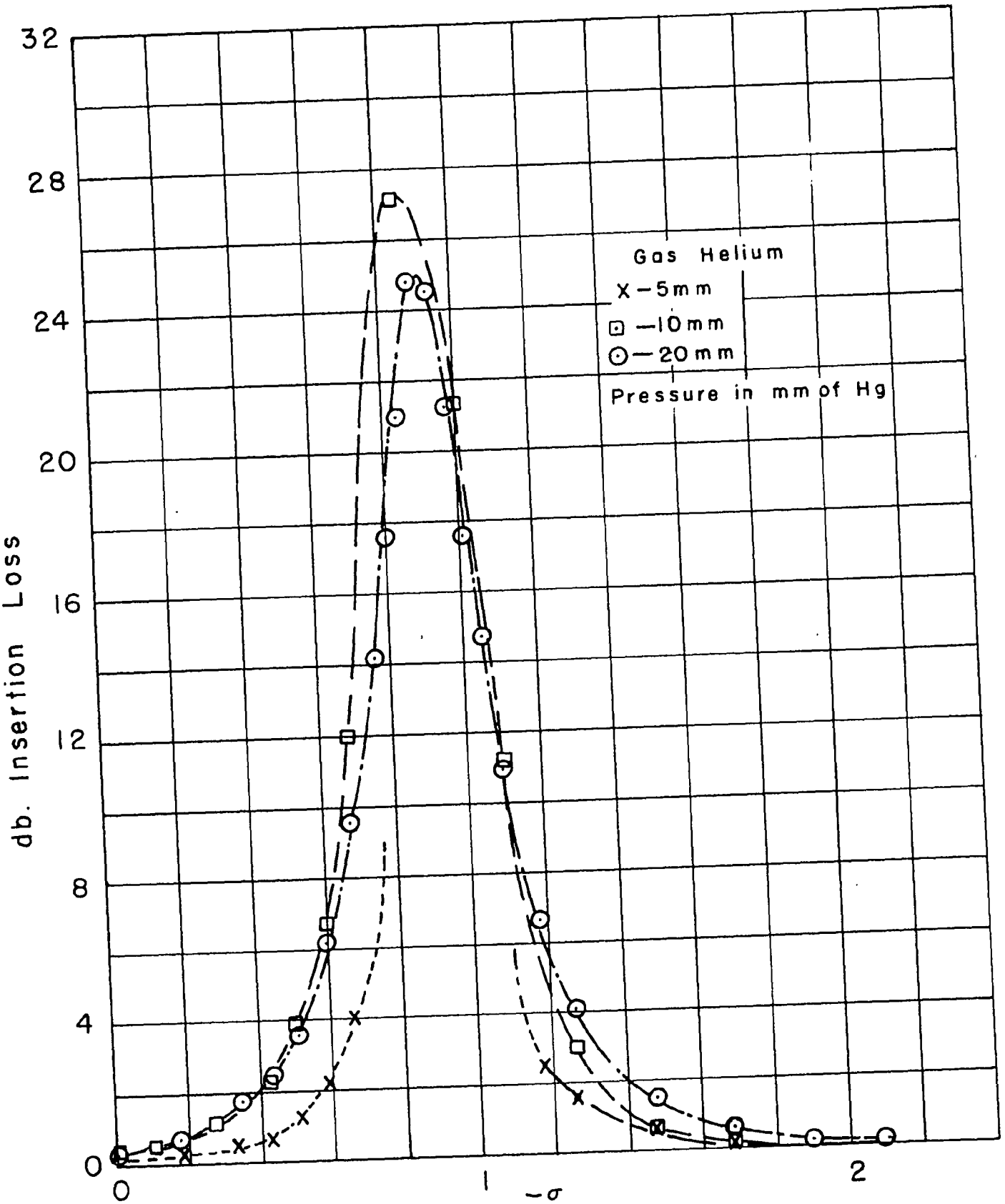

Figure 24. Insertion Loss of Incident Minus Wave - Helium Discharge

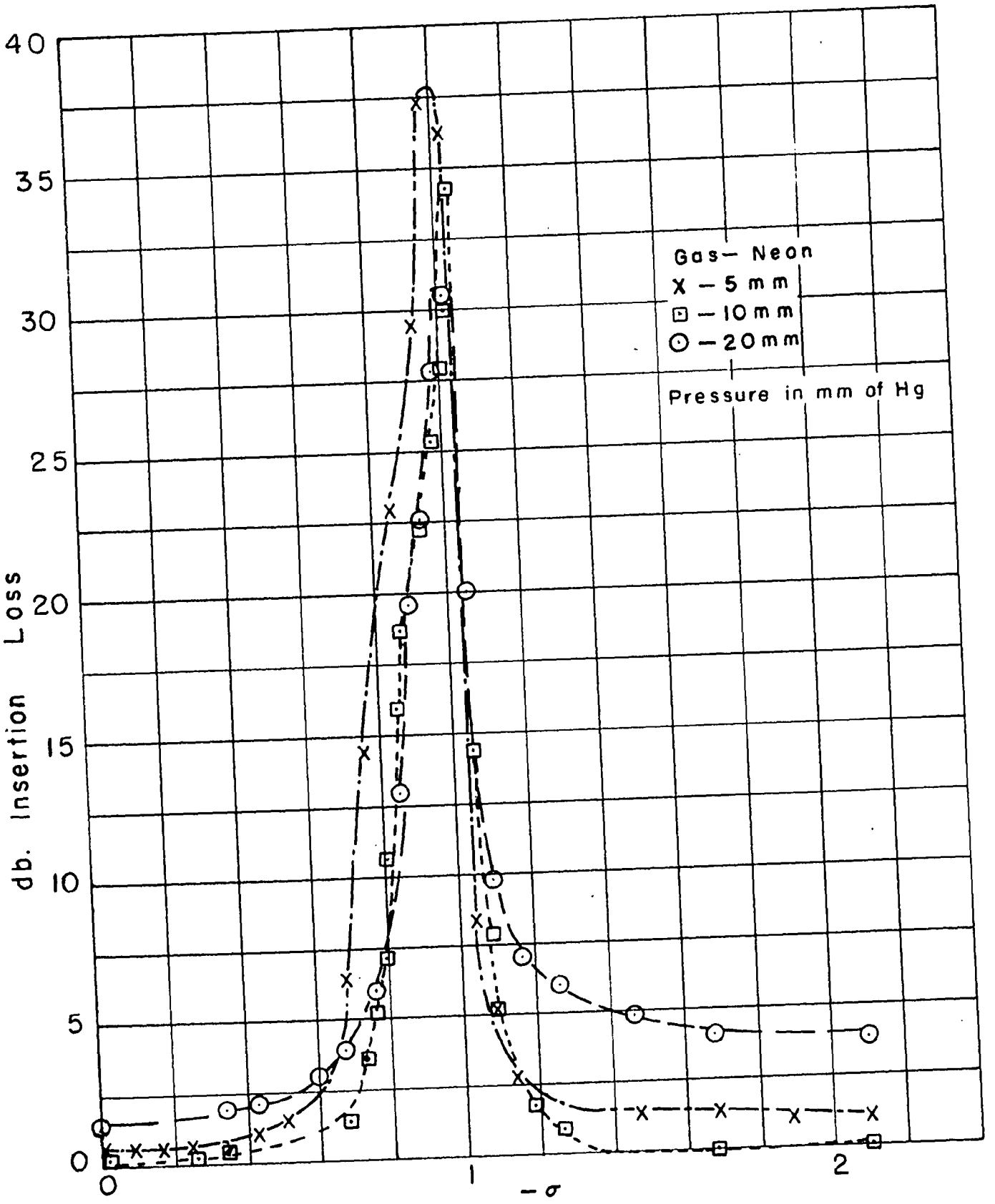

Figure 25. Insertion Loss of Incident Minus Wave - Neon Discharge

upon the phase shift may be obtained by considering the value of the tensor elements. In Section II we had

$$\eta = \epsilon_0 \frac{\sigma q^2}{\sigma^2 - (1 - ib)^2}$$

which for $b = \nu/\omega = 0$ reduces to

$$\eta = \epsilon_0 \frac{\sigma q^2}{\sigma^2 - 1} .$$

For $\nu/\omega \neq 0$, but small, the real part of η is given approximately by

$$\mathrm{RE}\ \eta = \epsilon_0 \frac{\sigma q^2}{\sigma^2 - 1 + \frac{4b^2}{\sigma^2 - 1}} .$$

Comparing the expressions for the real part of η considering losses and the value of η for $b = 0$, it is seen the effect of b is to reduce the no-loss value of η by a factor of the order of $4b^2/(\sigma^2-1)^2$. Thus for $b \leq 0.1$, an observable change due to the effect of collisions should not occur for very small or very large magnetic fields. The effect of collisions does become important as $-\sigma$ approaches unity.

Referring to Fig. 22 which shows the phase shifts vs magnetic field for minus waves propagation through the helium decay, measured values near $-\sigma = 0$ and $-\sigma = 2$ agee well with values calculated assuming $\nu/\omega = 0$, $q = 0.3$. Nearing $-\sigma = 1$, the measured values fall increasingly below the calculated magnitudes of phase shift. As ν/ω was lowered by successively reducing the gas pressure, the phase shifts approached the calculated values over an increasing range of $-\sigma$.

In neon, where for equal pressures the electron collision frequency is less than in helium, even closer agreement might be expected. However, this was not observed, since for the discharge in neon, the application of the magnetic field apparently altered the decay of the electron density. Referring to Fig. 23, it is seen that the change of phase with σ at $-\sigma = 0$ was the same for pressures of 5, 10, and 20 mm which indicates the same initial electron density. At higher $-\sigma$, the magnitude of the phase shift was significantly less than computed, decreasing with increasing pressure. Near $-\sigma = 2$, where the ratio ν/ω should not be of influence, the phase shifts were still low, indicating a decrease of electron density in the decay with increasing magnetic field.

The phase shift and insertion loss data may also be examined for cut-off of the minus wave. In section III the minus TE_{11}-limit wave was shown to be non-propagating for $.665 \leq -\sigma \leq 1$ if $q = 0.3$ and $b = 0$. Assuming minus TE_{11}- limit wave propagation within the three-inch length of discharge, then one would expect for the lossless case a high reactive insertion loss and little or no phase shift across the length of discharge at cutoff. If $\beta_o' = .445$ is the phase constant of the wave for $-\sigma = 0$, then in the cut-off region the phase of the analyzer signal will be increased by the phase corresponding to the removal of this section or to $\beta_o \times L \times \pi/180 \cong 195^\circ$. Actually an abrupt, complete cut-off cannot occur because of the presence of electron collisions, and possibly other factors such as a non-uniform electron density distribution. In addition the insertion loss associated with cut-off is altered by collisions and is further

complicated by resonance losses in the electron gas as $-\sigma$ approaches 1, the value required for electron gyroresonance at the rf signal frequency.

Nevertheless at the lower discharge pressures an approximate cut-off was quite evident as shown by the limit of the phase increase of the analyzer signal, and the asymmetry of the insertion loss curves about $-\sigma = 1$. Consider the data for a discharge in neon at 5 mm pressure (Figs. 23 and 25). At $-\sigma = .5$ the insertion loss and phase shift both abruptly increased as the magnetic field was increased. The insertion loss remained high between $-\sigma = .5$ and $-\sigma = 1$, and phase increases nearing 195° were measured. The pronounced increase in the insertion loss at $-\sigma = 1$ was probably associated with resonance losses in the electron gas. For $-\sigma$ just greater than 1, the value of insertion loss dropped sharply. Since the wave was propagating for $-\sigma$ just greater than 1. the behaviour of the insertion loss in this region is more representative of losses due to the gyroresonance than for values of $-\sigma$ less than 1 where the presence of the cut-off complicates the picture.

The behaviour in the region of cut-off for discharges in neon at 10 and 20 mm pressures supports the supposition made earlier that the magnetic field caused a reduction in density at these pressures. At $-\sigma = .665$, the electron gas should behave as a good dielectric, so that cut-off is expected if $q = 0.3$. It was observed that at these pressures, the insertion loss associated with cut-off began to rise at somewhat higher values of $-\sigma$. In addition the phase increases at $-\sigma = .665$ (75° for the 10 mm pressure, 60° for 20 mm) were well below the cut-off value of

195°. Both the low phase shift at $-\sigma = .665$ and the increase in magnetic field necessary to obtain cut-off are indications of lowering electron density with increasing magnetic field.

The asymmetry in the insertion loss curves is also present for data taken at 5, 10 and 20 mm pressure in helium. Here the collision frequency was sufficiently high so that the behaviour was not approximated very well by calculations assuming b = 0.

Similar data was taken for discharges in neon at 1, 110, and 200 mm pressure (Fig. 26). The phase shift for $0 \leq -\sigma < .2$ at the 1 mm pressure corresponded to $q = 0.3$ but increased much more rapidly to a cut-off value at $-\sigma = .43$. The TE_{11}- limit wave was calculated to cut-off at $q = 0.4$ for $-\sigma = .43$, indicating the magnetic field had caused an increase in density. Assuming $q = 0.4$ the phase shift at $-\sigma = 2$ was computed to be -98°, compared to a measured value of -102°.

At pressures of 110 and 200 mm the discharge in neon tended to be unstable and of a filamentary nature. Generally, the phase shift curves continued to show resonance behaviour of decreasing amplitude with increasing gas pressure.

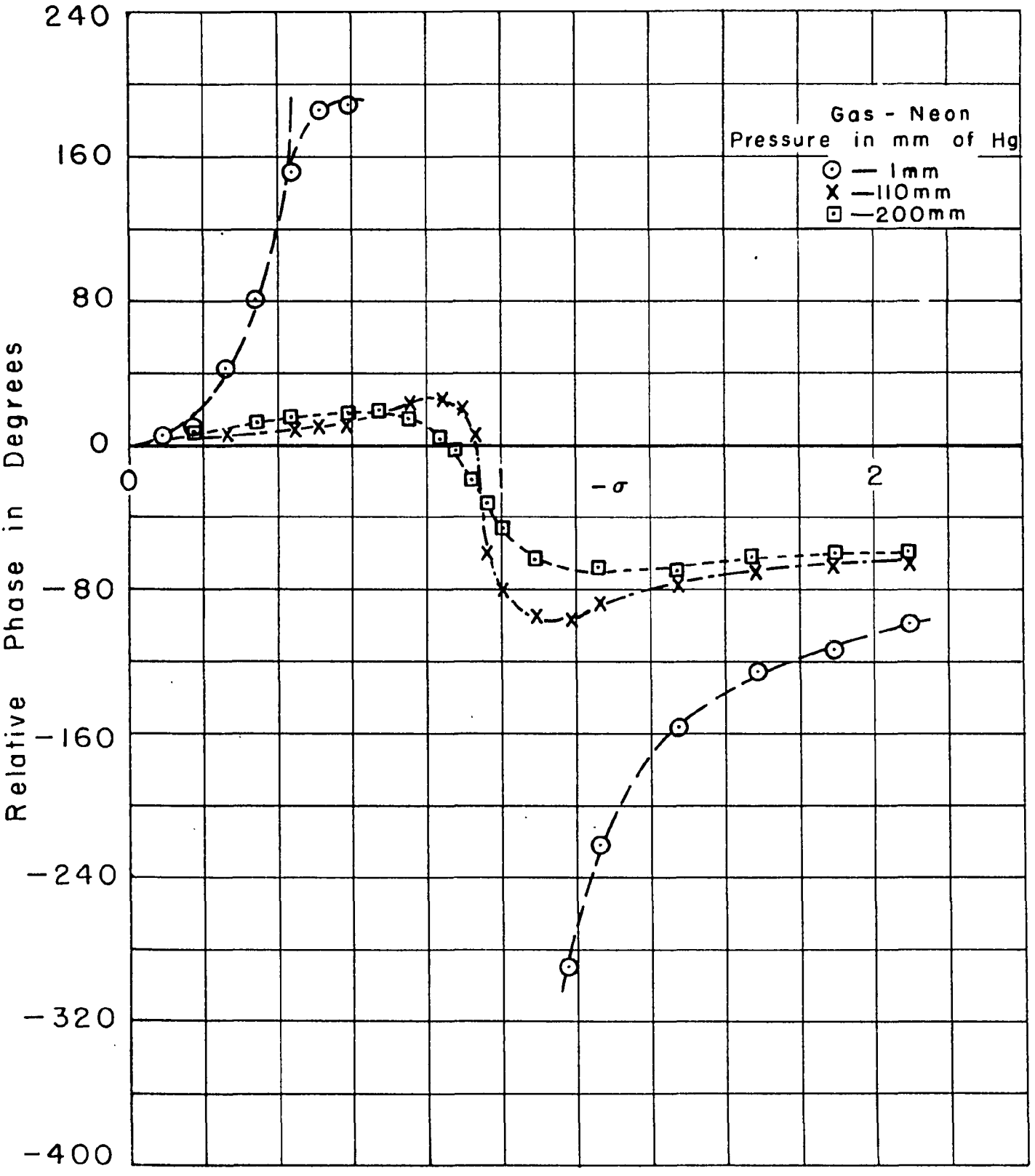

Figure 26. Phase of Analyzer Signal - Incident Minus Wave and Neon Discharge

2. Propagation of the Plus Wave

The measurements of the phase of the analyzer signal for plus circular polarization of the incident TE_{11} wave are shown in Figs. 27 and 28. The solid curves are computed values of phase shift assuming the electron gas to be uniform, $q = 0.3$ and TE_{11}-limit wave propagation.

The observed phase shift behaviour was similar to that calculated, but there was no quantitative agreement other than for very small magnetic fields. For $-\sigma < .4$, the phase shifts followed closely the approximate solution for small σ, rather than that of the full graphical analysis. The amplitude of the resonance variation near $-\sigma = 1$ was always much less than computed, and decreased with increasing pressure of the gas.

The insertion loss curves corresponding to the phase shift data of Figs. 27 and 28 are shown in Fig. 29. The data for insertion loss of the plus wave were in general not as consistent as those for the minus wave because the transmission of the plus wave was high and the effect of reflections and slight changes in transmitted polarization appear as a major portion of the observed insertion losses. For the lower pressure neon discharges however there were definite absorption peaks observed at resonance values of magnetic field. These are in accordance with the resonance predicted in Section III for this mode. The values of maximum insertion loss of the plus wave were much smaller than those of the minus wave. This difference was found to be due to the combined effects of electric field and electron density distribution within the discharge tube.

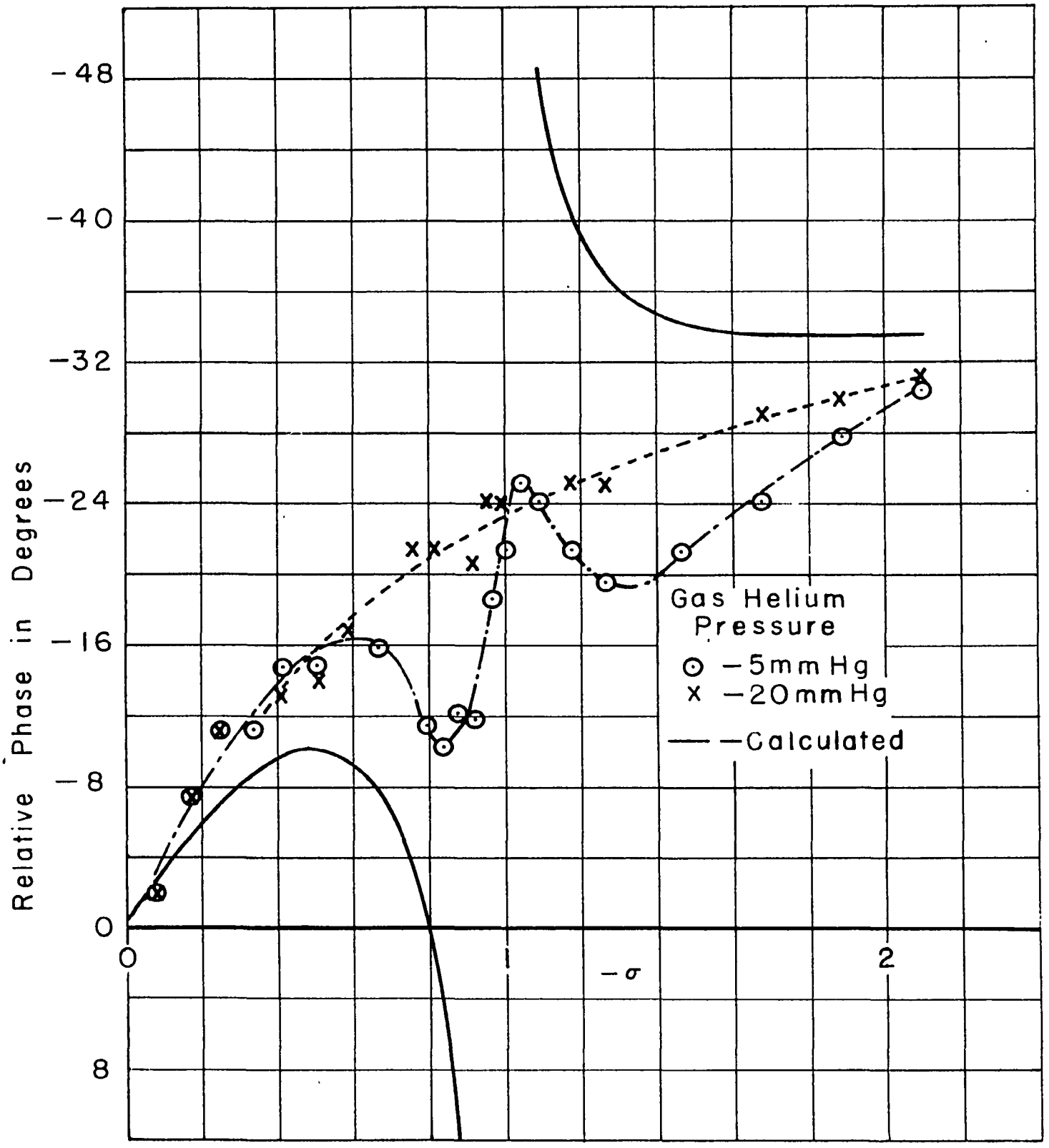

Figure 27. Phase of Analyzer Signal - Incident Plus Wave and Helium Discharge

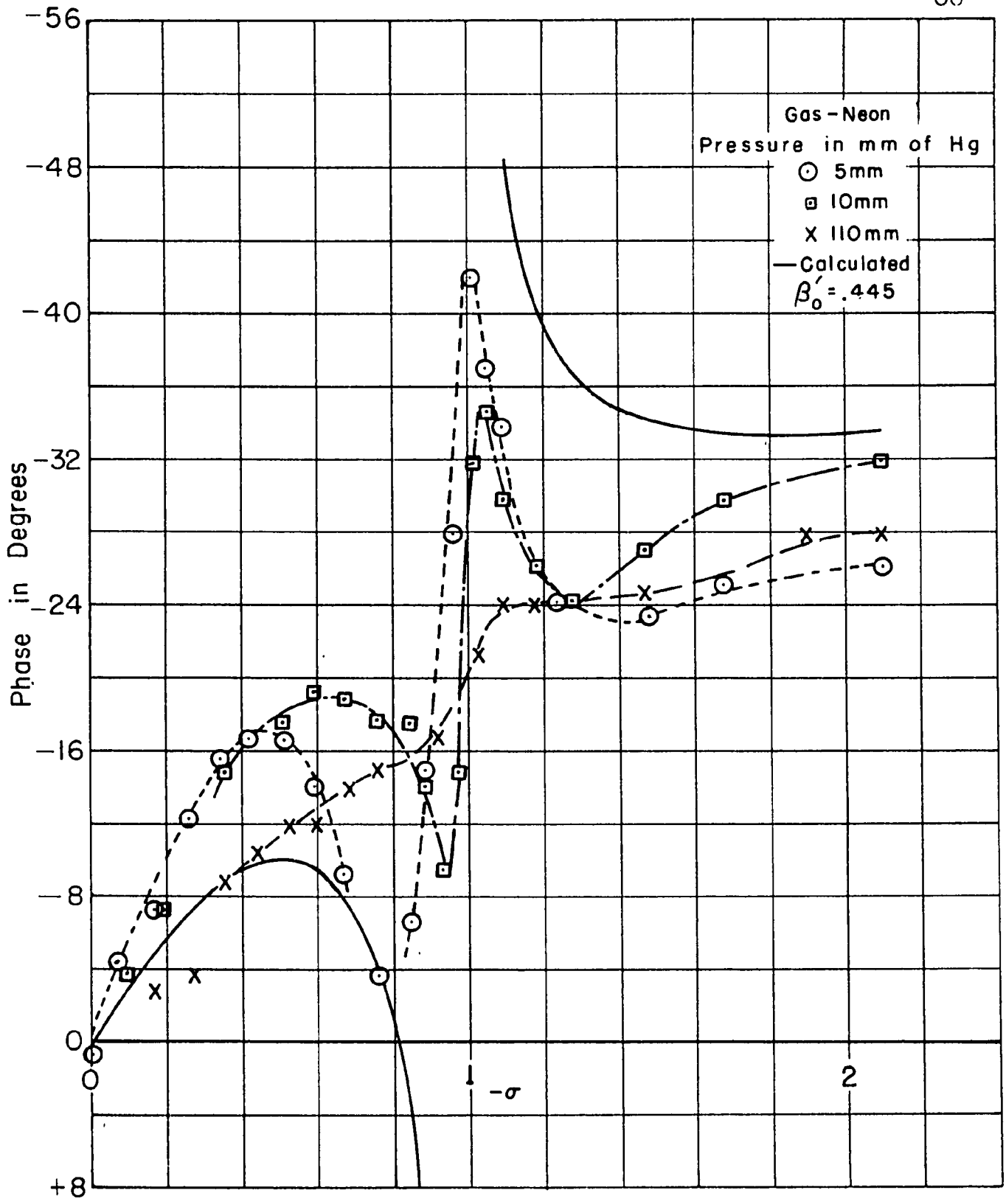

Figure 28. Phase of Analyzer Signal - Incident Plus Wave and Neon Discharge

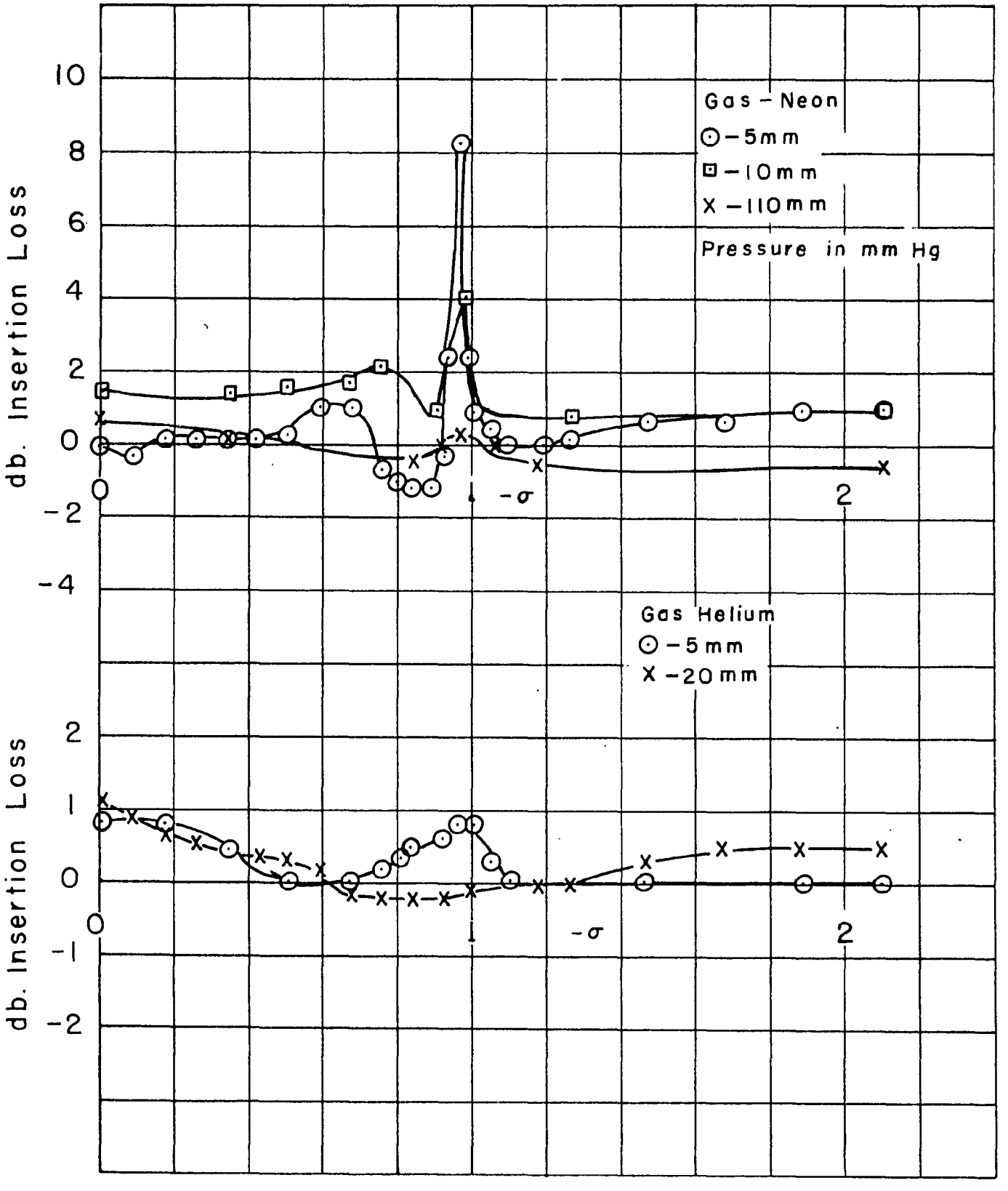

Figure 29. Insertion Loss of Incident Plus Waves

The differences in observed and calculated phase shifts were so large, especially in regions where the electron collisions could not be of influence, that other factors than collision damping must be considered. In the uniform wave analysis of Section II, it was shown that resonance phenomena are associated with transverse electric fields of minus circular polarization, and not with those of plus circular polarization. The plus TE_{11} wave has a minus circular polarization component of transverse electric field which is zero along the waveguide axis and increases to a maximum value at the guide wall. The plus component on the other hand is maximum at the guide center and diminishes in intensity outward. It seems reasonable to assume that the electrons in the region of high field intensity would have greatest effect upon the wave propagation, depending upon the polarization of the electric field. The resonant behaviour of the plus TE_{11} wave would thus be due primarily to the electron density in the region of high intensity of the minus circular polarization component of the transverse electric field. This region is approximately between the guide wall and half the distance to the guide center. A lower electron density in this portion of the discharge tube could then result in the observed small amplitude of resonance.

The effect of the absence of electrons in the volume near the wall was determined by placing a discharge tube coaxially in the waveguide, but having an inner diameter of only 2 cm. compared to the waveguide diameter of 4.1 cm. The discharge tube of 2 cm. diameter was three inches in length, the same length as the tube used in other experiments.

Fig. 30 and Fig. 31 show the phase shifts introduced by the discharge filling the guide cross section and the discharge in the smaller cross-section tube just described. In each case the time of propagation in the plasma decay was adjusted to give an initial phase shift of -44^{o}, and the gas was neon at five mm pressure. Although the one curve in Figure 31 is for minus polarization of the incident wave and negative B_o, this was equivalent to plus polarization and positive B_o.

It is seen that the small resonance of the plus wave (Fig. 30) was virtually eliminated by restricting the discharge to the center portion of the waveguide while the variation of the other polarization remained essentially the same.

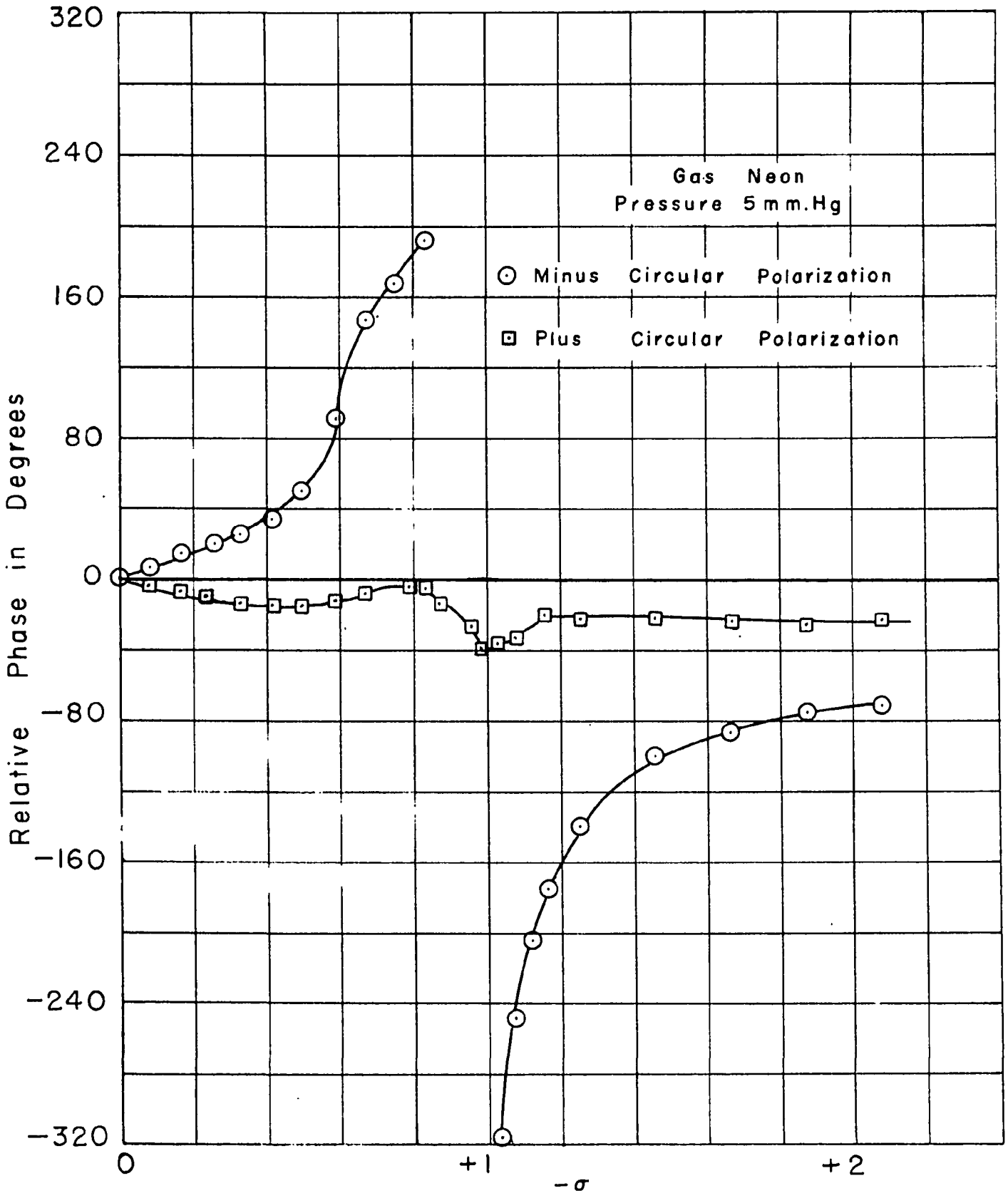

Figure 30. Phase of Analyzer Signal with Waveguide Cross Section Totally Filled with the Plasma

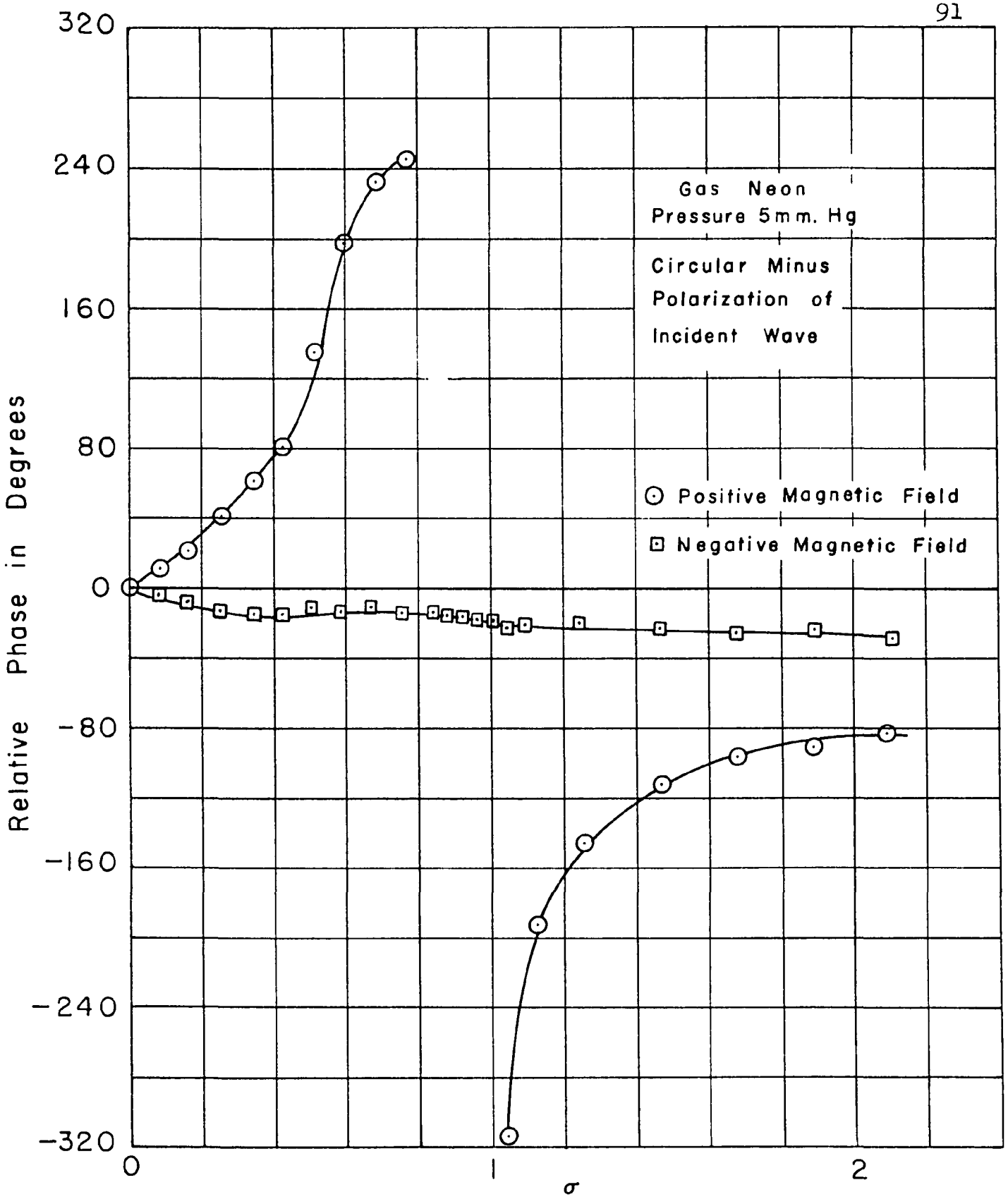

Figure 31. Phase of Analyzer Signal with Waveguide Cross Section only Partially Filled with Plasma

B. Linear Polarization of the Incident Wave

Nearly linear polarization of the incident wave could be obtained by adjusting the turnstile to give minimum analyzer signal with the analyzer plane positioned 45° from horizontal. In the absence of a discharge, the axial ratio of the resultant transmitted wave was greater than 40 db. With the discharge present, measurements of the axial ratio and the plane of polarization of the transmitted TE_{11} waves were made for values of electron density determined by the phase shift method.

1. Relation between Linear Wave and Circular Wave Behaviour

In Sections II and III it was developed that the behaviour of an initially linear wave in both the infinite media and the cylindrical guide could be expressed in terms of waves of opposite circular polarization. The position θ of the plane of polarization of a transmitted wave with respect to that of an incident linear wave was given as

$$\theta = \frac{\Phi_+ - \Phi_-}{2}$$

where Φ_+ and Φ_- are the phase shifts introduced into the plus and minus components of the transmitted wave by the length L of anisotropic electron gas. Angles of rotation of the plane of polarization as computed from $\theta = \frac{\Phi_+ - \Phi_-}{2}$ and the preceding phase shift data for circularly polarized waves were compared with those measured directly with linear polarization of the incident wave. An agreement between direct measurement and the synthesis from circular wave data was found. Fig. 32a compares these values for

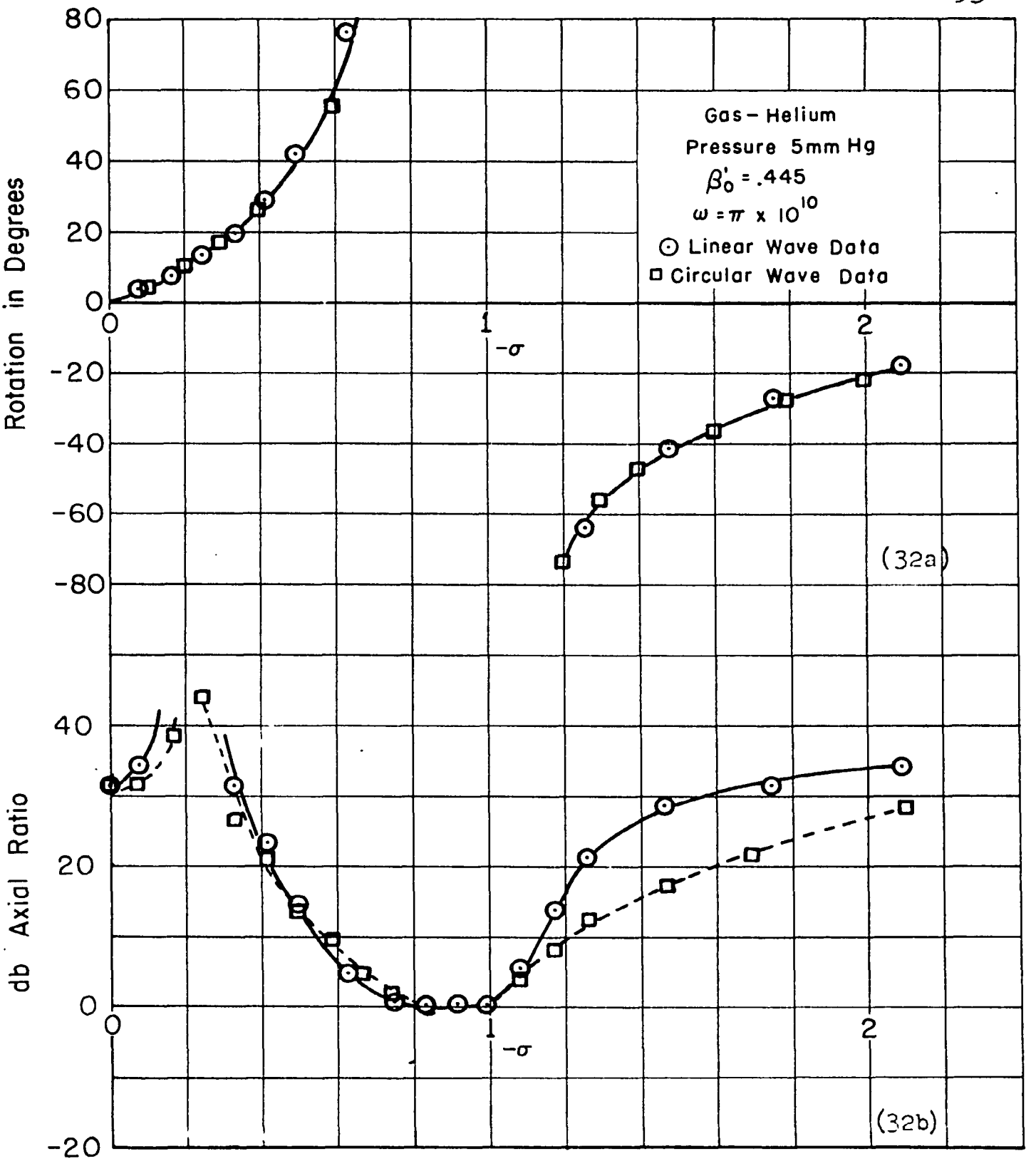

Figure 32. A Comparison of Incident Linear Wave Data with the Superposition of Circular Wave Data

a discharge in helium at a pressure of 5 mm. The phase shift values of the circularly polarized waves for these curves were taken from data presented in Figs. 22 and 27.

An axial ratio may be computed from the relative amplitudes of the individually transmitted circularly polarized waves. Exact agreement between this axial ratio and values measured from direct observation cannot be expected a priori since losses and power flow are not linear functions of the field quantities. However, curves of axial ratio vs σ obtained by both methods show fair agreement. and it appears that the axial ratio of a transmitted linear TE_{11} wave can be understood by considering the attenuation of the circularly polarized components individually.

Fig. 32b shows the observed and calculated axial ratios for the same discharge plasma in helium for which rotations were compared. Relative magnitudes of the oppositely circularly polarized waves were chosen so that the observed and calculated values agreed at $-\sigma = 0$. The maximum value of axial ratio which occurs at a low value of magnetic field is due to the unequal amplitudes of the component waves excited at $-\sigma = 0$.

2. Variation with Gas Pressure.

Complete curves of rotation and axial ratio of the transmitted wave were taken for $\beta_0' = .445$ and $q = 0.3$, values for which the phase constants of the TE_{11} lim t waves have been evaluated. This data is shown in Figs. 33 through 37. Figs. 33 and 34 are for discharges in helium; Figs. 35 36, 37 for discharges in neon. The solid curve in each of the figures represent-

ing rotation is computed assuming a uniform electron density such that $q = 0.3$ throughout a 7.62 cm length of the guide, and that the angle of rotation Θ can be expressed by $\Theta = \frac{\beta_+ - \beta_-}{2} L$.

The quantity $\frac{\beta_+ - \beta_-}{2}$ has been given previously by Fig. 15 as a function of σ. It may be worthwhile to mention that the discrepancies between the measured values of the angle of rotation and those calculated from β_+ and β_- can be related directly to the behaviour of the circularly polarized waves, which have been previously described.

Except for discharges at 100 and 200 mm pressure in neon which were unstable, the observed rotations at low magnetic field intensities agreed closely with calculated values. At higher magnetic fields, the rotation was found to depend largely upon the phase shift introduced in the minus circular wave components since the magnitudes of the minus wave phase shifts were much larger than those of the plus wave. For this reason, the large discrepancies between the calculated and measured values of plus wave phase shift account only for small differences in calculated and observed rotations.

The ellipticity curves also can be deduced from the circular wave insertion loss data, as shown previously. The variation of ellipticity with magnetic field, except at resonance, is due almost entirely to the attenuation of the minus wave, the plus wave being transmitted with relatively little loss. The asymmetry of the axial ratio vs curves about $-\sigma = 1$ is explained by the high insertion loss of the minus wave which occurs as cut-off of this component is approached At higher pressures, the increased electron collision frequency eliminates cut-off and the axial-

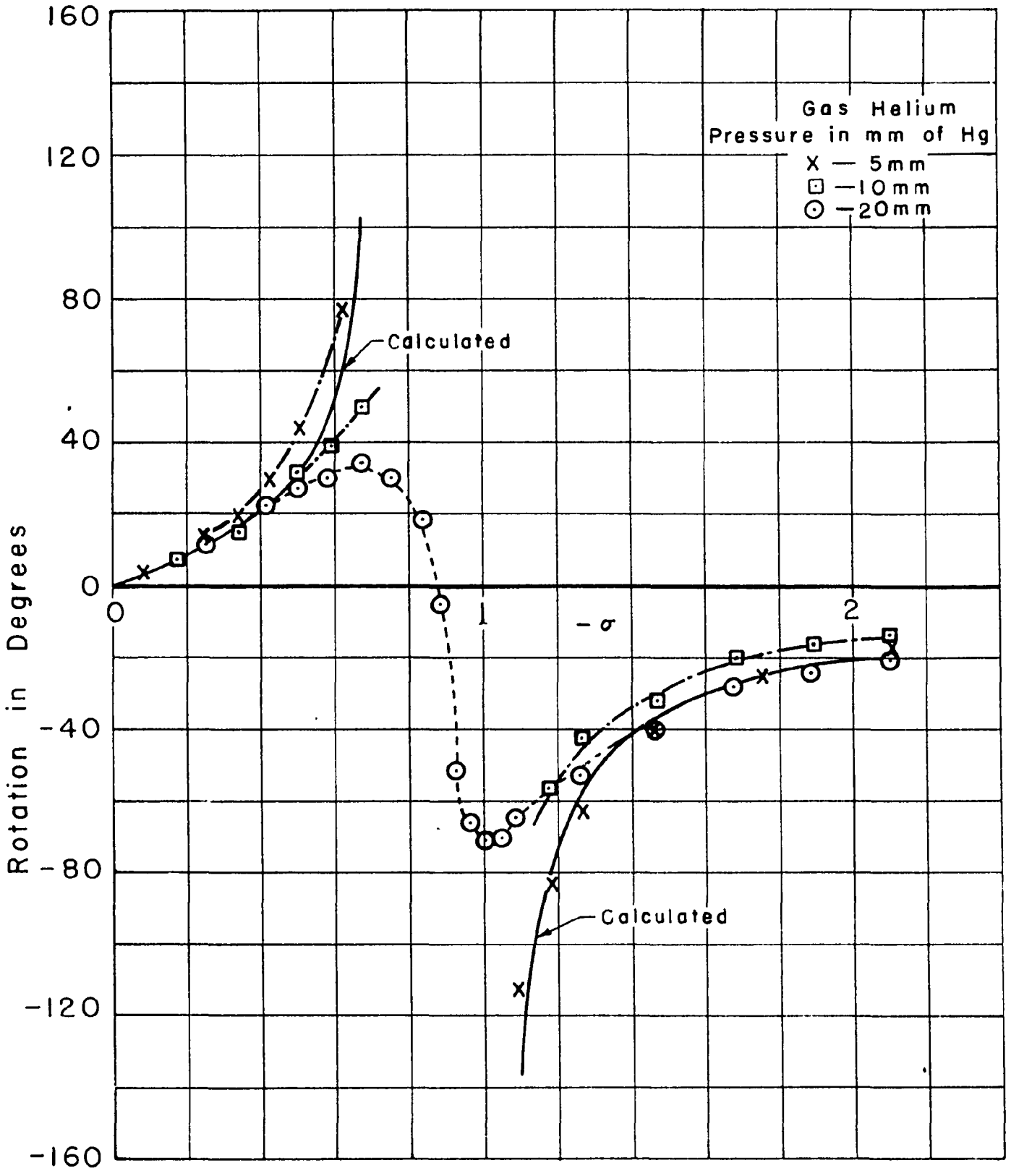

Figure 33. Rotation of Plane of Polarization of Transmitted Wave - Helium Discharge

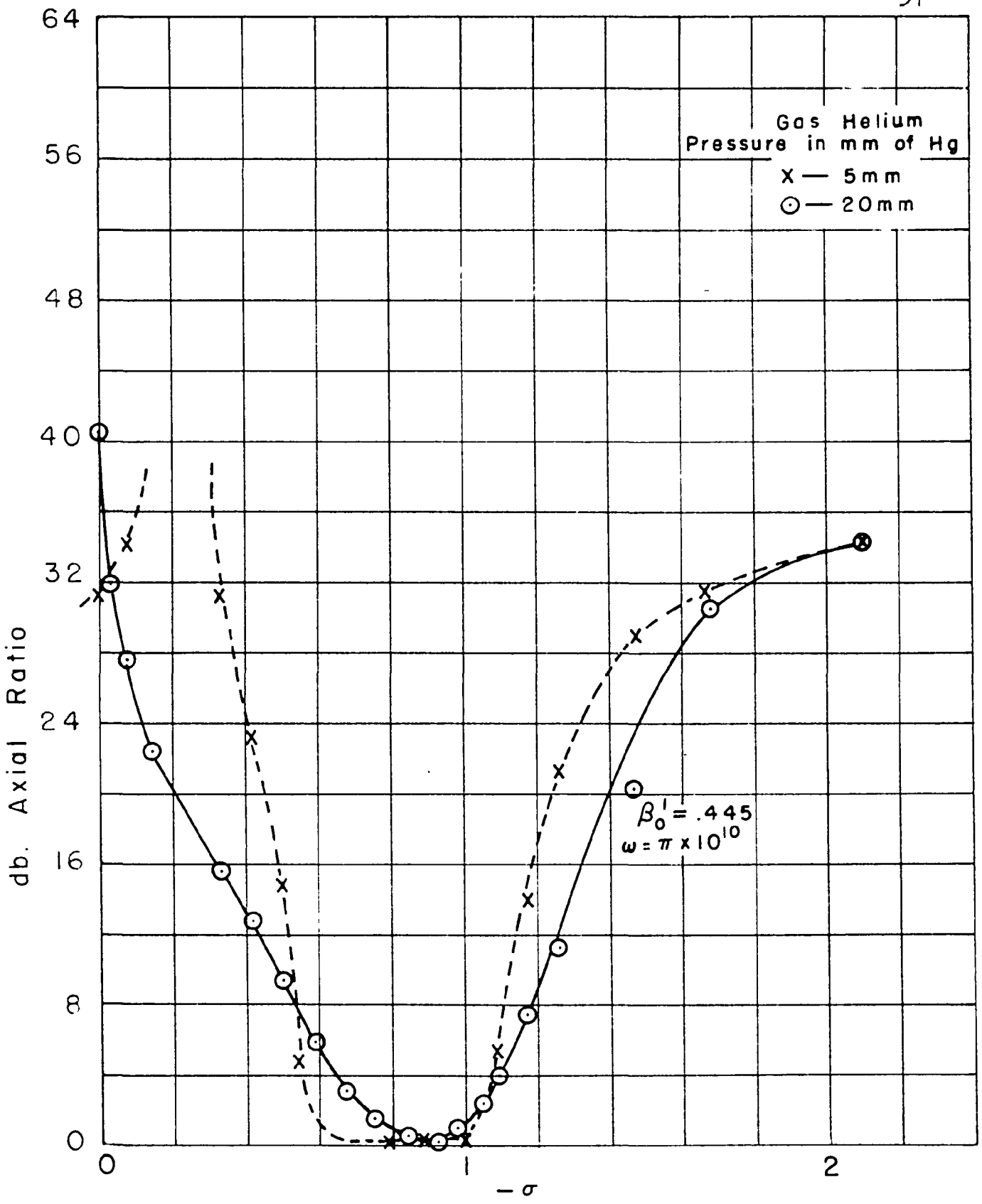

Figure 34. Axial Ratio of Transmitted Wave - Helium Discharge

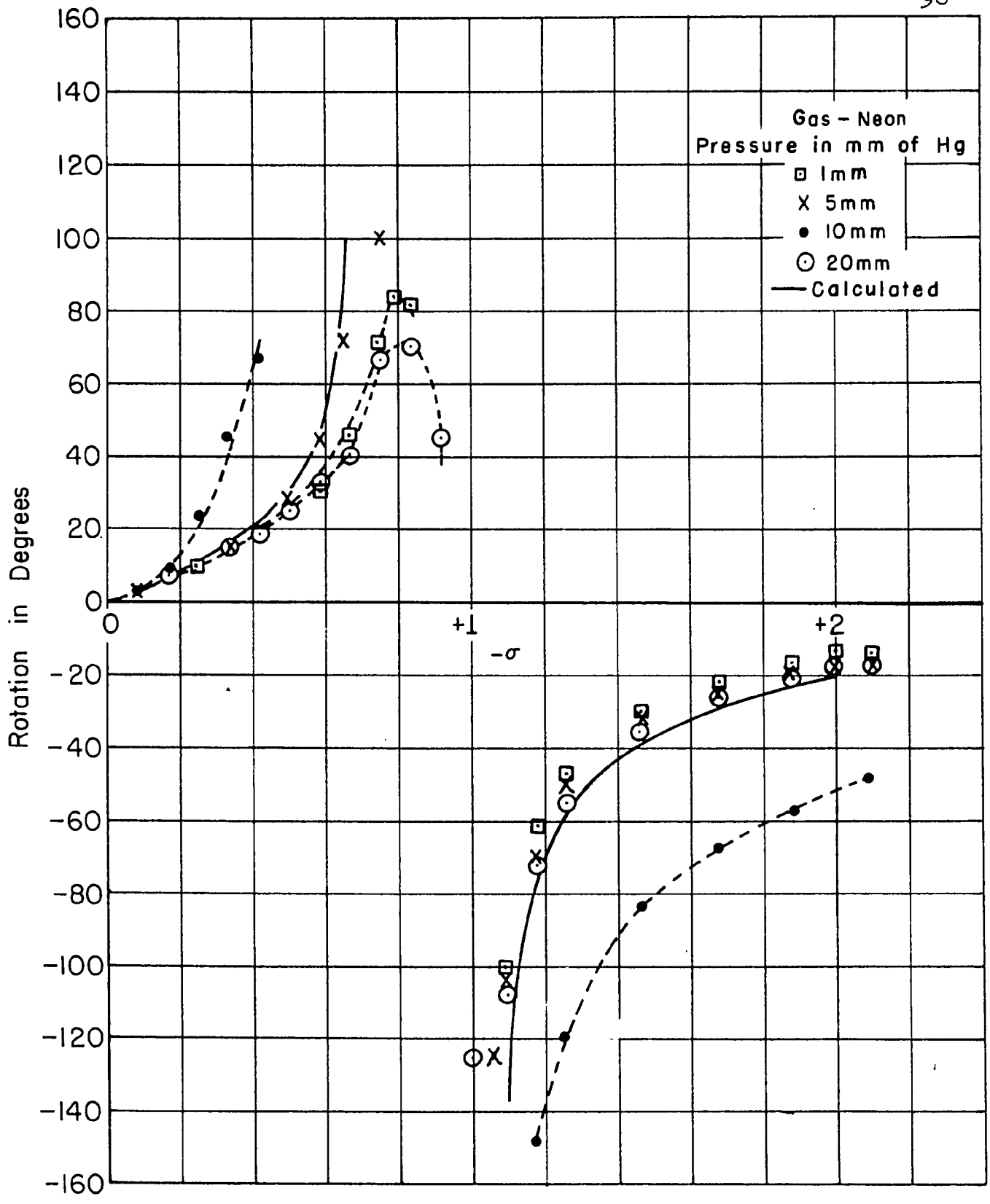

Figure 35. Rotation of Plane of Polarization of Transmitted Wave - Neon Discharge

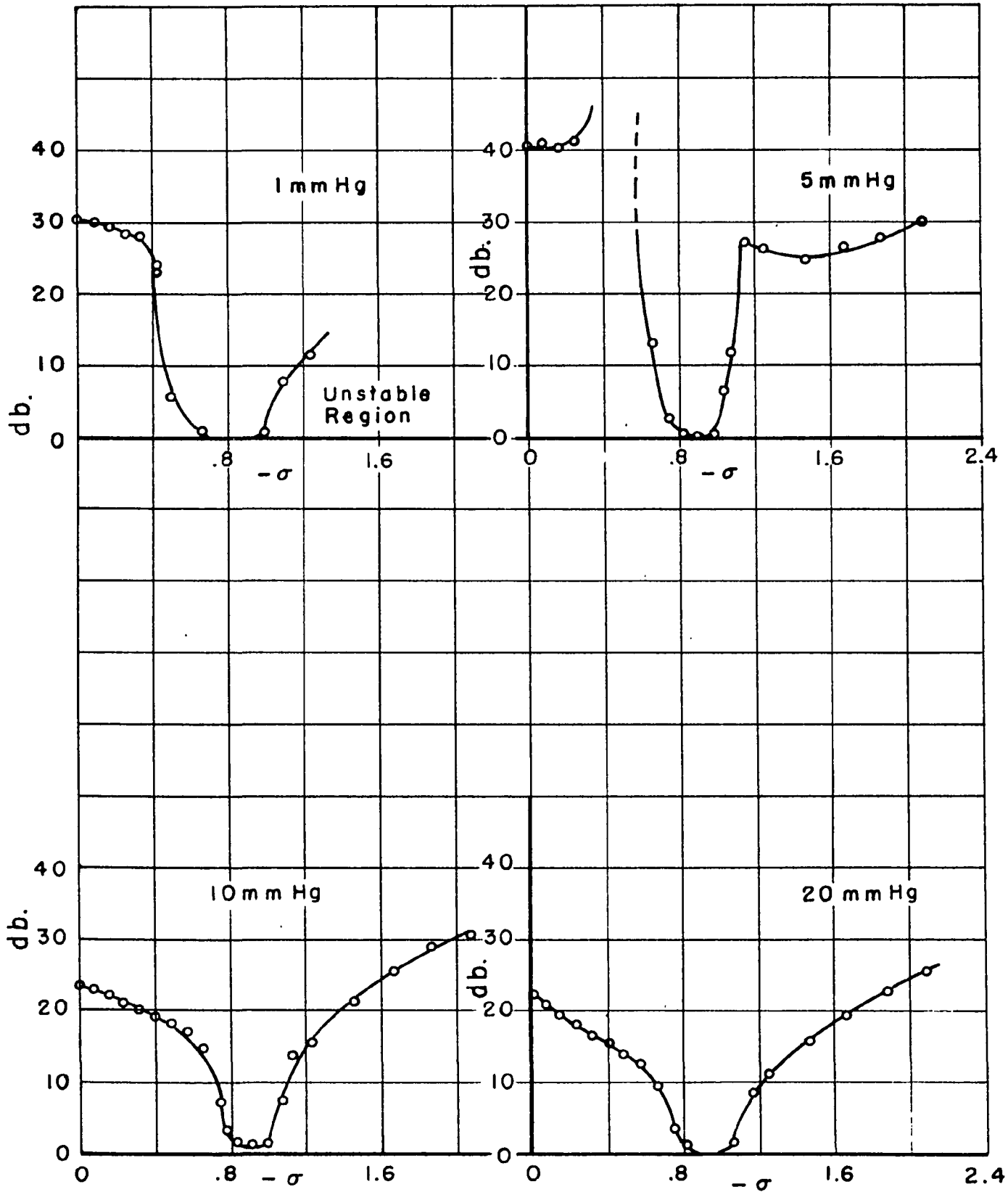

Figure 36. Axial Ratio of Transmitted Wave - Neon Discharge

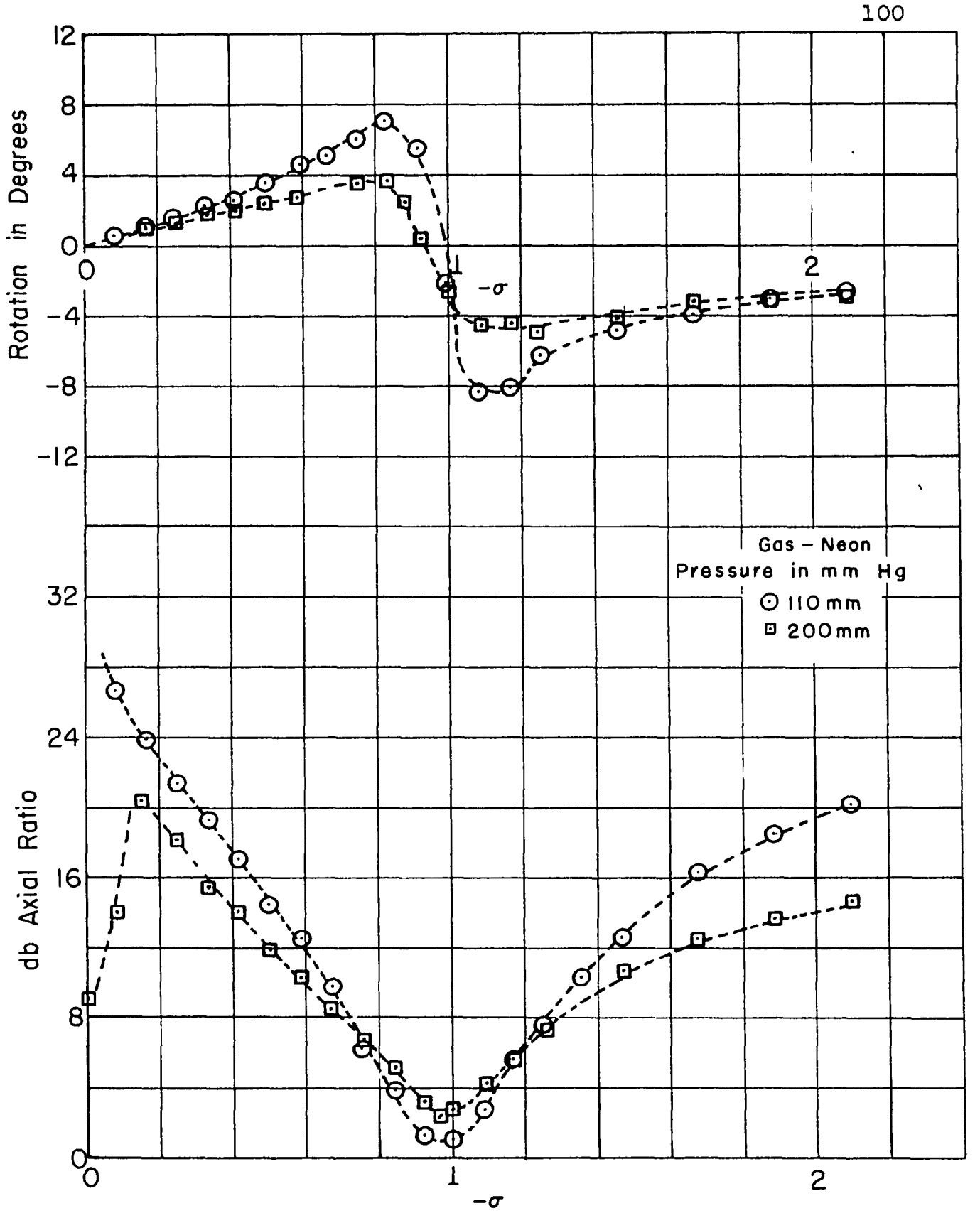

Figure 37. Rotation and Axial Ratio of Transmitted Wave - Neon Discharge

ratio curves are more symmetrical and broaden with increased pressure. This can be seen from the data for neon at pressures of 110 and 200 mm (Fig. 37). At resonance, the absorption of the minus wave is reduced by the increased collision frequency, so that the axial-ratio at resonance does not become zero. For these pressures, the axial ratio was measured to be approximately 1 and 2 db respectively.

It was also observed that at $-\sigma = 0$, the axial ratio of the transmitted wave was always less than that of the incident wave. Since the electron gas is isotropic at $-\sigma = 0$, both circular components of a linear wave should be equally affected, and as a result the axial ratio should be unchanged. The most likely reason for the decrease in axial ratio at $-\sigma = 0$ is non-uniformity of the discharge. There was no way of determining the variation of electron distribution experimentally, but it was observed that the discharges became unstable at higher pressures and angular variations in the light intensity were visible. Such discharge instabilities also were observed at pressures of 1 mm and below in both neon and helium discharges.

3. Variation with Electron Density: The Verdet Constant

In the region of magnetic field intensities corresponding to $0 \leq -\sigma < .5$, the rotation of the plane of polarization was measured for several values of the initial ($-\sigma = 0$) electron density in the decay of both helium and neon discharge plasmas. These data are presented in Fig. 38, and show clearly that for constant magnetic field intensity the rotation is correspondingly larger for greater electron densities. Within the accuracy of measurements, it is also seen that for a given electron density, the rotation is a linear function of magnetic field for $-\sigma$ close to zero. By approximating the slopes of the curves at $-\sigma = 0$ by the straight lines as shown in Fig. 38, the constants of proportionality or Verdet consiants were determined for each value of electron density. These values are compared to the theoretical values obtained from equation 3.28, Section III, in Figure 39.

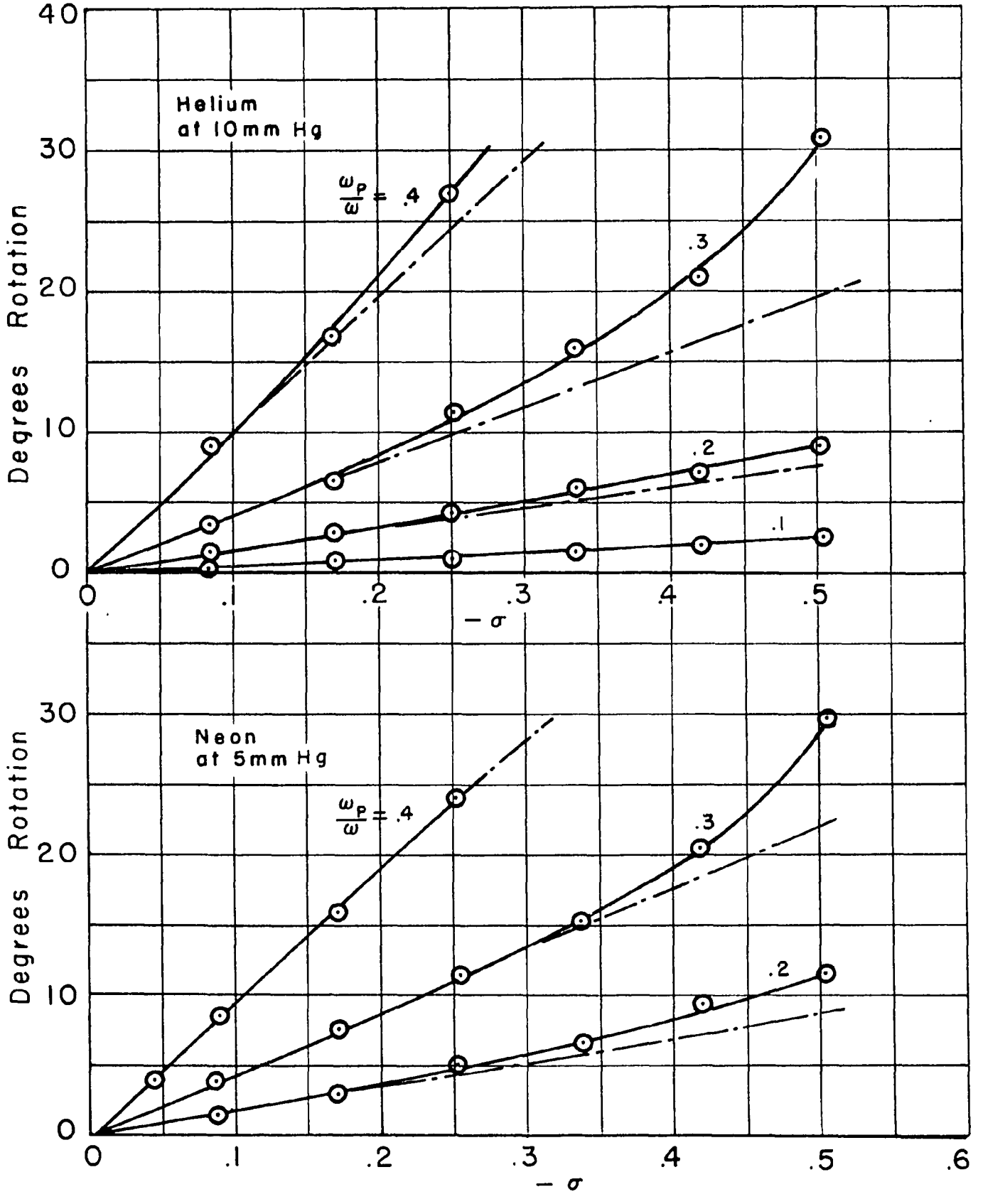

Figure 38. Faraday Rotation at Magnetic Field Intensities below Gyroresonance.

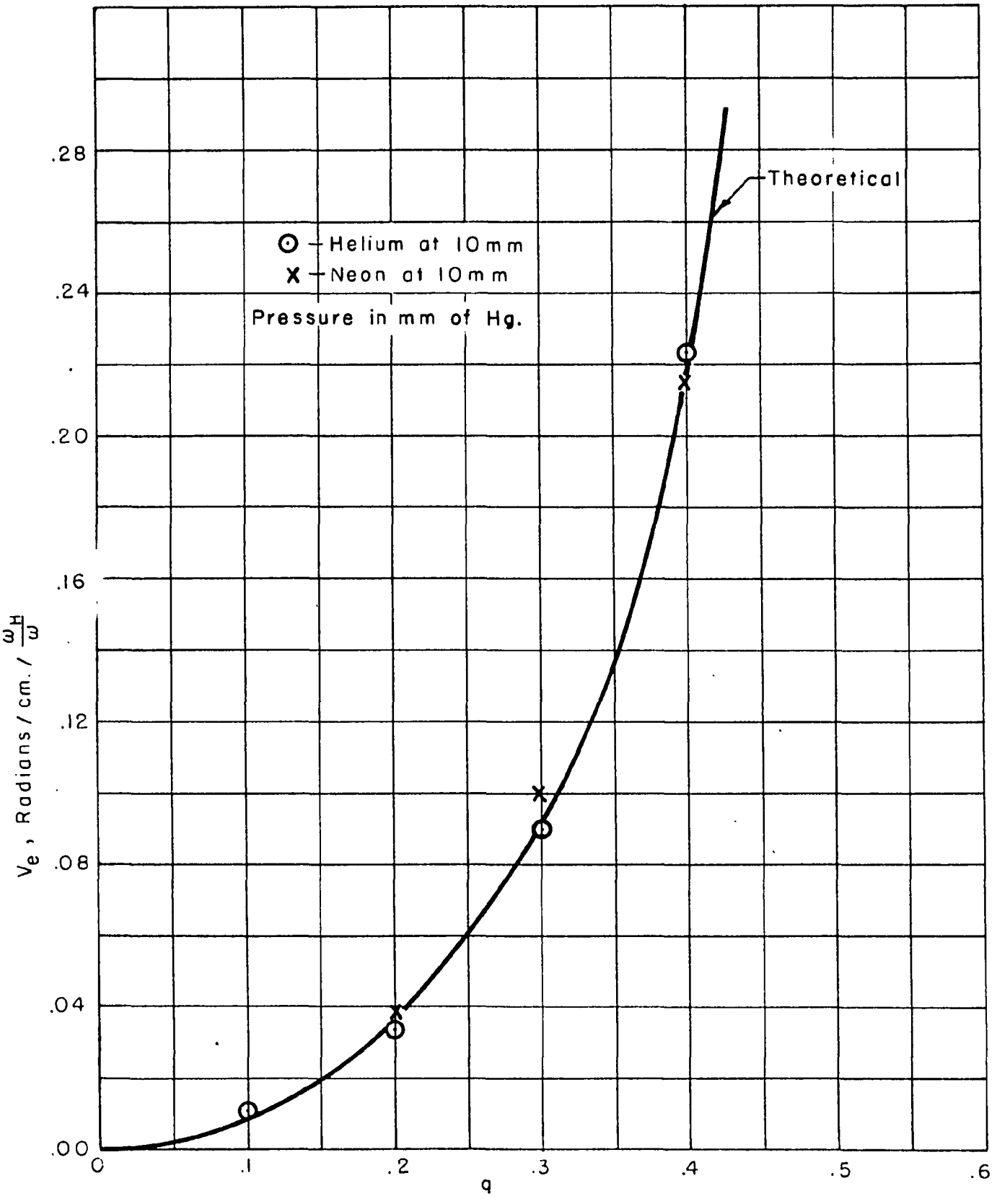

Figure 39. Measured and Calculated Values of the Verdet Constant

4. Non-Reciprocity of the Faraday Effect

The non-reciprocity of the phenomenon of Faraday rotation was demonstrated by an experiment using a modified waveguide circuit shown in Fig. 40.

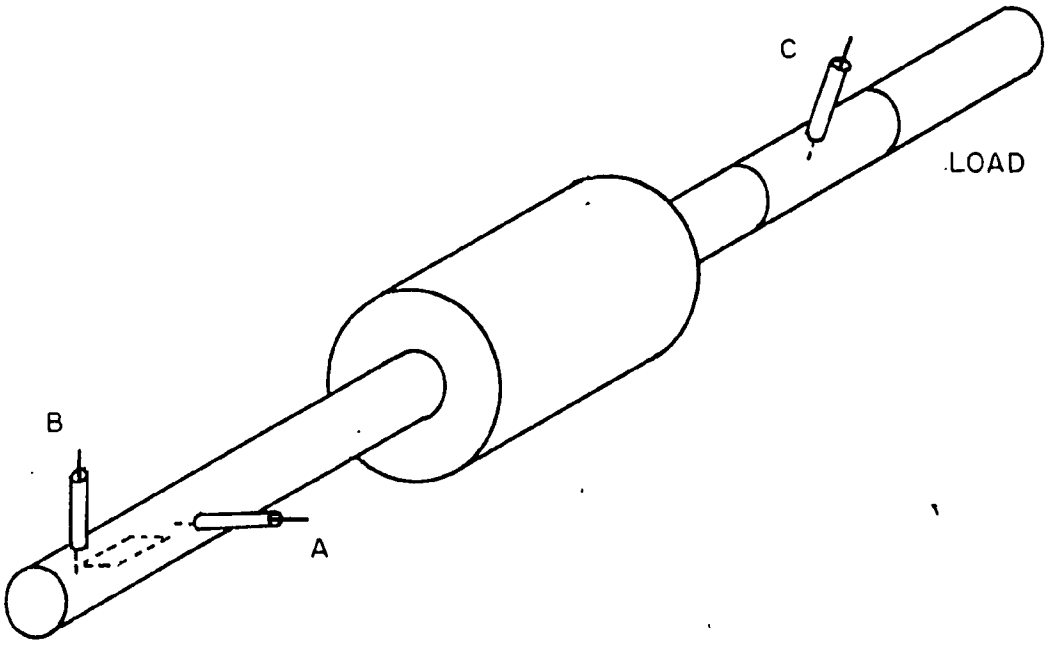

Figure 40. A Cutaway View of the Waveguide Arrangement for the Demonstration of Non-Reciprocity

The input antenna (A) launched a linear TE_{11} wave in the circular waveguide. A second antenna (B) shown to the left of the launching antenna was positioned 90 degrees about the waveguide axis with respect to the launching antenna. A conducting fin located in the waveguide and placed normal to the second antenna isolated the two antennas, and aided in matching the launching antenna to the waveguide.

The linear wave excited by antenna (A) was rotated by the discharge an amount measured by the rotating peripheral probe (C) with a matched load terminating the waveguide. The matched load was then replaced by a short. and the reflected wave further rotated by the second transmission through the discharge plasma. As the transmitted wave was rotated various amounts by changing the magnetic field from the solenoid, the relative power received by antenna (B) was measured.

The reflected wave was decomposed by the two antennae into linear components and each coupled from the waveguide by the antenna with corresponding polarization. The component from antenna (A) was dissipated in an attenuator and the other from antenna (B) was monitored by a crystal detector. The variation of the amplitude of the signal received at (B) with the rotation of the plane of the polarization of the transmitted wave is shown in Fig. 41.

If the plane of polarization of the transmitted wave is rotated θ degrees and an additional rotation of θ degrees occurs upon reflection, the wave returned toward the antenna system has its plane of polarization located an angle 2θ with respect to the incident wave polarization. By decomposing the reflected wave into two linear components polarized in the senses of the planes of the two antennas, it is readily established the power received by antenna (A) should vary as $\cos^2 2\theta$, and that received by antenna (B) as $\sin^2 2\theta$.

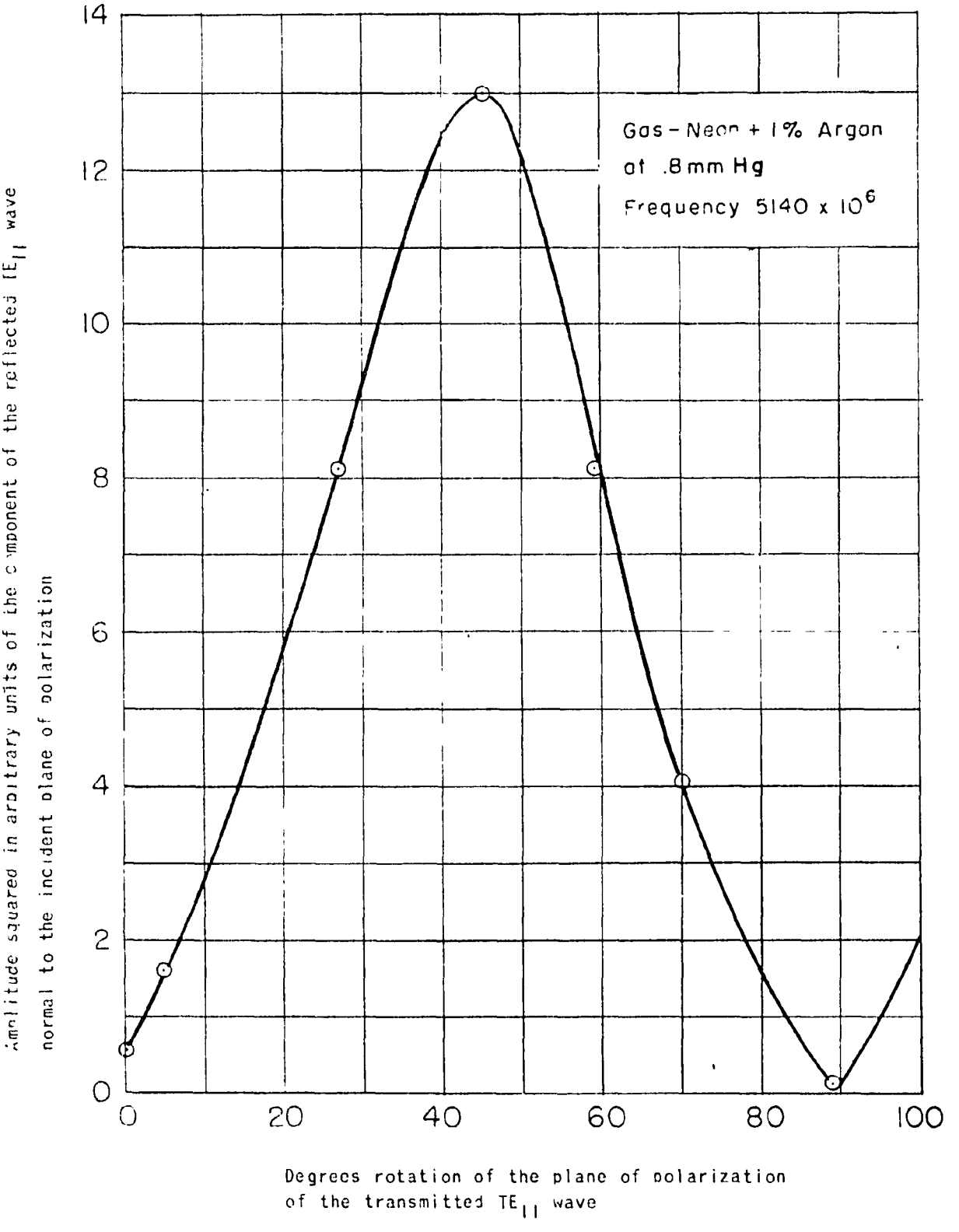

Figure 40. DEMONSTRATION OF THE NON RECIPROCITY OF THE ANISOTROPIC ELECTRON GAS

Therefore maximum power received at antenna (B) should occur for $\theta = 45^{\circ}$, and minimum power for $\theta = 0^{\circ}$ and 90° which is in agreement with the observations.

The use of a neon-argon gas mixture in the discharge tube for this experiment has no significance. since the effect depends only upon the electron density of the decaying plasma.

C. Summary and Conclusions

The Faraday rotation of TE_{11} waves in circular cross-section waveguide filled with the gyromagnetic electron gas of a discharge plasma has been investigated. Decaying isothermal plasmas in neon and helium gases were studied between gas pressures of 1 to 200 mm in neon and 5 to 20 mm in helium. The microwave signal was of low amplitude and at a frequency of 5000 megacycles.

The results of the experiments are in some respects explained qualitatively by a simple theory of propagation in an unbounded medium of uniform electron density. This theory gives correctly the observed effects of electron density, electron-molecule collision frequency, and applied magnetic field upon Faraday rotation of microwaves.

An explanation of the details of the phenomena is obtained by the more complete analysis of Suhl and Walker which, however, neglects electron molecule collisions. At the lower gas pressures and for magnetic fields away from that value required for electron gyroresonance, the electron collision frequencies obtained were sufficiently low to give good agreement between the observations and the calculations.

The superposition of circularly polarized data to yield the behaviour of initially linear TE_{11} waves propagated through the gyromagnetic electron gas demonstrates the validity of the interpretation of the Faraday rotation of a TE_{11} wave in terms of oppositely circularly polarized components. It was found that at an interface between the empty and filled portions of the waveguide, a circularly polarized TE_{11} wave could be used to excite a

corresponding circularly polarized wave essentially alone in the anisotropic region. This procedure was used to measure directly the phase constants of the modes of propagation in the anisotropic electron gas filled waveguide.

At low magnetic field intensities, the Faraday rotation of a guided wave is related to the magnetic field strength and length of the medium in a linear relation like that which is used to determine the rotation at light frequencies with transparent dielectric. The measured and theoretical values of the Verdet constant for the guided wave case agree well for plasmas in the two gases, neon and helium.

The non reciprocity of the Faraday effect has been demonstrated in a direct manner.

A conclusion to be drawn from the results is that Faraday rotation may be used as an aid in the investigation of discharge plasmas. At low magnetic field intensities, it has been shown the amount of rotation is directly proportional to the electron density. At higher magnetic field intensities, the relation is no longer linear, but a full analysis may be used in relating the observed rotations to the elements of the dielectric tensor of the plasma. It is worthwhile to consider other than the filled waveguide, since it was found difficult to obtain uniform electron densities throughout this structure. For instance, the behaviour of the plus wave did not agree well with calculations since its propagation was found to be determined largely by electrons in a region of the plasma near the waveguide wall where the average electron density was lower than at the guide center.

The results of the experiments give a good idea of the magnitudes of rotation and phase shift to be expected for actual discharge plasmas. It is seen that these values are of sufficient magnitude to be used in the control of guided microwave propagation. One immediate application, not new, is that of a one-way transmission device. This requires a rotation of 45 degrees, with high axial ratio of the transmitted wave, conditions which are met by the preceding experiments. Phase shift devices may also be obtained for circuits in which the mode of propagation is circularly polarized. Similarly attenuators, mode transducers and possibly many other waveguide circuit elements are realizeable using the Faraday rotation, resonance absorption, and phase shift properties of the anisotropic electron gas of a discharge plasma described in this thesis.

APPENDIX A

WAVE PROPAGATION IN CYLINDRICAL WAVEGUIDE TOTALLY FILLED WITH ANISOTROPIC DIELECTRIC

A. Derivation and Solution of the Wave Equation

The possible modes of propagation in cylindrical waveguide are obtained by applying the appropriate boundary conditions to solutions of Maxwells equations. when these equations are expressed in cylindrical polar coordinates (r, φ, z). The methods of obtaining the wave equations and their solutions in this Appendix are due to Suhl and Walker.[16],[17]

Maxwell's equation for the anisotropic medium are

$$\nabla \times \vec{E} = -\dot{\vec{B}} \qquad \nabla \times \vec{H} = \dot{\vec{D}} \quad . \tag{1}$$

$\vec{E}$, $\vec{D}$ $\vec{H}$, and $\vec{B}$ have their usual significance. and a dot appearing over a quantity denotes differentiation with respect to time.

In addition, we have the following relations:

$$\vec{B} = \mu_o \vec{H} \qquad \text{and} \qquad \vec{D} = \|\epsilon_e\| \cdot \vec{E} \tag{2}$$

where $\|\epsilon_e\|$ is a tensor of the form

$$\|\epsilon_e\| = \begin{Vmatrix} \epsilon & -i\eta & 0 \\ i\eta & \epsilon & 0 \\ 0 & 0 & \epsilon_z \end{Vmatrix} \quad . \tag{3}$$

The following definitions and operators are used:

1) Vectors are given by their components in the transverse (r, φ) plane and in the longitudinal (z) direction. The com-

ponents are indicated by the subscript t (transverse) or z (longitudinal)

$$\vec{A} = \vec{A}_t + \vec{A}_z$$

2) If $\vec{A}_t = (a,b)$, a "starring" operator is defined so that $\vec{A}_t^* = (b,-a)$

3) From statements 1 and 2 it follows that

$$\vec{A}_t^* \cdot \vec{A}_t^* = \vec{A}_t \cdot \vec{A}_t ,$$

$$\vec{A}_t^{**} = -\vec{A}_t ,$$

$$\vec{A}_t \cdot \vec{A}_t^* = 0,$$

$$\vec{A}_t \cdot \vec{B}_t^* = -\vec{A}_t^* \cdot \vec{B}_t = \left[\vec{A} \times \vec{B}\right]_z ,$$

and $\vec{k} \times \vec{A} = -\vec{A}_t^*$ where $\vec{k}$ denotes a unit vector in the z direction.

From Maxwells equations and the above relations, scalar wave equations are derived. The solutions to these equations are then used to express the field quantities within the cylindrical wave guide.

Assuming variations of the form $\exp i(\omega t - \beta z)$, noting $(\nabla \times \vec{A})_z = \nabla_t \cdot \vec{A}_t$ and $(\nabla \times \vec{A})_t = \nabla_t^* \vec{A}_z - \frac{\partial}{\partial z} \vec{A}_t^*$,

Maxwells curl relationships can be written in transverse and longitudinal components as

$$(\nabla \times \vec{E})_t = \nabla_t^* \vec{E}_z + i\beta \vec{E}_t^* = -i\omega\mu_0 \vec{H}_t , \qquad (4a)$$

$$(\nabla \times \vec{H})_t = \nabla_t^* \vec{H}_z + i\beta \vec{H}_t^* = i\omega(\epsilon \vec{E}_t - i\eta \vec{E}_t^*), \tag{4b}$$

and

$$(\nabla \times \vec{E})_z = \nabla_t \cdot \vec{E}_t^* = i\omega\mu_0 \vec{H}_z \tag{5a}$$

$$(\nabla \times \vec{H})_z = \nabla_t \cdot \vec{H}_t^* = i\omega\epsilon_z \vec{E}_z \quad . \tag{5b}$$

The following changes of variables are convenient:

1) All lengths are measured in units of $1/\beta_z$ where

$$\beta_z = \omega(\mu_0 \epsilon_z)^{\frac{1}{2}}$$

2) $\vec{\mathcal{H}} = (\mu_0/\epsilon_z)^{\frac{1}{2}} \vec{H}, \quad \vec{\mathcal{E}} = \vec{E},$

and 3) $\beta' = \beta/\beta_z$.

Using the above relations and setting $\nu_E = \epsilon/\epsilon_z$ and $\rho_E = \eta/\epsilon$ equations (4) and (5) become

$$\nabla_t^* \vec{\mathcal{E}}_z + i\beta' \vec{\mathcal{E}}_t^* = -i \vec{\mathcal{H}}_t \quad , \tag{6a}$$

$$\nabla_t^* \vec{\mathcal{H}}_z + i\beta' \vec{\mathcal{H}}_t^* = \nu_E (i \vec{\mathcal{E}}_t + \rho_E \vec{\mathcal{E}}_t^*) \quad , \tag{6b}$$

and $$\nabla_t \cdot \vec{\mathcal{E}}_t^* = -i \vec{\mathcal{H}}_z \quad , \tag{7a}$$

$$\nabla_t \cdot \vec{\mathcal{H}}_t^* = i \vec{\mathcal{E}}_z \quad . \tag{7b}$$

To simplify the notation, the prime will not be written with β', but is understood. Also the arrow denoting a vector will not be written.

Now operate on (6a) and (6b) with $\nabla_t \cdot$ and substitute from (7a) and (7b) so that

$$i\beta \nabla_t \cdot \mathcal{H}_t^* = \nu_E (i \nabla_t \cdot \mathcal{E}_t - i\rho_E \mathcal{H}_z) = -\beta \mathcal{E}_z \quad , \tag{8a}$$

and

$$i\beta \nabla_t \cdot \mathcal{E}_t^* = -i \nabla_t \cdot \mathcal{H}_t = \beta \mathcal{H}_z \quad . \tag{8b}$$

Similarly, operate on (6a) and (6b) with $\nabla_t^* \cdot$ and again substitute from (7a) and (7b) resulting in

$$\nabla_t^2 \mathcal{H}_z + i\beta \nabla_t \cdot \mathcal{H}_t = \nu_E (-\mathcal{H}_z + \rho_E \nabla_t \cdot \mathcal{E}_t) \quad , \tag{9a}$$

and

$$\nabla_t^2 \mathcal{E}_z + i\beta \nabla_t \cdot \mathcal{E}_t = -\mathcal{E}_z \quad . \tag{9b}$$

Eliminating first $\nabla_t \cdot \mathcal{E}_t$ and then $\nabla_t \cdot \mathcal{H}_t$ between (8) and (9) leads to

$$\nabla_t^2 \mathcal{H}_z + \nu_E (1 - \beta^2/\nu_E - \rho_E^2) \mathcal{H}_z = i\beta\rho_E \mathcal{E}_z \tag{10}$$

and

$$\nabla_t^2 \mathcal{E}_z + (1 - \beta^2/\nu_E) \mathcal{E}_z = -i\beta\rho_E \mathcal{H}_z \quad . \tag{11}$$

Solutions to equations (10) and (11) are obtained by determining the linear sums, $\mathcal{E}_z + i\kappa \mathcal{H}_z$, which satisfy both.

Multiplying (1) by $i\kappa$ and adding to (11) results in

$$\nabla_t^2 \mathcal{E}_z + i\kappa \nabla_t^2 \mathcal{H}_z + (1 - \frac{\beta^2}{\nu_E} + \beta\kappa\rho_E) \mathcal{E}_z + i\kappa \nu_E \left(1 - \frac{\beta^2}{\nu_E} - \rho_E^2 + \frac{\beta\rho_E}{\kappa \nu_E}\right) \mathcal{H}_z = 0 \quad . \tag{12}$$

Formulating $\Psi = \mathcal{E}_z + i\kappa \mathcal{H}_z$, Ψ is then a solution to equations (10) and (11) if κ is one of the roots κ_1, κ_2 of

$$\kappa^2 - \kappa \frac{\nu_E (1 - \beta^2/\nu_E - \rho_E^2) - (1 - \beta^2/\nu_E)}{\beta\rho_E} - 1 = 0 \tag{13}$$

Equation (12) may be written as

$$\nabla_t^2 \psi + \chi^2 \psi = 0 \tag{14}$$

where

$$\chi_{1,2}^2 = 1 - \beta^2/\nu_E + \beta \rho_E \kappa_{1,2} \tag{15a}$$

or $$\chi_{1,2}^2 = \nu_E \left(1 - \beta^2/\nu_E - \rho_E \right) - \rho_E \beta \kappa_{2,1} \quad . \tag{15c}$$

There are two ψ, ψ_1, and ψ_1, corresponding to χ_1 and χ_2 obtained from κ_1 and κ_2. Thus

$$\psi_1 = \mathcal{E}_z + i \kappa_1 \mathcal{H}_z \tag{16a}$$

and $$\psi_2 = \mathcal{E}_z + i \kappa_2 \mathcal{H}_z \quad . \tag{16b}$$

Solving for $\mathcal{E}_z$ and $\mathcal{H}_z$ we have

$$\mathcal{E}_z = \frac{\kappa_2 \psi_1 - \kappa_1 \psi_2}{\kappa_2 - \kappa_1} \tag{17a}$$

and $$\mathcal{H}_z = i \frac{\psi_1 - \psi_2}{\kappa_2 - \kappa_1} \tag{17b}$$

Solutions to equation (14) are required in cylindrical coordinates r, φ, z. Assuming the ψ to be of the form

$$\psi = \psi(r) \, e^{in\varphi} \, e^{i(\omega t - \beta z)} \tag{18}$$

where $\psi(r)$ is a function of r alone and

n = o, ± 1, ± 2, etc., equation (14) reduces to

$$\frac{d^2\psi(r)}{dr^2} + \frac{1}{r} \frac{d\psi(r)}{dr} + \left(\chi_{1,2}^2 - \frac{n^2}{r^2} \right) \psi(r) = 0 \quad . \tag{19}$$

A complete solution to equation (19) can be written

$$\psi(r) = C_1 J_m(\chi r) + C_2 Y_m(\chi r) \quad .$$

Since the field quantities must be regular at $r = 0$, the Y_n are not allowed. Therefore the final form of (18) is

$$\psi = A J_m(\chi r) e^{im\varphi} e^{i(\omega t - \beta z)} . \tag{20}$$

B. Application of the Boundary Conditions

Expressions for $\mathcal{H}_t$ and $\mathcal{E}_t$ in terms of the ψ are now obtained. Denoting the starring operation by the symbol P, equations (6a) and (6b) are written as

$$\nabla_t \mathcal{E}_z = -i\beta \mathcal{E}_t + i P \mathcal{H}_t \tag{21a}$$

and

$$\nabla_t \mathcal{H}_z = i\beta \mathcal{H}_t + (i\nu_E P - \rho_E \nu_E) \mathcal{E}_t \quad . \tag{21b}$$

Solving the above for $\mathcal{E}_t$ and $\mathcal{H}_t$ results in

$$(\nu_E - \beta^2 - i\rho_E \nu_E P) \mathcal{E}_t = -i\beta \nabla_t \mathcal{E}_z - i P \nabla_t \mathcal{H}_z \tag{22a}$$

and

$$(\nu_E - \beta^2 - i\rho_E \nu_E P) \mathcal{H}_t = \nu_E (iP - \rho_E) \nabla_t \mathcal{E}_z - i\beta \nabla_t \mathcal{H}_z \quad . \tag{22b}$$

Noting $\frac{1}{P + a} = \frac{1}{1 + a^2}(a - P)$, $P^2 = -1$, and $P^{-1} = -P$,

equations (22a) and (22b) may be rewritten as

$$\Omega \mathcal{E}_t = (1 - \beta^2/\nu_E + i\rho_E P)(-i\beta \nabla_t \mathcal{E}_z - i P \nabla_t \mathcal{H}_z) \tag{23a}$$

and

$$\Omega \mathcal{H}_t = \left(1 - \frac{\beta^2}{\nu_E} + i\rho_E P\right)\left[\nu_E(iP - \rho_E)\nabla_t \xi_z - i\beta \nabla_t \mathcal{H}_z\right] \quad , \tag{23b}$$

where

$$\Omega = \nu_E\left[\left(1 - \frac{\beta^2}{\nu_E}\right)^2 - \rho_E^2\right] \quad . \tag{24}$$

Substitution of (16a) and (16b) into (23a) and (23b) yields

$$\begin{aligned}(K_1 - K_2)\Omega \xi_t = {} & i\nabla_t \Psi_1\left[\beta K_2\left(1 - \beta^2/\nu_E\right) + \rho_E\right] - \nabla_t^* \Psi_1\left[1 - \beta^2/\nu_E + \beta\rho_E K_2\right] \\ & - i\nabla_t \Psi_2\left[\beta K_1\left(1 - \beta^2/\nu_E\right) + \rho_E\right] + \nabla_t^* \Psi_2\left[1 - \frac{\beta^2}{\nu_E} + \beta\rho_E K_1\right]\end{aligned} \tag{25}$$

and

$$\begin{aligned}(K_1 - K_2)\Omega \mathcal{H}_t = {} & \left[\left(1 - \beta^2/\nu_E\right)\left(\nu_E\rho_E K_2 - \beta\right) - \nu_E \rho_E K_2\right] \nabla_t \Psi_1 \\ & - i\left[\nu_E K_2\left(1 - \beta^2/\nu_E\right) - \rho_E\left(\rho_E \nu_E K_2 - \beta\right)\right] \nabla_t^* \Psi_1 \\ & - \left[\left(1 - \beta^2/\nu_E\right)\left(\nu_E \rho_E K_1 - \beta\right) - \nu_E \rho_E K_1\right] \nabla_t \Psi_2 \\ & + i\left[\nu_E K_1\left(1 - \beta^2/\nu_E\right) - \rho_E\left(\rho_E \nu_E K_1 - \beta\right)\right] \nabla_t^* \Psi_2 \quad .\end{aligned} \tag{26}$$

The following boundary conditions may now be applied:

at $r = r_o$, $\xi_\varphi = \xi_z = 0$.

From equation (17a), $(K_2 - K_1)\xi_z = K_2 \Psi_1 - K_1 \Psi_2$.

Using equation (2), this is written as

$$(K_1 - K_2)\,\xi_{\varphi_z} = K_1\psi_2 - K_2\psi_1 = \left[K_1 A_2 J_m(\chi_2 r) - K_2 A_1 J_m(\chi_1 r)\right] e^{im\varphi} .$$

$\xi_{\varphi_z} = 0$ at $r = r_0$ independent of the value of φ if

$$K_1 A_2 J_n(\chi_2 r_0) - K_2 A_1 J_n(\chi_1 r_0) = 0 .$$

A_1 and A_2 can then be chosen as

$$A_1 = \frac{J_n(\chi_2 r_0)}{K_2} \quad \text{and} \quad A_2 = \frac{J_n(\chi_1 r_0)}{K_1} ,$$

so that finally

$$\psi_{1,2} = \frac{J_n(\chi_{2,1} r_0)}{K_{2,1}} J_n(\chi_{1,2} r)\, e^{im\varphi} . \qquad (27)$$

Substitution of equation (27) into (25) and expansion of $\nabla\psi$ and $\nabla\psi^*$ leads to

$$(K_1 - K_2)\Omega\,\xi_\varphi = \frac{J_m(\chi_2 r_0) e^{im\varphi}}{K_2}\left[-\frac{m}{r}\left\{\beta K_2\left(1-\frac{\beta^2}{\nu_E}\right)+\rho_E\right\}J_m(\chi_1 r)+\left\{1-\frac{\beta^2}{\nu_E}+\beta\rho_E K_2\right\}\chi_1 J_m'(\chi_1 r)\right]$$

$$-\frac{J_m(\chi_1 r_0) e^{im\varphi}}{K_1}\left[-\frac{m}{r}\left\{\beta K_1\left(1-\frac{\beta^2}{\nu_E}\right)+\rho_E\right\}J_m(\chi_2 r)+\left\{1-\frac{\beta^2}{\nu_E}+\beta\rho_E K_1\right\}\chi_2 J_m'(\chi_2 r)\right] . \qquad (28)$$

Evaluating equation (28) at $r = r_0$ and noting that $K_{2,1} K_{1,2} = -1$ results in

$$(K_1-K_2)\Omega\,\xi_\varphi = \frac{J_m(\chi_1 r_0)\,J_m(\chi_2 r_0)}{r_0}\,e^{im\varphi}\left[m\rho_E(K_1-K_2)\right.$$

$$\left.+\left\{\beta\rho_E-K_1\left(1-\frac{\beta^2}{\nu_E}\right)\right\}\frac{\chi_1 r_0\,J_m'(\chi_1 r_0)}{J_m(\chi_1 r_0)}-\left\{\beta\rho_E-K_2\left(1-\frac{\beta^2}{\nu_E}\right)\right\}\frac{\chi_2 r_0\,J_m'(\chi_2 r_0)}{J_m(\chi_2 r_0)}\right] . \qquad (29)$$

Expressions of the form $\frac{u\,J_m'(u)}{J_m(u)}$ occur repeatedly and will be denoted as $F_n(u)$.

At $r = r_0$, $\xi_\varphi = 0$, so that (24) reduces to

$$m\rho_E(K_1-K_2)+\left[\beta\rho_E-K_1\left(1-\frac{\beta^2}{\nu_E}\right)\right]F_m(\chi_1 r_0)-\left[\beta\rho_E-K_2\left(1-\frac{\beta^2}{\nu_E}\right)\right]F_m(\chi_2 r_0)=0 \qquad (30)$$

which after manipulation is written as

$$\frac{m}{\beta}\left(\chi_2^2-\chi_1^2\right)=\frac{\chi_2^2}{K_2}F_m(\chi_1 r_0)-\frac{\chi_1^2}{K_1}F_m(\chi_2 r_0) \quad . \qquad (31)$$

C. Application to the Anisotropic Electron Gas in a Stationary Discharge Plasma.

Equations 13, 15, and 31 are sufficient to determine β , K , and χ given r_0, n, ρ_E and ν_E . If an electron gas is considered, a further simplification can be made. The elements of the tensor are then

$$\epsilon = \epsilon_0\left[1+\frac{q^2}{\sigma^2-1}\right] \quad , \quad \epsilon_z = \epsilon_0\left[1-q^2\right] \quad , \quad \text{and}$$

$$\eta = \epsilon_0\left[\frac{\sigma q^2}{\sigma^2-1}\right] \qquad \text{where } q=\frac{\omega_p}{\omega}=\frac{1}{\omega}\left(\frac{Ne^2}{\epsilon_0 m}\right)^{1/2}$$

and $\sigma = e\mu_0 H_0/\omega m$.

Then $$\rho_E = \eta/\epsilon = \frac{\sigma q^2}{\sigma^2 + q^2 - 1}$$

and $$\nu_E = \epsilon/\epsilon_2 = 1 - \frac{\sigma^2 q^2}{(\sigma^2-1)(q^2-1)} \quad .$$

ν_E and ρ_E are shown in Figures 41 and 42 as a function of σ.

The relation between ν_E and ρ_E is

$$\left(1 - \frac{1}{\nu_E}\right)\frac{1}{\rho_E} = \sigma \quad . \tag{32}$$

If a parameter h is substituted for βK, we have

$$h_{1,2} = \beta K_{1,2} \text{ so that,}$$

$$\beta^2 = -h_1 h_2. \tag{33}$$

Using equation (33), equation (31) becomes

$$\frac{1}{\chi_1^2}\left[h_1 F_m(\chi_1 r) + m\right] = \frac{1}{\chi_2^2}\left[h_2 F_m(\chi_2 r) + m\right] \quad . \tag{34}$$

Equations (13) and (15a) become

$$h^2 - h\,\frac{\nu_E\left(1-\rho_E^2-\beta^2/\nu_E\right) - \left(1-\beta^2/\nu_E\right)}{\rho_E} - \beta^2 = 0 \tag{35}$$

and $$\chi_{1,2}^2 = 1 - \beta^2/\nu_E + \rho_E h_{1,2} \quad . \tag{36}$$

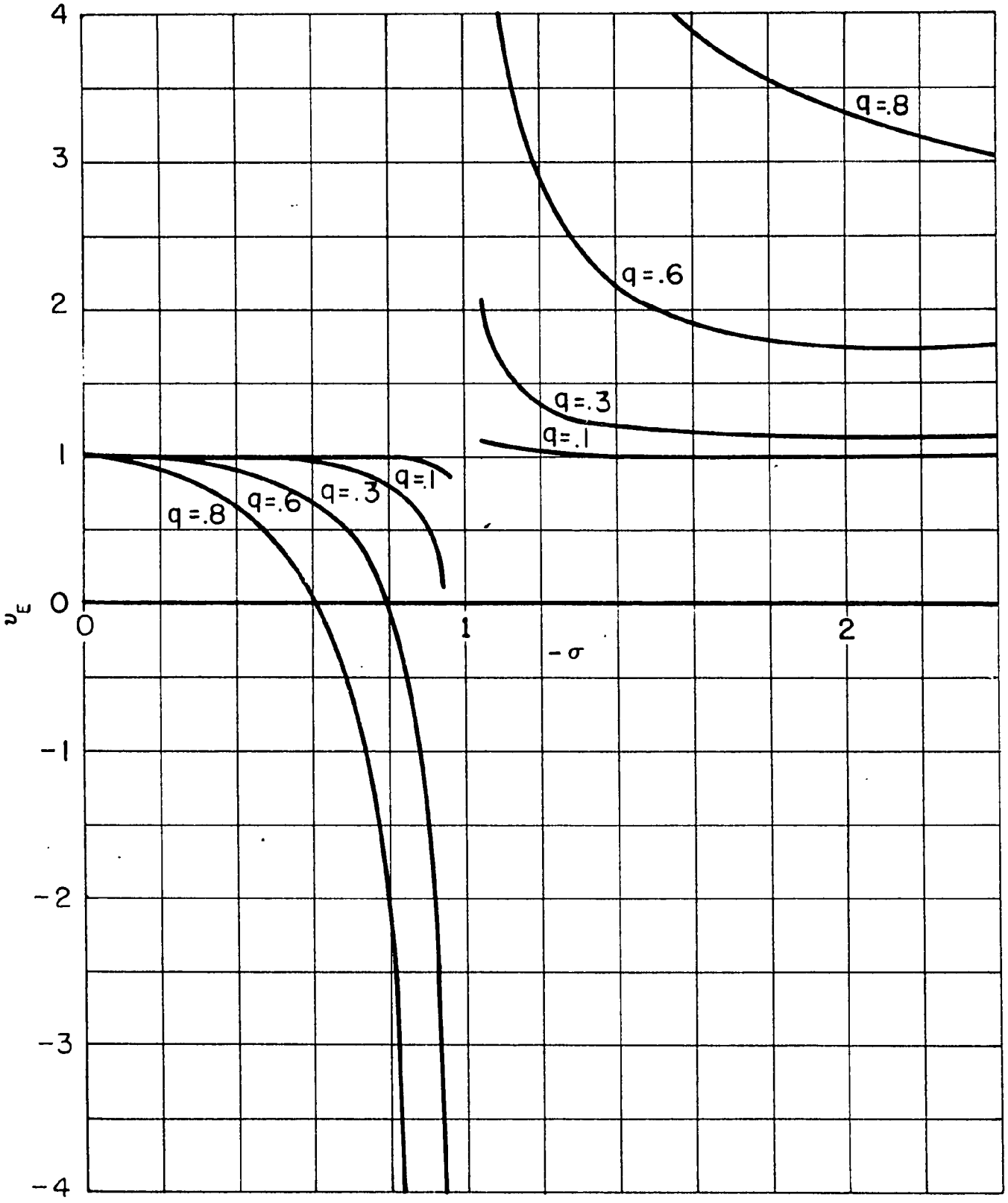

Figure 41. The Tensor Element Ratio ν_ε

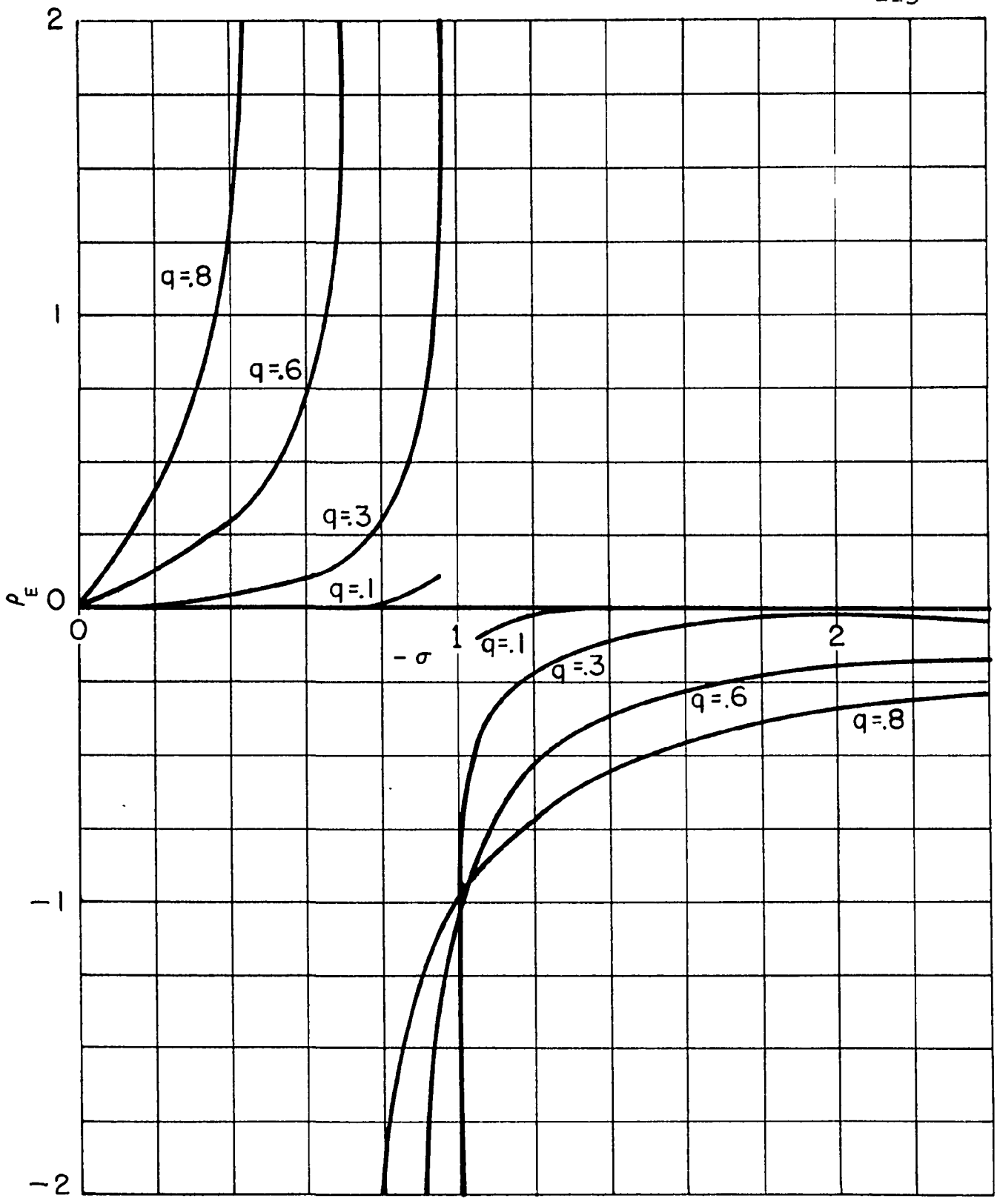

Figure 42. The Tensor Element Ratio ρ_E

Eliminating β between (35) and (36) results in

$$h_{1,2}^2 - \chi_{1,2}^2 \; h_{1,2} \left\{ \frac{1 - 1/\nu_E}{\rho_E} \right\} + \chi_{1,2}^2 - 1 = 0 \qquad (37)$$

Substituting (32) into (37) yields

$$\chi_{1,2}^2 = \frac{1 - h_{1,2}^2}{1 - h_{1,2}} \quad . \qquad (38)$$

Using relation (38), equation (34) reduces to

$$\frac{1-\sigma h_1}{1-h_1^2}\left[h_1 F_m\left(\sqrt{\frac{1-h_1^2}{1-\sigma h_1}}\,\eta\right) + m\right] = \frac{1-\sigma h_2}{1-h_2^2}\left[h_2 F_m\left(\sqrt{\frac{1-h_2^2}{1-\sigma h_2}}\right) + m\right] \quad . \qquad (39)$$

From equation (36), $\chi_1^2 - \chi_2^2 = \rho_E (h_1 - h_2)$, so that, for equation (38) we can write,

$$\frac{1-h_1^2}{1-\sigma h_1} - \frac{1 - h_2^2}{1 - \sigma h_2} = \rho_E (h_1 - h_2)$$

which simplifies to

$$h_1 + h_2 - \sigma h_1 h_2 = \frac{\sigma - \rho_E}{1 - \sigma \rho_E} = \frac{\sigma}{1 - q^2} \quad . \qquad (40)$$

The procedure of solution is to determine h_1 and h_2 from (39) and (40) given q and σ. The χ's are obtained from (38), and β^2 follows from equation (33).

The expressions for the field components in terms of h, r_0, and χ are

$$\mathcal{E}_z = \left[\frac{J_m(\chi_1 r)}{J_m(\chi_1 r_0)} - \frac{J_m(\chi_2 r)}{J_m(\chi_2 r_0)}\right] \quad e^{im\varphi} \quad , \tag{41}$$

and $$\mathcal{H}_z = i\beta\left[\frac{1}{h_1}\frac{J_m(\chi_1 r)}{J_m(\chi_1 r_0)} - \frac{1}{h_2}\frac{J_m(\chi_2 r)}{J_m(\chi_2 r_0)}\right] e^{im\varphi} \, . \tag{42}$$

By expansion of (25) and (26) the transverse components are

$$\mathcal{E}_r = -\frac{i}{\beta}\left[\frac{1}{r}\frac{J_m(\chi_1 r)}{J_m(\chi_1 r_0)}\frac{1}{\chi_1^2}\left\{(1-\chi_1^2)F_m(\chi_1 r) + m\right\}\right.$$

$$\left. - \frac{1}{r}\frac{J_m(\chi_2 r)}{J_m(\chi_2 r_0)}\frac{1}{\chi_2^2}\left\{(1-\chi_2^2)F_m(\chi_2 r) + m\right\}\right] e^{im\varphi} \, , \tag{43}$$

$$\mathcal{E}_\varphi = \frac{1}{\beta}\left[\frac{1}{r}\frac{J_m(\chi_1 r)}{J_m(\chi_1 r_0)}\frac{1}{\chi_1^2}\left\{h_1 F_m(\chi_1 r) + m(1-\chi_1^2)\right\}\right.$$

$$\left. - \frac{1}{r}\frac{J_m(\chi_2 r)}{J_m(\chi_2 r_0)}\frac{1}{\chi_2^2}\left\{h_2 F_m(\chi_2 r) + m(1-\chi_2^2)\right\}\right] e^{im\varphi} \, , \tag{44}$$

$$\mathcal{H}_r = -\left[\frac{1}{r}\frac{J_m(\chi_1 r)}{J_m(\chi_1 r_0)}\frac{1}{\chi_1^2}\left\{h_1 F_m(\chi_1 r) + m\right\}\right.$$

$$\left. - \frac{1}{r}\frac{J_m(\chi_2 r)}{J_m(\chi_2 r_0}\frac{1}{\chi_2^2}\left\{h_2 F_m(\chi_2 r) + m\right\}\right] e^{im\varphi} \, , \tag{45}$$

and

$$\mathcal{H}_\varphi = -i\left[\frac{1}{r}\frac{J_m(\chi_1 r)}{J_m(\chi_1 r_0)}\frac{1}{\chi_1^2}\left\{F_m(\chi_1 r) + m h_1\right\}\right.$$

$$\left. - \frac{1}{r}\frac{J_m(\chi_2 r)}{J_m(\chi_2 r_0)}\frac{1}{\chi_2^2}\left\{F_m(\chi_2 r) + m h_2\right\}\right] e^{im\varphi} \quad . \quad (46)$$

A common factor $\dfrac{K_2 - K_1}{J_n(\chi_1 r_0)\, J_n(\chi_2 r_0)}$ has been removed from the left side of equations (41) thru (46).

BIBLIOGRAPHY

1. H. G. Booker, An Outline of the Magneto-Ionic Theory, Technical Report No. 1, Contract W36-039-sc-44518, Cornell University, Ithaca, N.Y., March, 1950.

2. H. Gamo, The Faraday Rotation of Waves in a Circular Wave-Guide, Jour. Phys. Soc. Japan, v. 8, No. 2, pp. 176-182, May 15, 1953.

3. L. Goldstein, M. Lampert, and Geiger, Determination of Electron Density and Electron Collision Frequency in a Gaseous Discharge by Microwave Propagation Measurements, Electrical Communication, v. 29, no. 3, p. 243, Sept. 1951.

4. L. Goldstein, M. Lampert, and J. Heney, Magneto-Optics of an Electron Gas with Guided Microwaves, Phys. Rev., v. 82, pp. 956-957, June 15, 1951.

5. L. Goldstein, M. Lampert, and J. Heney, Magneto-Optics of an Electron Gas for Guided Microwaves: Propagation in Rectangular Waveguide, Phys. Rev. v. 82, p. 1255, Sept. 15, 1951.

6. C. L. Hogan, The Ferromagnetic Faraday Effect at Microwave Frequencies and its Applications, Bell System Tech. Jour., v. 31, no. 1, pp. 1-31, January, 1952.

7. E. C. Jordan, Electromagnetic Waves and Radiating Systems, Prentice-Hall, Inc., 1950.

8. H. A. Lorentz, The Theory of Electrons, Dover, 1952.

9. N. W. McLachlan, Bessel Functions for Engineers, Oxford University Press, 1948.

10. C. G. Montgomery, Technique of Microwave Measurements, MIT Rad. Lab. Series, v. 11, McGraw Hill, 1947.

11. C. G. Montgomery, R. H. Dicke, and E. M. Purcell, Principles of Microwave Circuits, MIT Rad. Lab. Series, v. 8, McGraw Hill, 1948.

12. A. V. Phelps, O. T. Fundingsland, and S. C. Brown, Microwave Determination of the Probability of Collision of Slow Electrons in Gases, Phys. Rev., v. 84, no. 3, pp. 559-562, Nov. 1, 1951.

13. R. Rompe and M. Steenbeck, Der Plasmazustand der Gase, Ergebnisse der Exakten Naturwissenschaften, Berlin, 1939.

BIBLIOGRAPHY (continued)

14. A. L. Samuel and C. F. Crandell, A Waveguide Bridge for Measuring Gain at 4000 Mc., Proc. I.R.E., v. 36, no. 11, pp. 1414-1418, Nov., 1948.

15. Stratton, Electromagnetic Theory, McGraw-Hill, 1941.

16. H. Suhl and L. R. Walker, Faraday Rotation of Guided Microwaves, Phys. Rev., v. 86, no. 1, p. 122, 1952.

17. H. Suhl and L. R. Walker, Topics in Guided Wave Propagation through Gyromagnetic Media, Bell System Tech. Jour., v. 31, no. 3, pp. 579-659, May, 1954.

18. C. H. M. Turner, Birefringence in Crystals and the Ionosphere, Canadian Jour. of Physics, v. 33, no. 1, pp. 16-34, January, 1954.

19. A. A. Th. M. Van Trier, Guided Electromagnetic Waves in Anisotropic Media, Applied Scientific Research, Sec. B, v. 3, nos. 4-5, pp. 305-371, 1953.

VITA

James E. Etter was born at Piqua, Ohio on the twenty-first of May, 1925.

After graduating from Covington High School, Covington, Ohio, in 1942 Mr. Etter entered the Ohio State University as a student in Engineering Physics. During his second year of study, he was drafted into the United States Navy, and was later assigned to the V-12 program at the University of Illinois in March, 1944. Mr. Etter received his BSEE in February, 1946 from the University of Illinois and continued in the U.S. Navy until discharged in May, 1946 with the rank of Ensign.

Mr. Etter re-entered the University of Illinois in September, 1946 as a graduate student and received the M.S.E.E. in February 1948. During this period, he held a research assistantship in the Electron Tube Research Group. Following his Masters Degree, Mr. Etter became a research associate with this group, a position he presently holds.

He is a member of Sigma Xi, Eta Kappa Nu, and Pi Mu Epsilon.